AD

TECHNICAL REPORT ECOM-0189-F

ELECTROMAGNETIC INTERFERENCE MEASUREMENT METHODOLOGY, COMMUNICATION EQUIPMENT

FINAL REPORT

By

W. R. FREE AND C. W. STUCKEY

October 1969

ECOM

UNITED STATES ARMY ELECTRONICS COMMAND • FORT MONMOUTH, N.J.

Contract DAAB07-68-C-0189

Engineering Experiment Station
GEORGIA INSTITUTE OF TECHNOLOGY
Atlanta, Georgia

NOTICES

Disclaimers

The findings in this report are not to be construed as an official Department of the Army position, unless so designated by other authorized documents.

Disposition

Destroy this report when it is no longer needed. Do not return it to the originator.

Reports Control Symbol
OSD-1366

TECHNICAL REPORT ECOM-0189-F

October 1969

ELECTROMAGNETIC INTERFERENCE MEASUREMENT METHODOLOGY, COMMUNICATION EQUIPMENT

FINAL REPORT

1 FEBRUARY 1968 TO 31 MAY 1969

CONTRACT NO. DAAB07-68-C-0189
DA PROJECT NO. 1H6 20501 D449 01 56

Prepared By

W. R. FREE AND C. W. STUCKEY

ENGINEERING EXPERIMENT STATION
GEORGIA INSTITUTE OF TECHNOLOGY
ATLANTA, GEORGIA

For

U. S. ARMY ELECTRONICS COMMAND
FORT MONMOUTH, N. J.

ABSTRACT

This report summarizes the accomplishments on a program to develop improved test techniques and procedures for performing radiated measurements in shielded enclosures which can be correlated with measurements made in the open-field.

A set of three short hooded probe antennas to cover the 1 to 12 GHz frequency range were developed and evaluated. Results from this program indicate that reliable radiated measurements, which can be correlated with open-field measurements, can be made in shielded enclosures with short hooded probe antennas over the 200 MHz to 12 GHz frequency range.

Coupling nulls were observed in shielded enclosures in the frequency range from 10 to 100 MHz. The presence of these nulls could not be explained on the basis of cavity resonances or multi-path reflections from the enclosure walls since the dimensions on the enclosures were quite small in terms of wavelengths. It was concluded that a different coupling mechanism must be responsible for the existance of these coupling nulls. A theory was developed to explain the nulls in terms of near-field coupling between the radiating source and the enclosure walls and between the enclosure walls and the probe antenna. The results from extensive experimental measurements supported the validity of this theory. The coupling nulls were essentially eliminated by isolating the probe antenna from the enclosure walls.

While it was concluded that radiated measurements performed in shielded enclosures over the 14 kHz to 20 MHz frequency range yielded essentially the same results as equivalent measurements performed in the open-field, there is considerable question as to the value of measurement results obtained in either location over this frequency range where the probe antenna is in the very near-field of the unit under test. This investigation also re-emphasized the need for more efficient, balanced probe antennas for use in the 14 kHz to 20 MHz frequency range.

FOREWORD

This report was prepared at the Georgia Tech Engineering Experiment Station on Contract No. DAAB07-68-C-0189. The work covered by this report was performed within the Electronics Division under the suprevision of Mr. D. W. Robertson, Head of the Communications Branch. The report covers the activities and results of a fifteen month effort on a project to develop improved test setups, procedures and equipment for measurement of radiated emission and susceptibility characteristics of military communication - electronic equipment in shielded enclosures.

TABLE OF CONTENTS

TABLE OF CONTENTS (Continued)

LIST OF ILLUSTRATIONS

LIST OF ILLUSTRATIONS (Continued)

LIST OF ILLUSTRATIONS (Continued)

LIST OF ILLUSTRATIONS (Continued)

LIST OF ILLUSTRATIONS (Continued)

I. FACTUAL DATA

A. Introduction

1. Purpose and Objectives of the Program

This report covers the work performed under contract DAAB07-68-C-0189 for the period from 1 February 1968 to 31 May 1969.

The purpose of this program was to conduct theoretical and experimental investigations directed toward the development of improved test setups, procedures and equipment for the measurement of radiated emission and susceptibility characteristics of military communication - electronic equipment. These measurements are to be made within shielded enclosures, in the near-field of the equipment under test and at frequencies at which RF absorbers are not economically feasible, and where present hooded antennas are not effective.

The primary objectives of the program were (1) the development of techniques for measuring radiated interference and susceptibility characteristics in shielded enclosures over the frequency range from 20 to 200 MHz, (2) an investigation to determine the availability of broadband, balanced, electric-field antennas suitable for radiated emission and susceptibility measurements in shielded enclosures over the frequency range from 14 kHz to 200 MHz and (3) the development of broadband hooded antennas which minimize the narrowing effect of the hood on the antenna field pattern.

2. Background

Present techniques for case and cable emission and susceptibility measurements are seriously inadequate, and need to be improved to assure repeatability and correlation between measurement data taken at different times and/or different locations. If these measurements are made in the "open-field", strong man-made and atmospheric background interference make measurements difficult and often impossible. If the measurements are made in a shielded enclosure to avoid the environmental interference, standing waves and enclosure resonances make the measurements highly susceptible to minor variations in equipment placement, enclosure dimensions, and personnel location.

A typical measurement setup in a shielded enclosure is shown in Figure 1. The diagram shows some of the multiple signal paths which exist with this measurement configuration. Extensive measurement programs were conducted on previous research efforts[1,2] to determine the

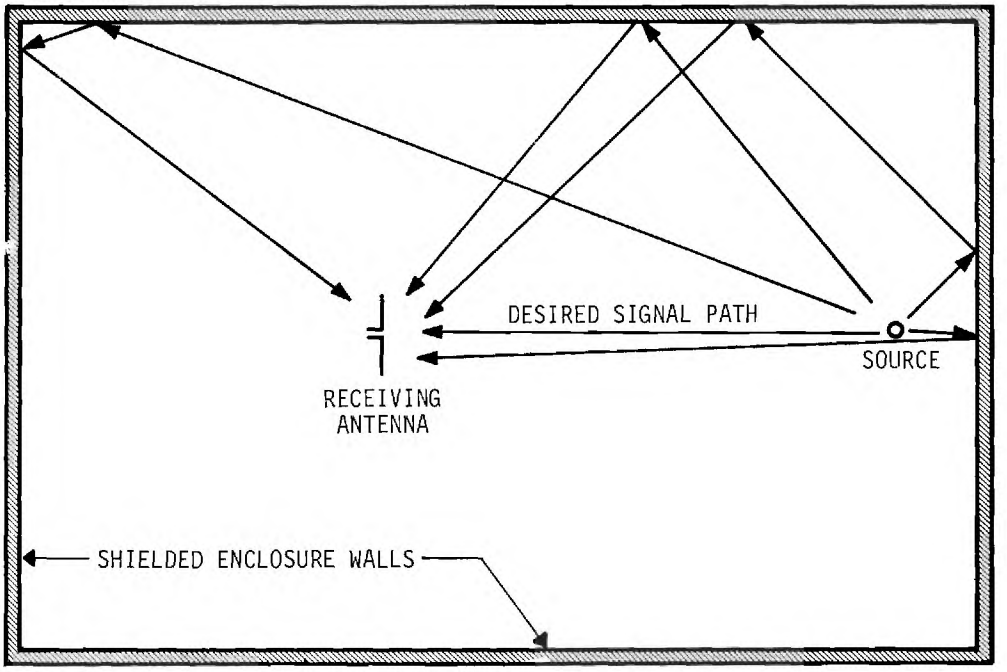

Figure 1. Diagram of a Conventional Measurement Setup in a Shielded Enclosure Showing Multiple Signal Paths.

magnitude and nature of the effects of shielded enclosures on radiated measurements. Measurements were made to determine the effects of a shielded enclosure on the coupling between two antennas (a) at a fixed separation as a function of frequency, (b) at a fixed frequency as a function of separation and (c) as a function of the location of the test setup within the shielded enclosure.

A curve showing the coupling between two antennas spaced 1 meter apart in an 8 x 8 x 20 foot shielded enclosure over the frequency range from 1 MHz to 1 GHz is shown in Figure 2. This curve has been normalized with respect to an open-field coupling curve to remove the coupling variations due to the antenna characteristics, and hence, all coupling variations shown in the normalized coupling curve result from the presence of the shielded enclosure walls. The results indicate that coupling variations in the order of ±40 dB are possible as a function of frequency of operation. Similar results were obtained as a function of separation between the two antennas at 615 and 930 MHz and are shown in Figure 3. It is obvious that measurements made under these conditions are of little value and the possibility of correlating these measurements with measurements made in the open-field is small.

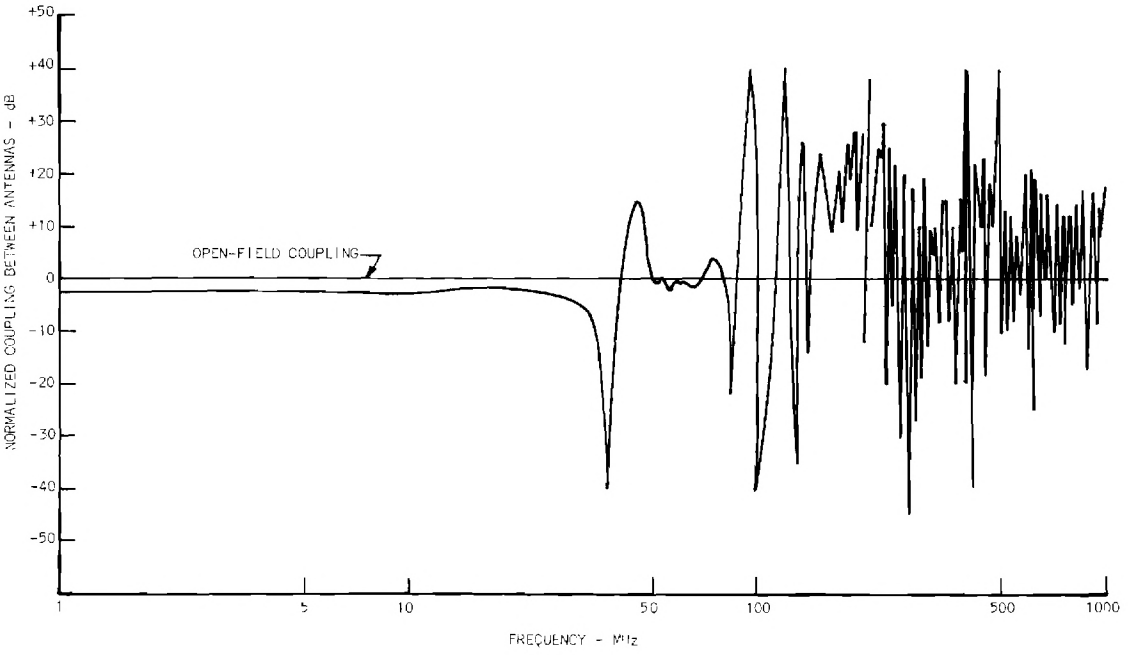

Figure 2. Coupling Between Antennas in a Shielded Enclosure as a Function of Frequency at a Spacing of 1 Meter.

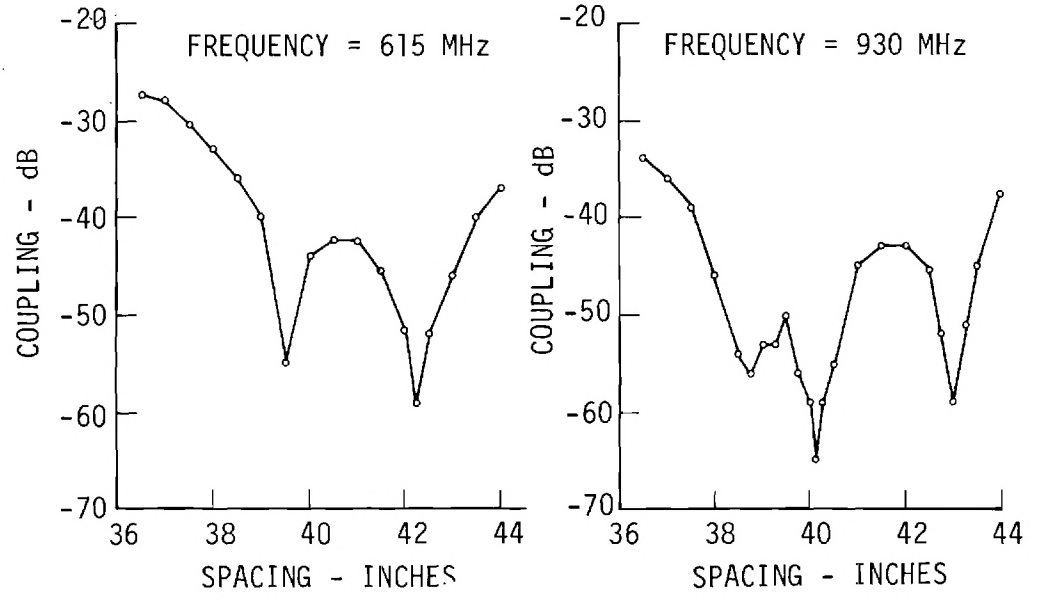

Figure 3. Coupling Between Antennas in a Shielded Enclosure as a Function of Spacing.

A number of techniques for reducing multipath reflections within shielded enclosures were investigated on previous programs under Contracts Nos. DA 36-039 AMC-02294(E) and DA 28-043 AMC-02381(E). As a result of these programs, a hooded antenna measurement technique was developed. A diagram showing a typical hooded antenna measurement setup in a shielded enclosure is shown in Figure 4. A number of possible signal paths are shown in the shielded enclosure, but as illustrated, only that signal traveling the desired path reaches the shielded probe antenna. Results from evaluations of the hooded antenna technique over the frequency range from 200 MHz to 10 GHz indicate that this technique is capable of reducing the multipath reflections in shielded enclosures to a level comparable with the reflections normally encountered in open-field measurements.

To substantiate these results, the coupling between two antennas was measured for a spacing of one meter in an 8 x 8 x 20 foot shielded enclosure over the frequency range of 1 MHz to 10 GHz. Conventional dipole probe antennas were used as the receiving antennas over the range from 1 to 200 MHz, and hooded probe antennas were used over the 200 MHz to 10 GHz range.

The results of these measurements are shown in Figure 5. The shielded enclosure coupling curve shown in the figure has been normalized with respect to the coupling curve obtained in the open-field. The curve shows that the measurement results obtained in the enclosure over the frequency range from 1 to 30 MHz are approximately 2 to 3 dB lower than the results obtained in the open-field. In the range from 20 to 200 MHz, the curve indicates that the enclosure results deviate as much as ±40 dB from the open-field results. From 200 MHz to 10 GHz, using the hooded antenna technique, it is seen that the enclosure results remain within 2 to 3 dB of the open-field results. It is apparent from Figure 5 that the 20 to 200 MHz range is the remaining area requiring improved measurement techniques.

B. Study of Near-Field Measurement Problems

1. General

At low frequencies, where the shielded enclosure dimensions and probe antenna spacings are small relative to the wavelengths involved, the coupling between the equipment under test and the probe antenna becomes much more complicated and includes additional components of the more complex near-field. The behavior of these near-field components in the shielded enclosure is not well understood, and there is a very limited amount of information on this subject in the literature. In order to determine the measurement problems

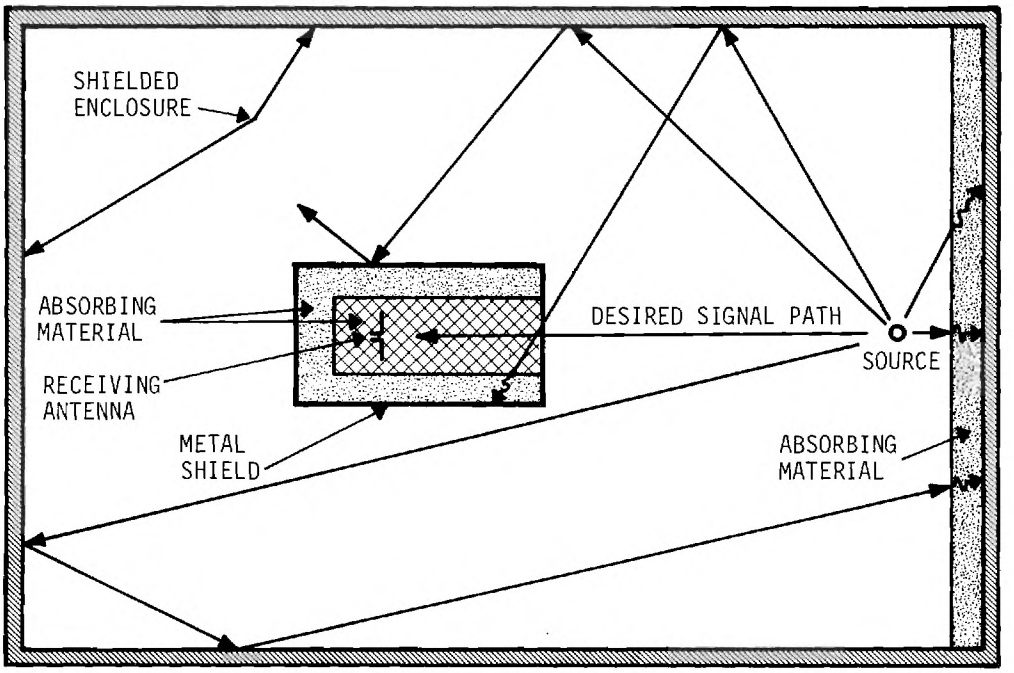

Figure 4. Diagram of a Hooded Antenna Measurement Setup in a Shielded Enclosure.

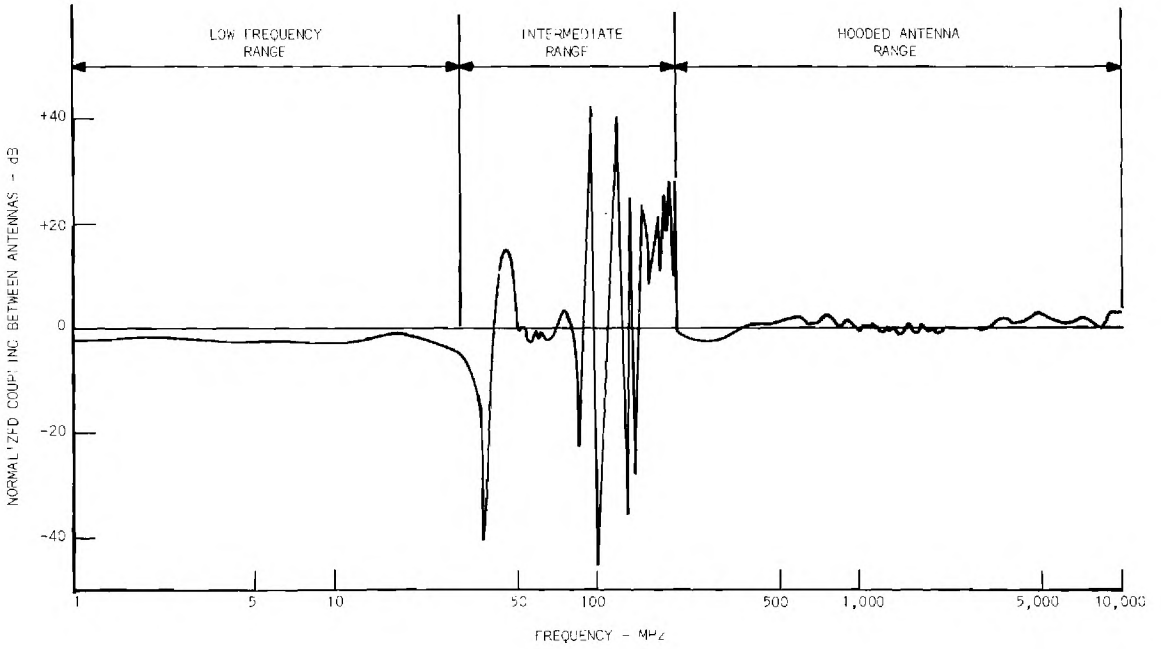

Figure 5. Coupling Between Antennas in a Shielded Enclosure at 1 Meter Separation Over the Frequency Range from 1 MHz to 10 GHz.

to be anticipated in this frequency range, a series of experimental measurements were made on the previous programs. The measurements were made over the frequency range of 1 to 150 MHz, both on and off the axis of a shielded enclosure for different source antenna locations. The test setup used in making these measurements consisted of two "identical" bow-tie antennas, 30 inches long, with a 45 degree flare angle. The off-axis setup differed from the on-axis setup in that both antennas were located two feet off-axis toward a sidewall.

Typical results from these measurements (for 30 MHz and 50 MHz) are shown in Figures 6 and 7. From Figure 6, it is apparent that at 30 MHz the coupling nulls occur well beyond a one-meter separation between the antennas and out to a one-meter spacing there is good correlation between all the coupling curves obtained in the shielded enclosure and the open-field coupling curve. This was true for all test frequencies below 30 MHz. Figure 7 shows that at 50 MHz, the coupling nulls occur within a one-meter spacing from the radiating source and there is no correlation between the various coupling curves obtained in the shielded enclosure and the open-field coupling curve over the spacing range from 12 to 40 inches from the radiating source. This condition was apparent at all test frequencies above 50 MHz. On the basis of the results from these experimental measurements, it was concluded that additional investigation was needed to develop a measurement technique which will make it possible to make reliable, repeatable measurements in shielded enclosures over the frequency range from 20 to 200 MHz.

On the previous programs, no satisfactory explanation was developed for the presence of sharp coupling nulls in shielded enclosures at low frequencies. Several attempts were made to explain these nulls on the basis of simple cancellation and addition of waves reflected from the enclosure walls. However, since the transmission path lengths within the shielded enclosure, both direct and reflected, were small fractions of a wavelength at the lower frequencies, it was not possible to justify the rapid phase shifts necessary to obtain the observed sharp coupling nulls and hence these attempts were unsuccessful.

2. A Near-Field Coupling Hypothesis

In order to assure that the measurement problem was approached in the most direct and efficient manner, it was considered necessary that the mechanism causing the problem be defined and understood. Hence, the attempt to explain the sharp coupling nulls in close proximity to the radiating source was continued.

With the normal multi-path reflections from the walls eliminated as the cause, it was hypothesized that the nulls must be caused by components of the near-fields of the two antennas. The near-fields

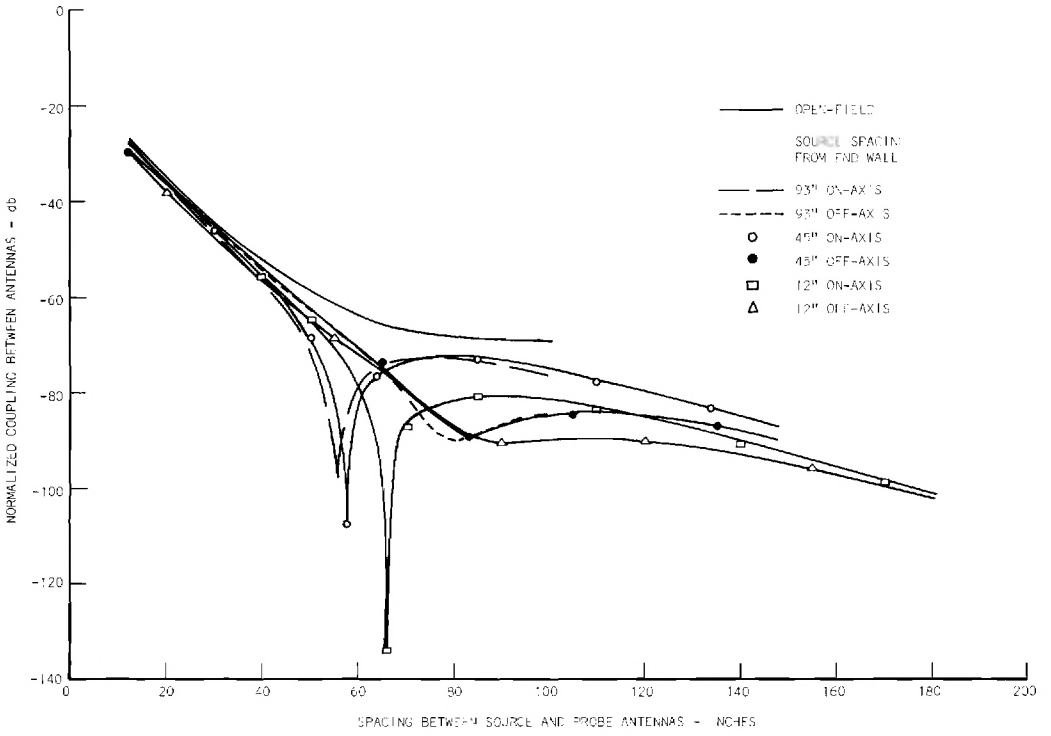

Figure 6. Coupling Between Antennas as a Function of Spacing and Source Location in a Shielded Enclosure at 30 MHz.

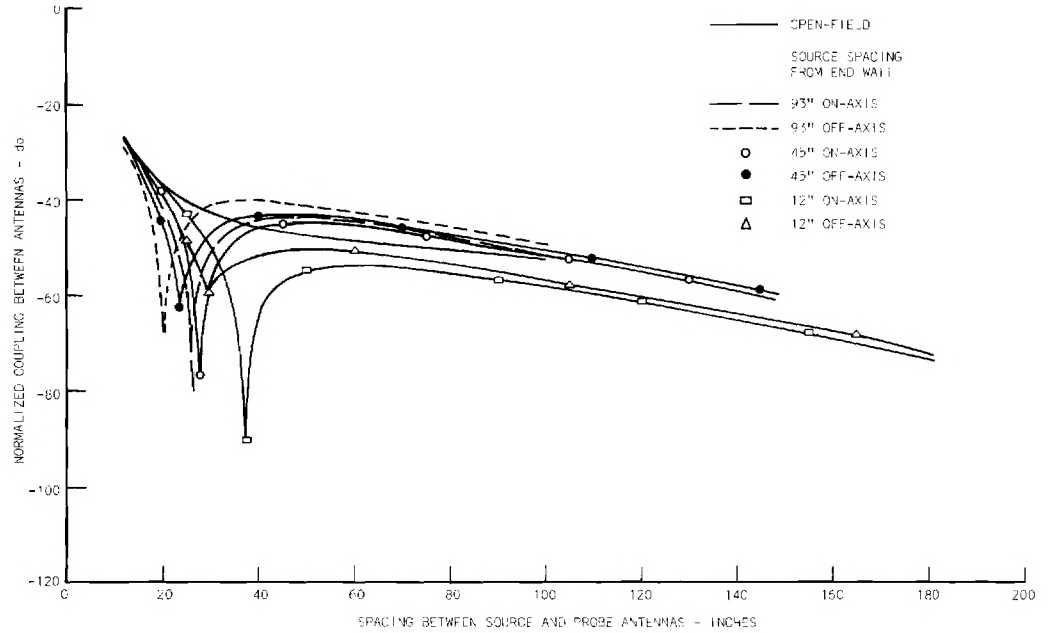

Figure 7. Coupling Between Antennas as a Function of Spacing and Source Location in a Shielded Enclosure at 50 MHz.

from a dipole contain three components E_r, E_θ and H_Φ and are described by Kraus[3] by the expressions:

$$E_\theta = \frac{I_o L \sin\theta\, e^{j\omega(t - \frac{r}{c})}}{4\pi\epsilon} \left[\frac{j\omega}{c^2 r} + \frac{1}{cr^2} + \frac{1}{j\omega r^3}\right] , \qquad (1)$$

$$H_\Phi = \frac{I_o L \sin\theta\, e^{j\omega(t - \frac{r}{c})}}{4\pi} \left[\frac{j\omega}{cr} + \frac{1}{r^2}\right] , \text{ and} \qquad (2)$$

$$E_r = \frac{I_o L \cos\theta\, e^{j\omega(t - \frac{r}{c})}}{2\pi\epsilon} \left[\frac{1}{cr^2} + \frac{1}{j\omega r^3}\right] . \qquad (3)$$

The near-field patterns of these components are shown in Figure 8. From (1) and (2) it is apparent that E_θ and H_Φ are both proportional to $\sin\theta$ and hence the solid pattern in Figure 8 applies to both the E_θ and H_Φ terms. This pattern is independent of Φ, so that the space pattern is doughnut-shaped, and is a figure of revolution of the pattern about the axis of the dipole. For the E_θ and H_Φ components, the near-field patterns are the same as the far-field patterns, being proportional to $\sin\theta$. However, the near-field pattern for E_r is proportional to $\cos\theta$ as indicated by the dashed pattern in Figure 8. The space pattern for E_r is a figure of revolution of this pattern around the dipole axis, and hence, the maximum intensities of the E_r field occur on the axis of the dipole.

A diagram of a two-dipole measurement setup in a shielded enclosure is shown in Figure 9. If it is assumed that there is an appreciable E_r field off the ends of the radiating dipole, it is apparent from the figure that a significant E_r field will be incident on and perpendicular to the enclosure side walls adjacent to the ends of the radiating dipole.[4] In a similar manner, the receiving dipole will exhibit maximum response to these fields and energy can be coupled into the antenna. Thus three coupling paths between the two dipole antennas in a shielded enclosure can be assumed and are depicted in Figure 8 as $P(\Phi)_1$, $P(\Phi)_2$, and $P(\Phi)_3$. $P(\Phi)_1$ represents the direct radiation between the radiating and

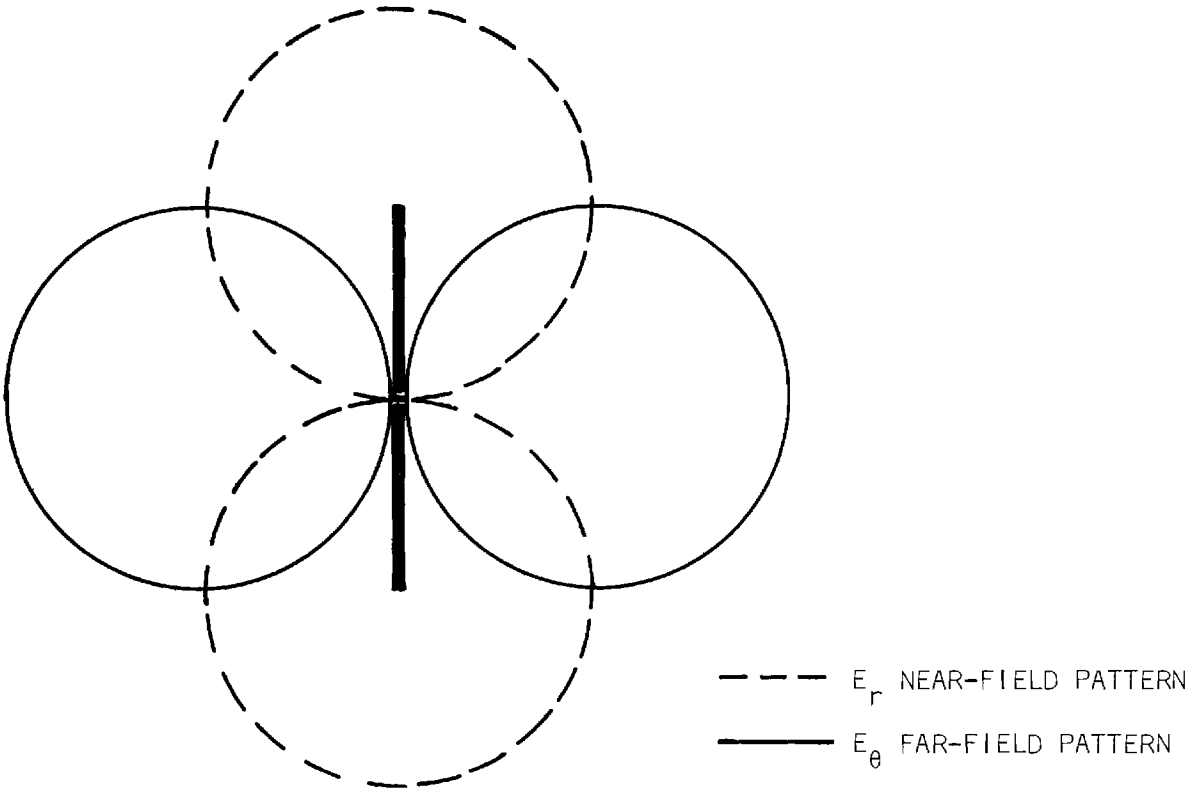

Figure 8. Near-Field and Far-Field Patterns of Short Dipole Antenna.

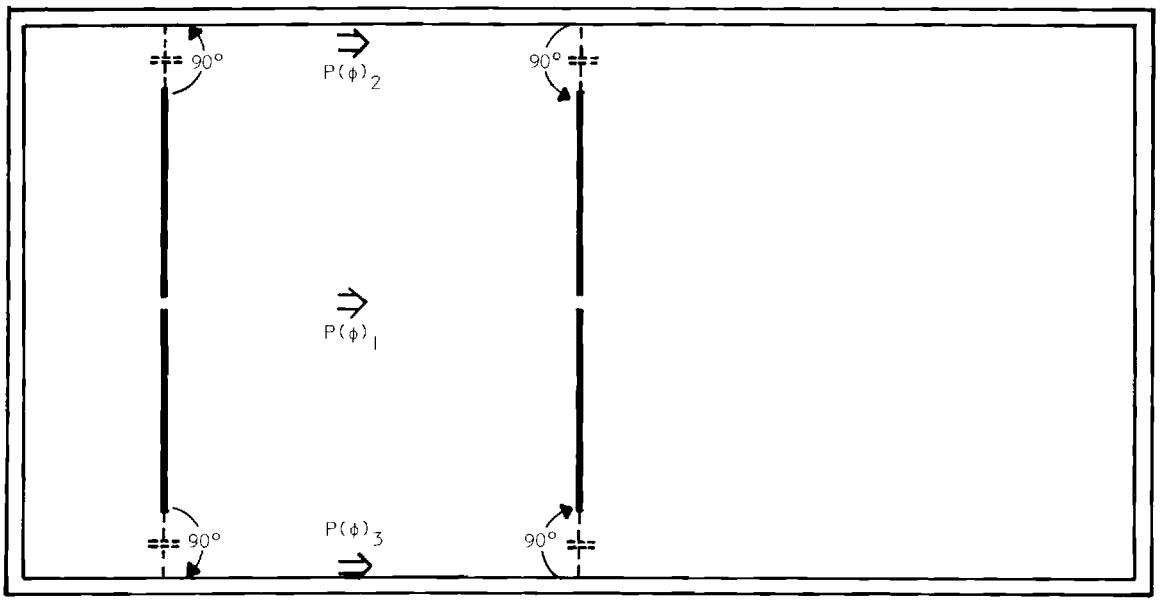

Figure 9. Diagram Showing Three Primary Coupling Paths Between Two Dipole Antennas in a Shielded Enclosure at Low Frequencies.

receiving antennas and $P(\Phi)_2$ and $P(\Phi)_3$ represent the path along the two side walls. If it is assumed that the E_r field experiences a 90 degree phase shift coupling from the radiating antenna to the wall and from the wall to the receiving antenna, and also, that the velocity of propagation along each side wall is equal to the velocity of propagation of the direct radiation so that each phase shift is the same for the three propagation paths, it is apparent from the figure that $P(\Phi)_2$ and $P(\Phi)_3$ arrive at the receiving antenna 180 degrees with respect to $P(\Phi)_1$ independent of the spacing between the two dipoles.

A set of postulated signal levels obtained from the three signal paths are shown in Figure 10. The solid curve depicts the direct coupling between the antennas as a function of spacing between the two dipoles. As shown in the curve, this coupling decreases quite rapidly (approximately 18 dB per octave of distance) at small spacings due to the near-field coupling between the antennas. The dashed curve represents the sum of the two side wall couplings. The side wall coupling can be expected to decrease with range at a lower rate than the near-field direct path coupling, $P(\Phi)_1$. Since the spacings between the ends of the dipoles and the side walls (near-field couplings) do not change as the spacing between the dipoles is varied, the side wall coupling is far less sensitive to dipole spacing than the direct coupling path. The solid-dash curve depicts the summation of all the coupled signals,

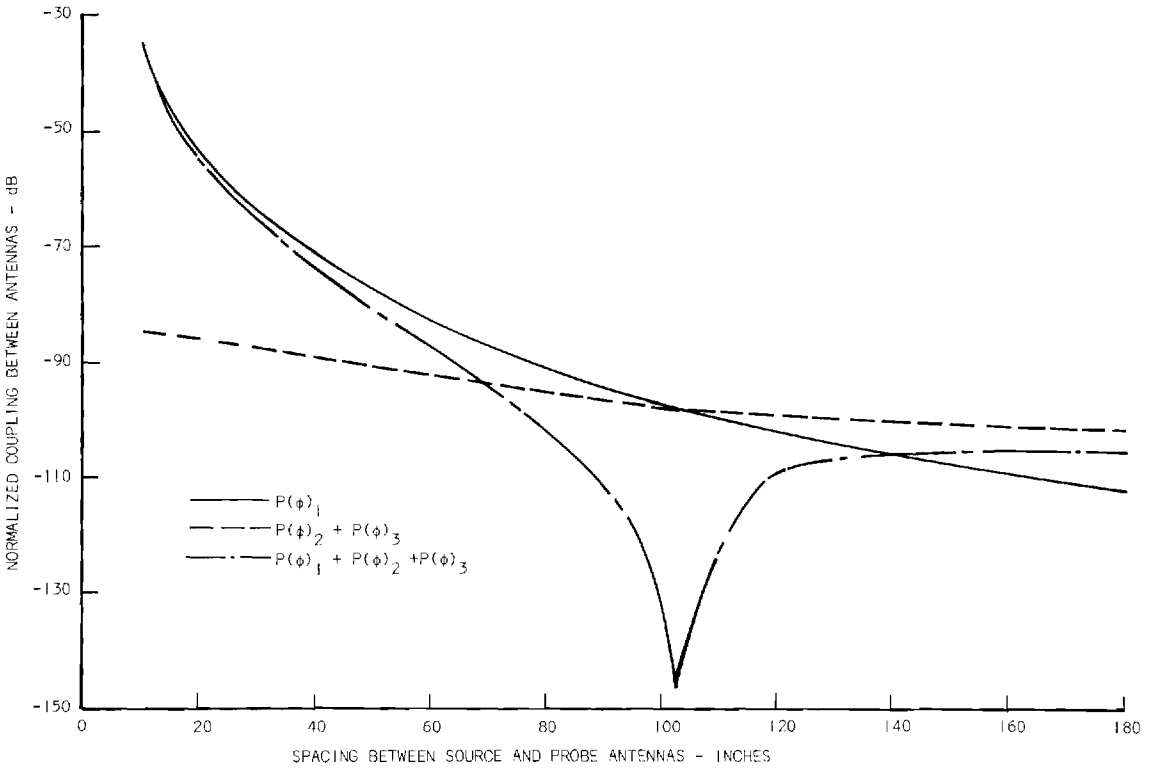

Figure 10. Diagram of Theoretical Coupling Null in a Shielded Enclosure.

noting that $P(\Phi)_2$ and $P(\Phi)_3$ are 180 degrees out of phase with $P(\Phi)_1$. Note that at a spacing of 10 inches, the signal contribution from the side walls is approximately 50 dB below the direct signal and has very little effect on the overall coupling curve. However, as the spacing is increased, the direct coupling rapidly approaches the side wall coupling and the side wall contribution significantly reduces the overall coupling. For the example shown in Figure 10 at a spacing of slightly over 100 inches, the magnitudes of the direct signal and the side wall signal are equal and a null is obtained in the overall coupling. If the side wall signals were exactly 180 degrees with respect to the direct signal, the depth of this null would be infinite. Thus the depth of the null is apparently an indication of the phase relationship between the two signals. Referring to the measured coupling curves in Figures 6 and 7, the depth of the deep null in Figure 6 was established by the limitations of the instrumentation system indicating that the phase relationship between the two signals was very nearly 180 degrees at 30 MHz. The bottom of the deepest null in Figure 7 is approximately 40 dB above the lower limit of the instrumentation system, indicating that the phase relationship between the two signals at 50 MHz is not exactly 180 degrees.

Some preliminary measurements were made in an attempt to validate the E_r side wall coupling theory. The lengths of the dipole antennas were increased and it was found that this caused the coupling nulls to occur at smaller spacings between the antennas. These results support the theory, for increasing the antenna lengths increases the coupling between the ends of the antennas and the side walls, increases the level of the side wall coupling curve, causes the direct and side wall coupling curves to intersect at smaller spacings and hence results in the coupling nulls occurring at smaller spacings between antennas. Reducing the lengths of the dipole antennas caused the coupling nulls to occur at larger spacings. It had previously been observed that increasing the frequency of operation caused the nulls to occur at shorter spacings and decreasing the frequency caused the nulls to occur at greater spacings, which also supports the theory.

The E_r side wall coupling theory not only explains the existence of coupling nulls in shielded enclosures at low frequencies, but it explains other phenomena observed in measured data. For example, the theory explains why good correlation was obtained between open-field and enclosure measurements at a spacing of 12 inches at all frequencies below 100 MHz.

3. Near-Field Coupling Measurements

A series of experimental measurements were performed to determine the relative end-to-end and boresight couplings between two bow-tie

antennas at spacings where the coupling is primarily near-field. The objectives of this study were to further substantiate the side wall coupling theory and to define the spacings between the end of the probe antenna and the enclosure walls necessary to eliminate the side wall coupling. Diagrams depicting the measurement setups used to perform the experimental measurements are shown in Figure 11. The upper diagram shows the setup used for the boresight coupling measurements. Two 30-inch bow-tie antennas with a 45-degree flare angle were operated as horizontal dipoles and they were aligned so that they were at the same height and each was boresighted on the other. The spacing between the antennas was defined as the distance between the two planes containing the two bow-tie antennas. The lower diagram shows the measurement setup used for the end-to-end coupling measurements. The bow-tie antennas were again operated as horizontal dipoles at the same height, but they were aligned so that they were both contained in the same plane. This resulted in the primary coupling between the two antennas being end-to-end. The spacing between the two antennas was defined as the distance between the adjacent antenna ends as shown in the diagram. Photographs of the actual measurement setups are shown in Figure 12. The upper photograph shows the end-to-end coupling setup. One antenna is mounted on a movable cart which runs on a calibrated track. This arrangement makes it possible to conveniently vary the spacing between the antennas from 0 to 100 inches. The equivalent setup for the boresight coupling measurements is shown in the lower photograph.

Utilizing these measurement setups, boresight and end-to-end coupling measurements as a function of spacing between antennas were made on an outdoor range at eight frequencies in the range from 10 to 100 MHz. The results from these measurements are plotted in Figures 13-20. Figure 13 shows the end-to-end and boresight coupling as the spacing between antennas was varied from 0 to 100 inches. It is apparent from the figure that the end-to-end and boresight couplings are equal at a spacing of approximately 60 inches and in the range from 60 to 100 inches the end-to-end coupling exceeds the boresight coupling. Figure 14 shows that at 25 MHz, the couplings are equal at approximately 42 inches and in the range from 50 to 100 inches, the end-to-end coupling is significantly greater than the boresight coupling. At 30 MHz, Figure 15 indicates that the couplings are equal at 35 inches, and again, in the 50 to 100 inch range the end-to-end coupling is significantly greater than the boresight coupling. Figure 16 shows that the coupling curves intersect twice at 40 MHz, at approximately 33 inches and again at approximately 63 inches. In the range from 33 to 63 inches, the two couplings are approximately equal and above and below this range, the boresight coupling exceeds the end-to-end coupling. Figure 17 indicates a similar situation at 50 MHz with the two intersections occurring at approximately 23 and 53 inches. At 62 MHz, Figure 18 indicates that the two coupling curves approach each other in the range from 15 to 30 inches but never intersect and the boresight coupling is always greater than the end-to-end coupling. Figures 19 and 20 indicate that at 70 and 100 MHz the boresight coupling is always greater than the end-to-end coupling and that the coupling curves diverge with increased spacing.

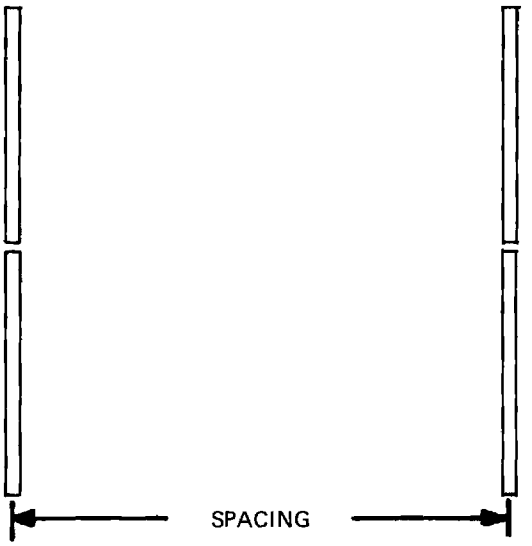

BORESIGHT COUPLING MEASUREMENT SETUP

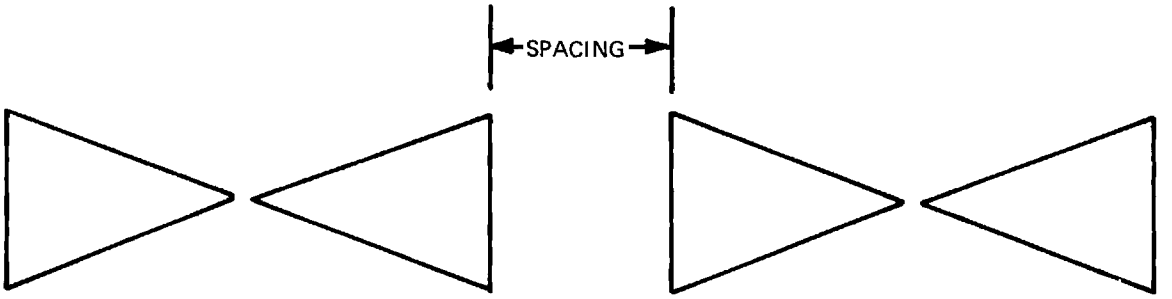

END-TO-END COUPLING MEASUREMENT SETUP

Figure 11. Setups for Coupling Measurements Between Two Bow-Tie Antennas.

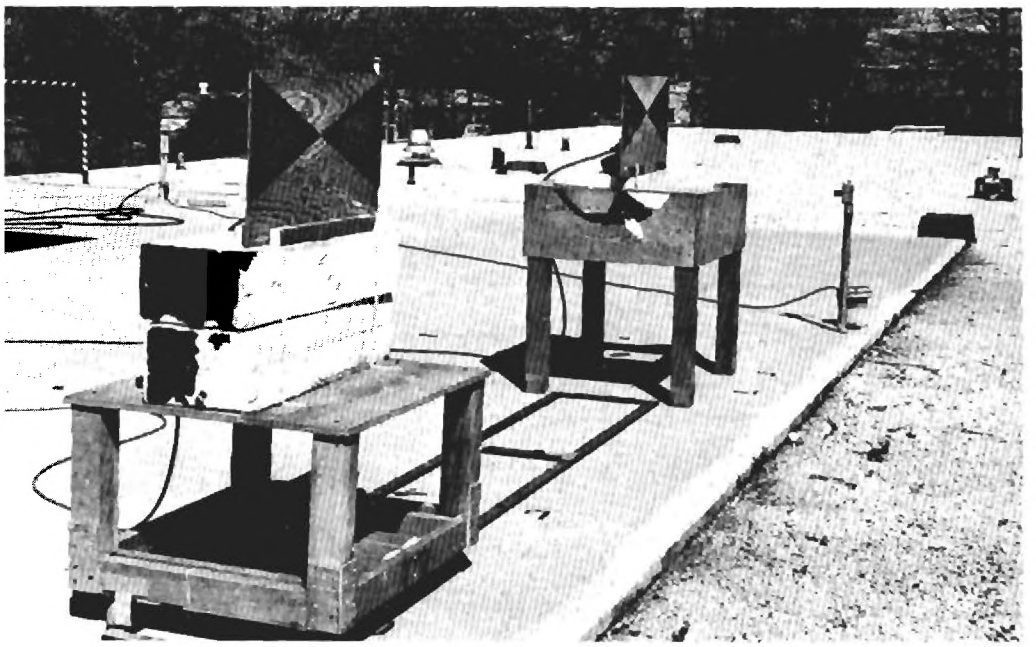

(a)

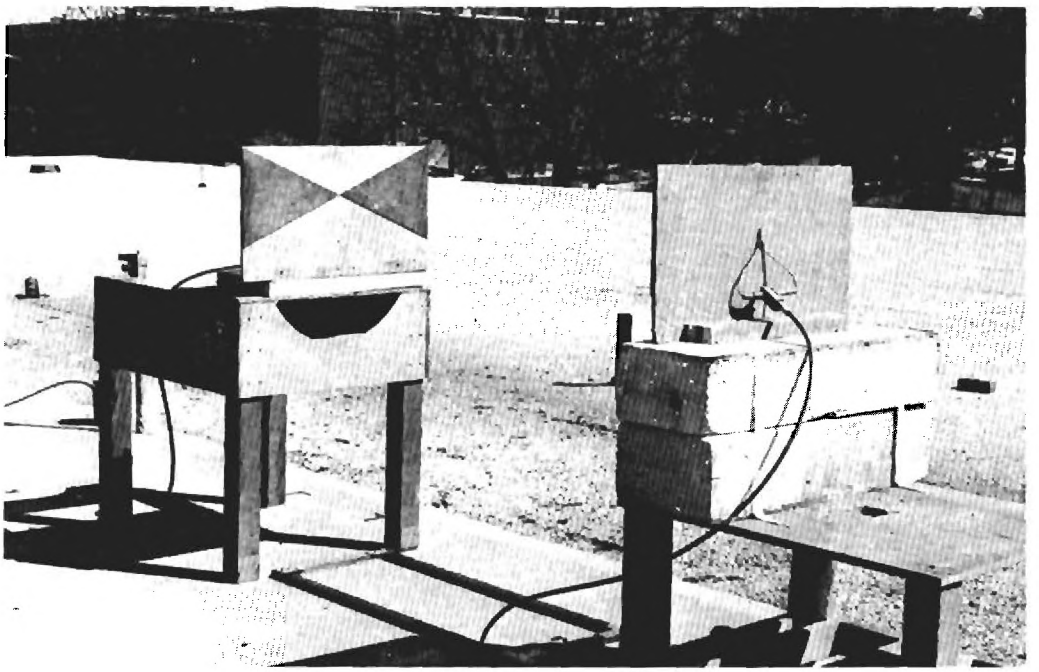

(b)

Figure 12. Two Views of the Coupling Measurement Setups..

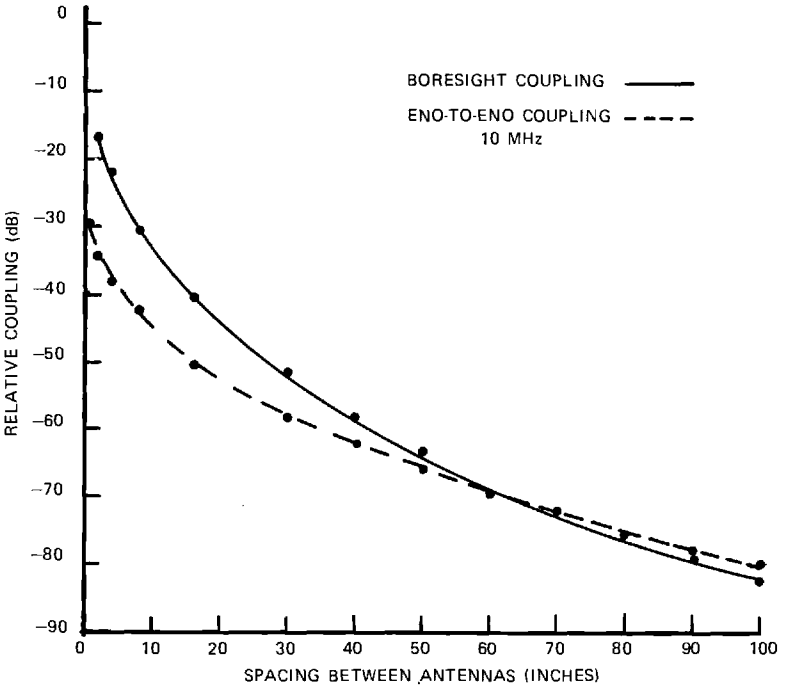

Figure 13. Boresight and End-To-End Coupling Between Two Bow-Tie Antennas as a Function of Spacing at 10 MHz.

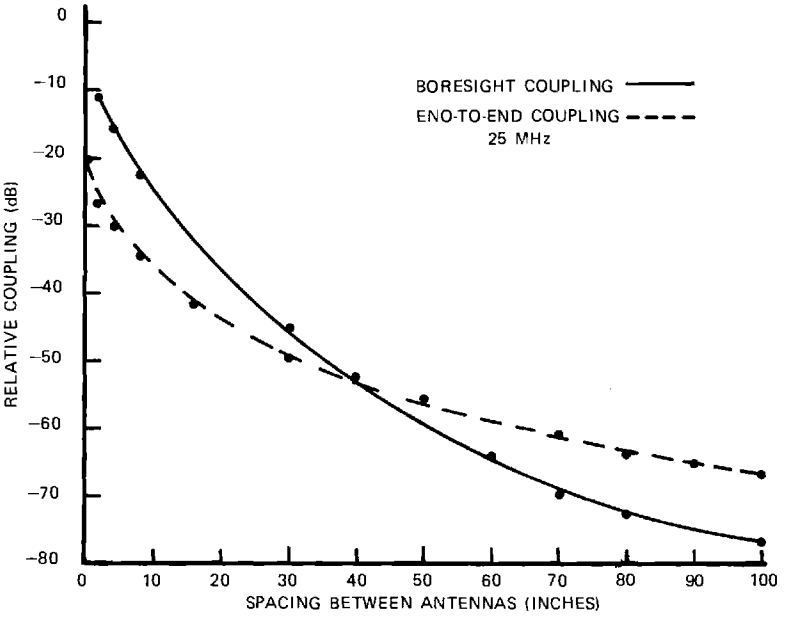

Figure 14. Boresight and End-To-End Coupling Between Two Bow-Tie Antennas as a Function of Spacing at 25 MHz.

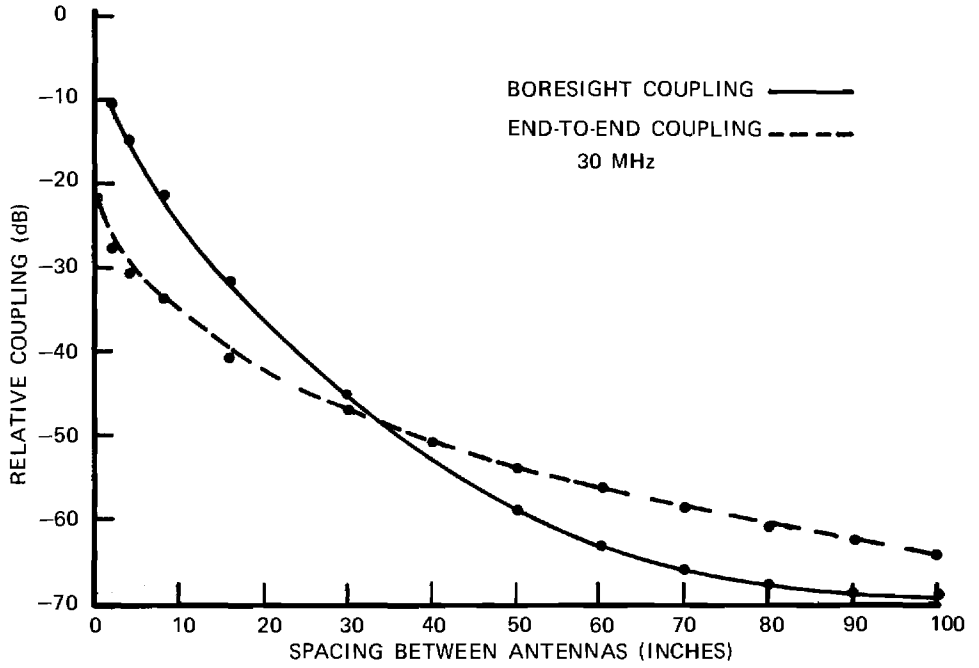

Figure 15. Boresight and End-To-End Coupling Between Two Bow-Tie Antennas as a Function of Spacing at 30 MHz.

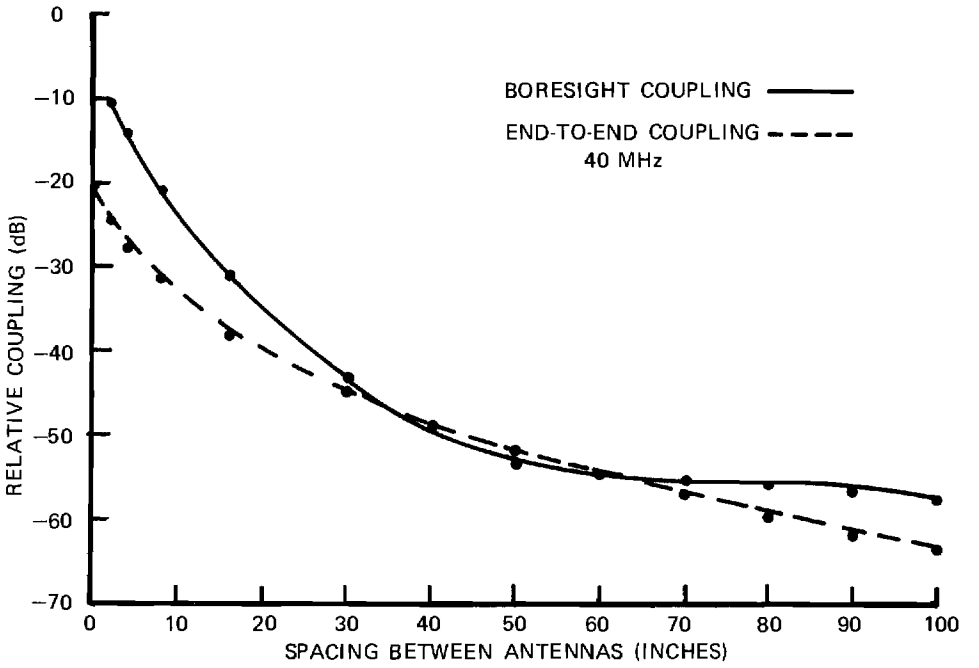

Figure 16. Boresight and End-To-End Coupling Between Two Bow-Tie Antennas as a Function of Spacing at 40 MHz.

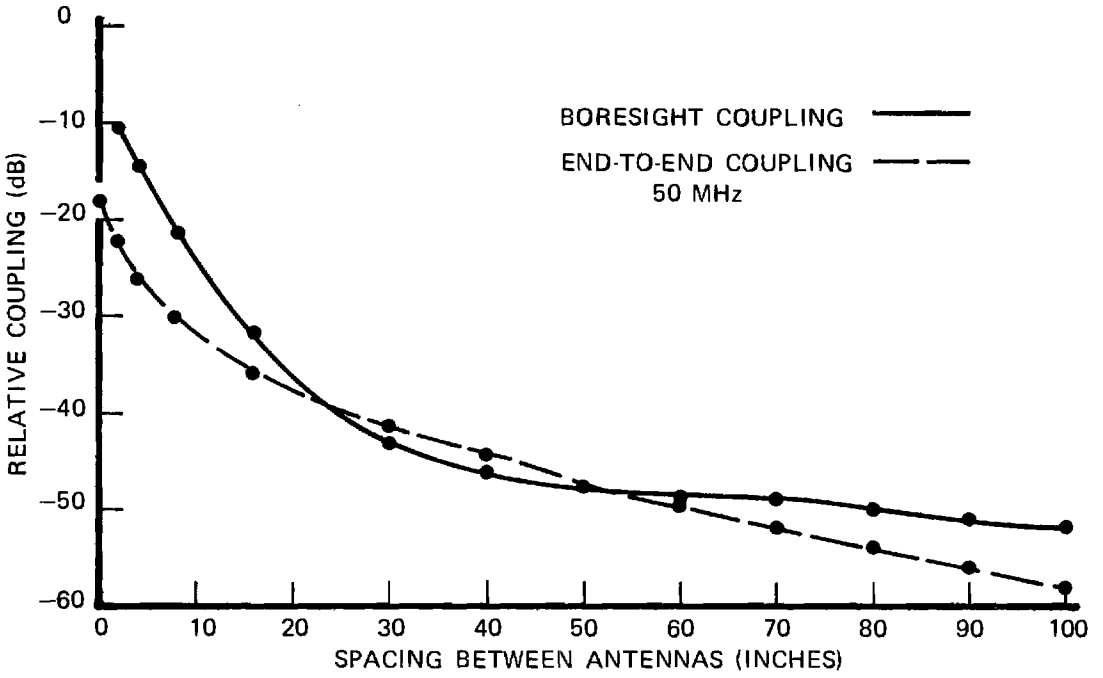

Figure 17. Boresight and End-To-End Coupling Between Two Bow-Tie Antennas as a Function of Spacing at 50 MHz.

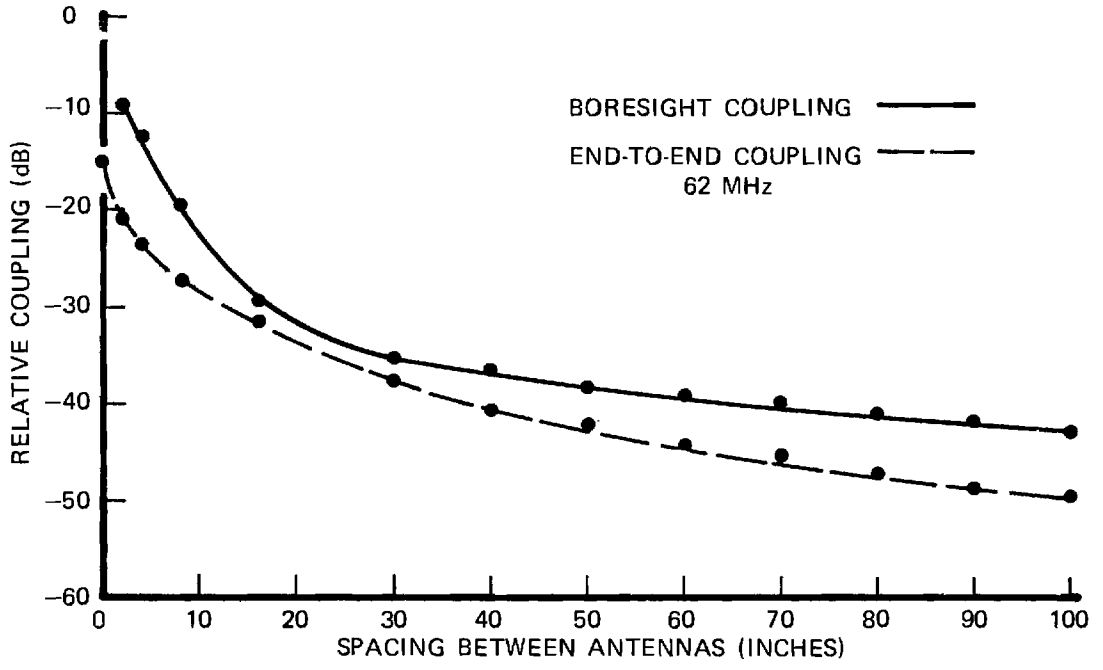

Figure 18. Boresight and End-To-End Coupling Between Two Bow-Tie Antennas as a Function of Spacing at 62 MHz.

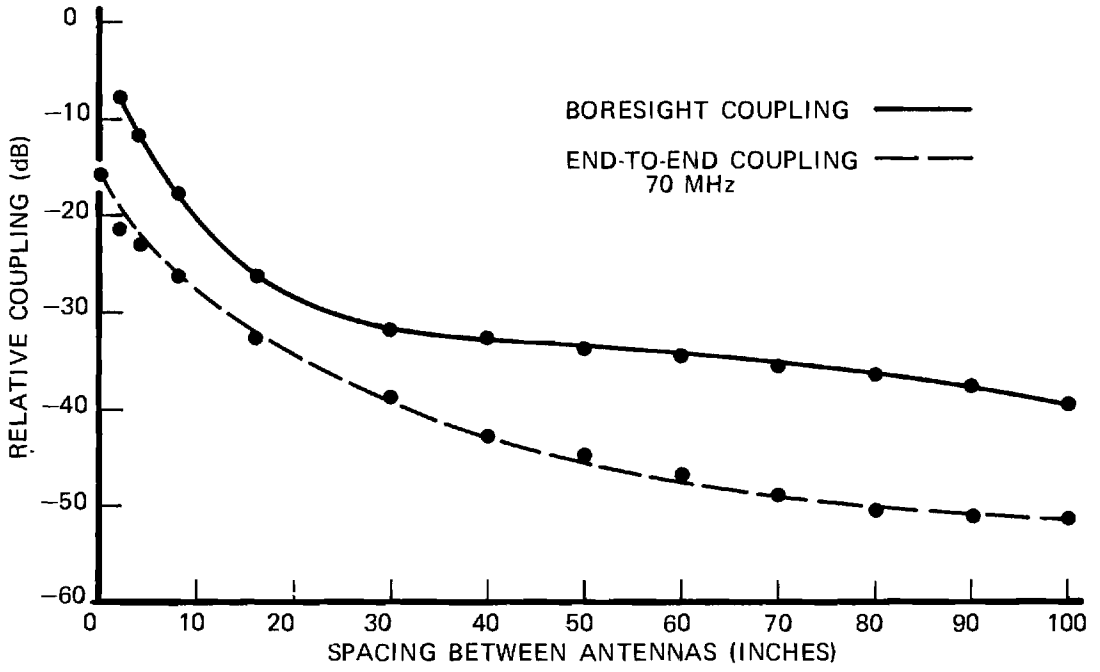

Figure 19. Boresight and End-To-End Coupling Between Two Bow-Tie Antennas as a Function of Spacing at 70 MHz.

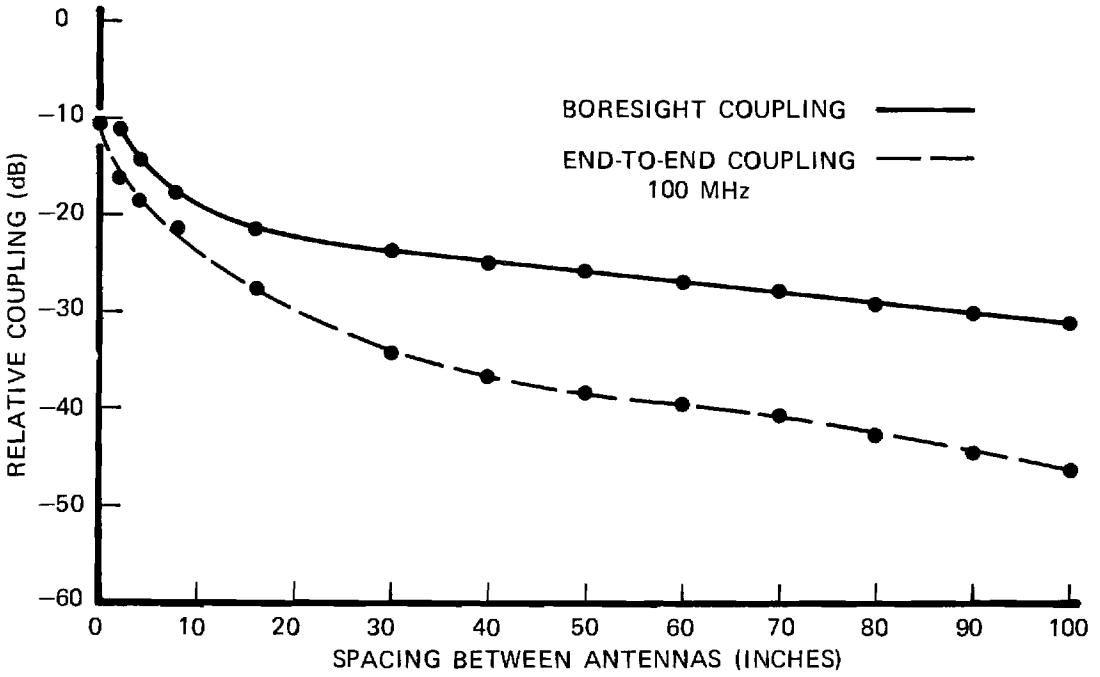

Figure 20. Boresight and End-To-End Coupling Between Two Bow-Tie Antennas as a Function of Spacing at 100 MHz.

On the basis of these measured data it was concluded that it is definitely possible to obtain equivalent boresight and end-to-end couplings between antennas in the near-field. In addition, it is apparent from Figures 13-17 that it is not necessary that the end-to-end spacing be less than the boresight spacing in order to get equivalent couplings. At 25 and 30 MHz, it appears possible to obtain equivalent couplings when the end-to-end spacing is significantly greater than the boresight spacing.

While these data demonstrate the possibility of obtaining coupling nulls in a shielded enclosure in the frequency range from 10 to 100 MHz, it is not possible to predict the location of the nulls as a function of the spacing between the ends of the antennas and the enclosure walls because the measured end-to-end coupling data do not include the effect of the enclosure wall on the coupling.

In order to obtain more realistic antenna coupling data and a measurement of the relative phase of the end coupled and boresight coupled signals, additional measurements were made utilizing the measurement setups depicted in the diagrams shown in Figure 21. The upper diagram shows the measurement setup used to measure the magnitude of the side wall coupling as a function of the spacing of the ends of the antennas from the enclosure wall. The two bow-tie antennas were positioned as shown in the diagram at an outside corner of a shielded enclosure. This arrangement minimized the boresight coupling due to the fact that the antennas were in quadrature with respect to each other and the corner of the enclosure provided shielding between the antennas. On the other hand, the side wall coupling was preserved, since one end of each antenna is in close proximity to a continuous enclosure wall. Each bow-tie antenna was positioned 48 inches above the floor and $12\frac{1}{2}$ inches from the corner of the enclosure. This provides a 25-inch total wall path distance which was considered average for the nulls of interest.

The lower diagram in Figure 21 shows the measurement setup used to measure the phase of the wall coupled signal relative to the boresight coupled signal. This measurement setup was used because it afforded considerably more isolation from the boresight coupling and for the phase measurement, the magnitude of the coupling was of no interest.

Photographs of the actual measurement setups are shown in Figure 22. The upper photograph shows the measurement setup at the corner of an enclosure and the lower photograph shows the phase measurement setup with the antennas on opposite sides of the enclosure.

The two bow-tie antennas were spaced 100 inches apart and boresighted. A signal generator tuned to 50 MHz was connected to one antenna and a Vector Voltmeter was connected to the other antenna.

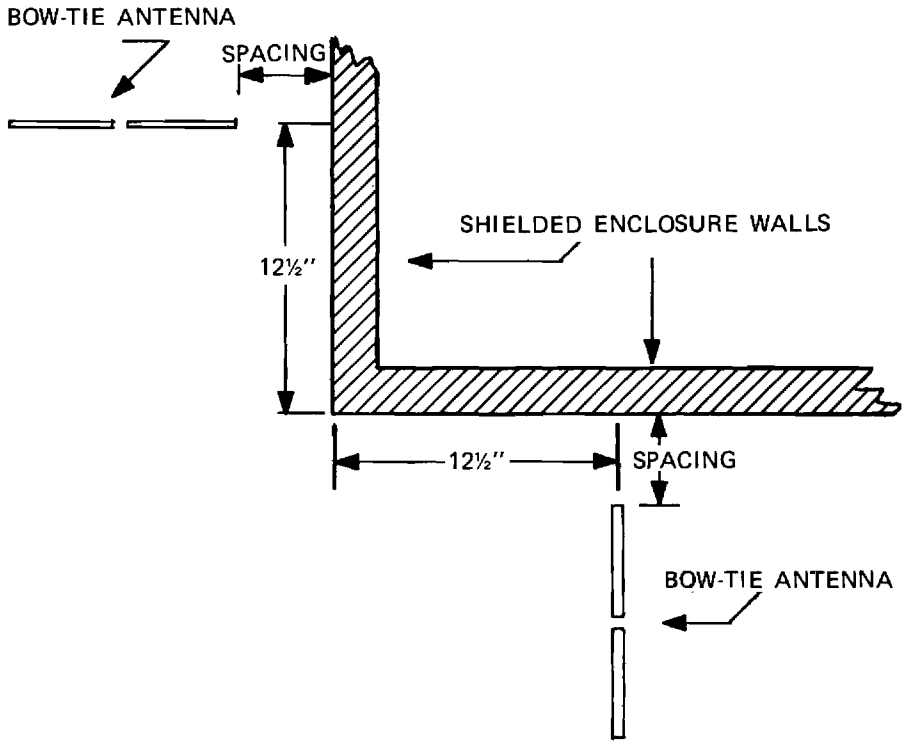

(A) MEASUREMENT SETUP FOR COUPLING MAGNITUDE MEASUREMENTS

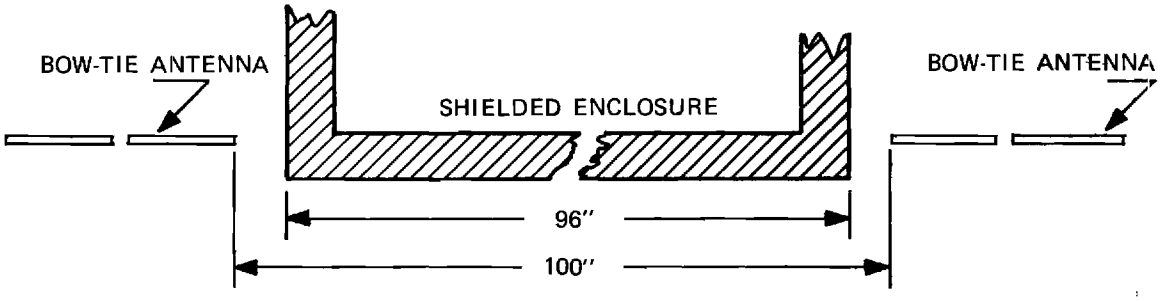

(B) MEASUREMENT SETUP FOR PHASE MEASUREMENTS

Figure 21. Diagrams Showing Setups for Measuring Antenna End-To-Wall Coupling.

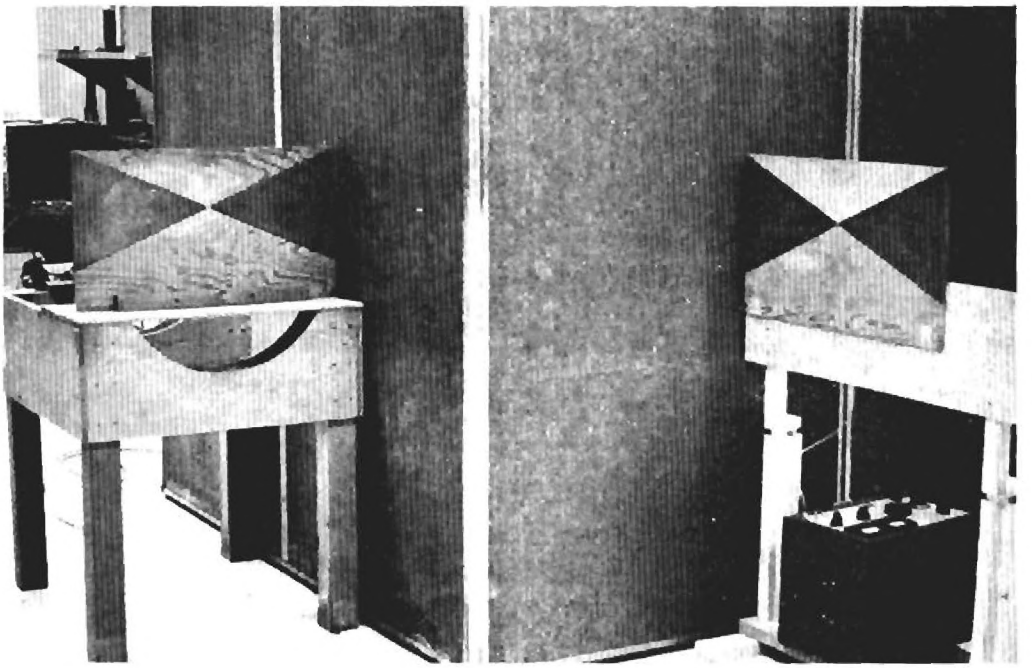

(a)

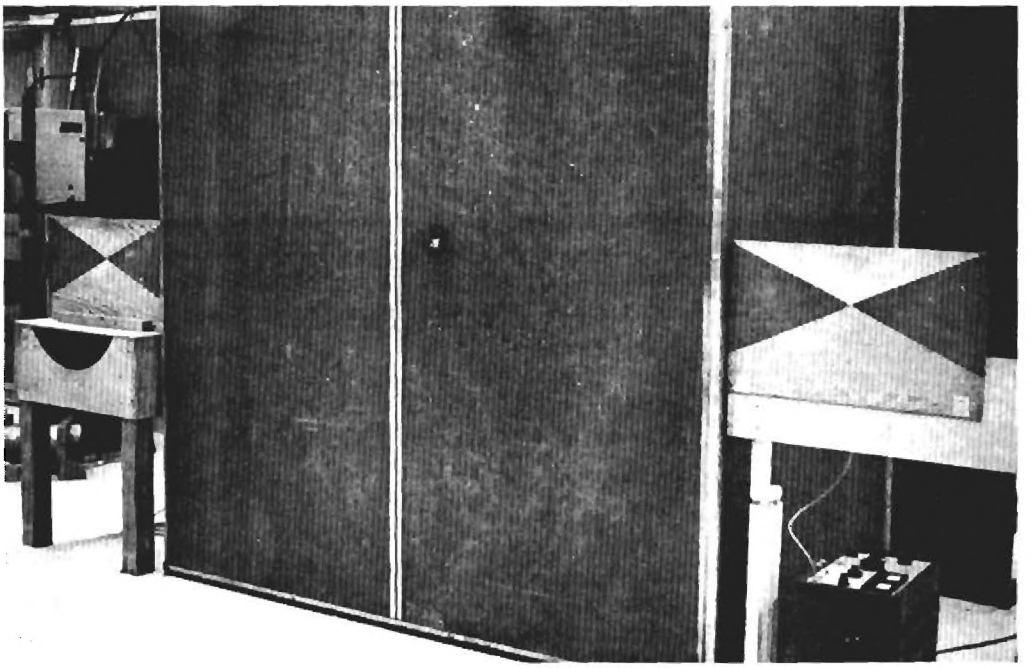

(b)

Figure 22. Two Views of Antenna End-To-Wall Coupling Measurement Setups.

The phase of the received signal was measured on the vector voltmeter. The antennas were then positioned on opposite sides of an enclosure as shown in the lower photograph of Figure 22. The antennas were positioned so that the spacing between the ends of the antennas was 100 inches. The phase of the received signal was again measured with the vector voltmeter. The relative phase of the boresight coupled signal and the wall coupled signal was determined to be 175 degrees. This result supports the assumption in the side wall coupling theory that the two signals are approximately 180 degrees out of phase. This result also supports the discussion in the last section that the relatively shallow null at 50 MHz indicates that the phase relationship between the two signals at 50 MHz is not exactly 180 degrees.

Measurements of the magnitude of the side wall coupling as a function of the spacing of the ends of the antennas from the enclosure wall were performed at 30 and 50 MHz. The two bow-tie antennas were positioned at the outside corner of a shielded enclosure as shown in the upper diagram of Figure 21 and the upper photograph of Figure 22. Measurements were made with the spacing between the ends of the antennas and the enclosure wall at 0.5, 1, 2, 4, 8, 16, 32, and 64 inches. The results of these measurements at 30 MHz are shown plotted in the upper curves of Figure 23. The boresight coupling over the spacing range of 2 to 70 inches is also plotted in this figure. For the boresight curve, the abscissa is the actual spacing between antennas as shown in the top diagram of Figure 11. The side wall coupling measurements described above only measure the coupling along one wall. For a measurement setup inside a shielded enclosure where both ends of the antennas were equally spaced from the walls, it would be expected that the side wall coupling would be increased by a factor of two (or 3 dB). The original coupling curves made in a shielded enclosure which revealed the coupling nulls in the 10 to 100 MHz frequency range were made in an 8 x 8 x 20 foot enclosure with the 30-inch bow-tie antennas. The 8 foot enclosure dimension and the 30-inch antenna length results in the ends of the antennas being approximately 32.5 inches from the enclosure walls for a symmetrical measurement setup in the enclosure. From Figure 23, the end-to-wall-to-end coupling for a spacing of 32.5 inches from the wall is seen to be approximately -64.5 dB. If this value is increased 3 dB to account for the coupling of the opposite wall, and the -61.5 dB coupling value is translated horizontally to intersect the boresight coupling curve (shown by the graphical construction lines on the figure) it is seen that the side wall coupling and boresight coupling are equal at a boresight spacing of approximately 56.5 inches. Hence, on the basis of the measured end-to-wall-to-end coupling data the null in the shielded enclosure would be predicted to occur at a spacing of 56.5 inches at 30 MHz. The actual measured coupling in the shielded enclosure at 30 MHz (shown in Figure 6), shows that the null occurs at 55 inches. The good correlation between the predicted and actual location of the coupling null at 30 MHz is quite encouraging and tends to add confidence to the side wall coupling measurement technique.

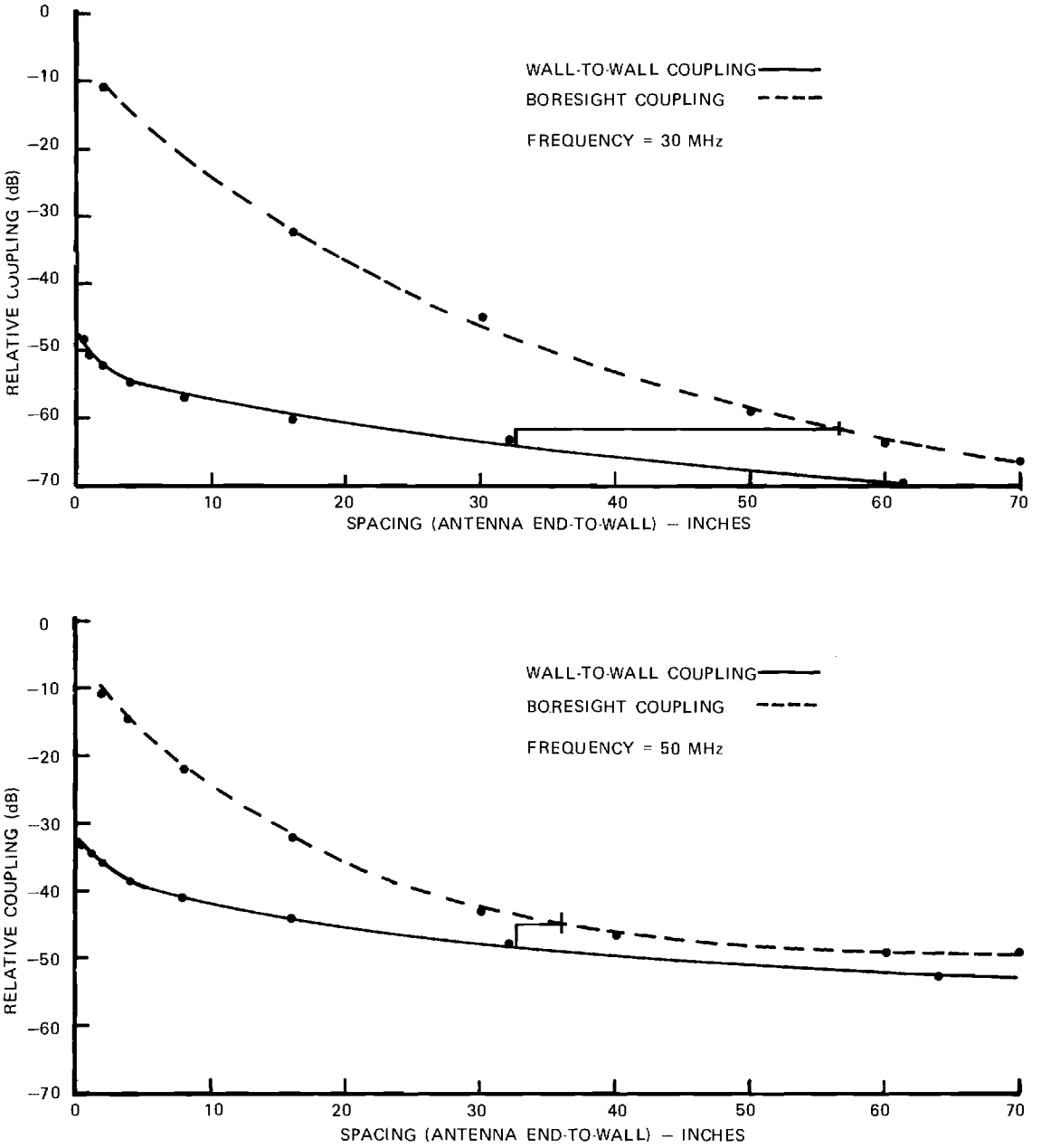

Figure 23. End-To-Wall-To-End Coupling Between Two Bow-Tie Antennas as a Function of Distance From Wall.

The results from the side wall coupling measurements at 50 MHz are shown in the lower curves of Figure 23. The predicted location of the coupling null at 50 MHz is seen to be 36 inches. Figure 7 shows that the measured coupling null occurs at approximately 25 inches. A significant difference between the predicted and actual location of the coupling null is evident; however, examination of the coupling curves shows that the coupling curves are so flat in the region of interest that very small errors in the coupling measurements would result in several inches error in the predicted null location.

4. Model Enclosure Experiments

While the results of preliminary measurements supported the side wall coupling theory, it was felt that further evidence was needed prior to commencing the investigation of antennas with the characteristic of low sensitivity to near-field, electric-field components polarized in the radial direction. An experiment was needed to test the concept that the side walls of the enclosure were both necessary and sufficient for the existance of a null in the coupling characteristics of two horizontal dipoles in an enclosure. The results of such an experiment would be quite valuable in evaluating the validity of the near-field coupling theory and the desirability of pursuing the search for antenna configurations which exhibit a low near-field component polarized in the radial direction.

Since the removal of the side walls of a full-size shielded enclosure was impractical, a model enclosure was designed and fabricated to carry out the desired measurements. The model enclosure was designed to be a 10:1 scale model of an 8 x 8 x 20 foot shielded enclosure. Figures 24(A) and 24(B) show some of the details of the model enclosure. The back wall of the enclosure was made of metal and lined with Emerson and Cumings Eccosorb HPY-12 pyramidal absorbing material. The absorbing material was used to eliminate any reflections from the back wall. The ceiling and side walls were fabricated from a single piece of metal so that the enclosure could be used either conventionally (two side walls, floor, ceiling) or, by inverting the top member, could be used as an enclosure with no side walls.

It was also necessary to fabricate model antennas for use in the model enclosure. Two 10:1 scale models were made of the 30-inch bow-tie antennas normally used for coupling measurements in the full-size shielded enclosure. Broadband balun transformers were wound on ferrite cores for use with the model antennas. These model bow-tie antennas are also shown in Figures 24(A) and 24(B). Sufficient measurements were made on the model antennas to assure that the patterns of Figure 8 were generally representative of those of the model antennas.

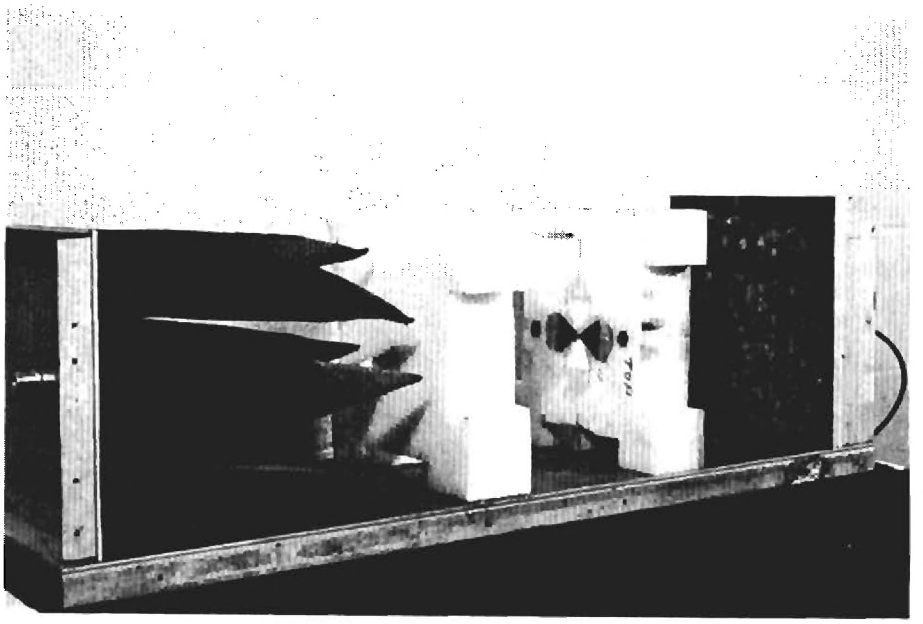

(a)

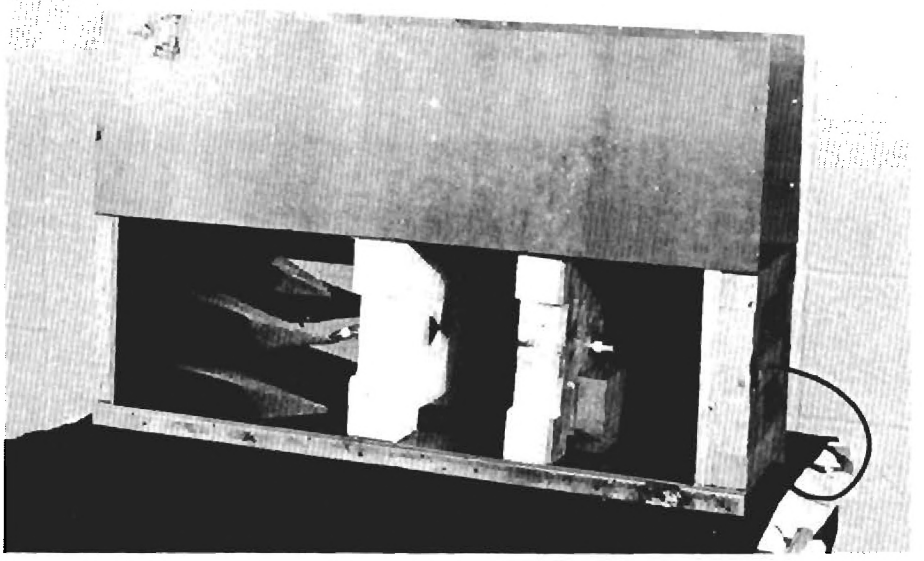

(b)

Figure 24. Two Views of the Model Enclosure.

Coupling measurements were made at 0.1 inch increments at antenna separation distances of 1.0 to 10.0 inches at a frequency of 400 MHz. The 400 MHz frequency was chosen because it was the lowest frequency at which reasonably good absorption could be obtained with the material lining the back wall of the model enclosure. The antenna closest to the absorber lined end wall was placed 9.3 inches from the wall to correspond to the 93-inch source spacing used in the full-size chamber.

Initially the model enclosure was operated with the antennas in the orientation shown in Figure 25(A). It can be seen from this figure, that while the antennas are actually shown vertically polarized, this antenna configuration is equivalent to horizontal dipole antenna operation in an enclosure with side walls only. The near-field coupling theory implies that the presence of the side walls only is sufficient for the existance of a coupling null.

That a coupling null does indeed exist in the presence of only the side walls is shown by the results of the measurements plotted in Figure 26. The null occurs at an antenna separation distance of 4.5 inches, which corresponds to a separation distance of 45 inches in the full-size enclosure. It has previously been established[2] that coupling nulls occur with the 30-inch bow-tie antennas in the full-size enclosure at a separation distance of 40 inches at 37.5 MHz and 23 inches at 50 MHz. Since 400 MHz in the 10:1 model enclosure corresponds to 40 MHz in the full-size enclosure, the null in the model enclosure at 400 MHz would be expected to occur at slightly less than 4.0 inches if the small bow-tie antennas were perfect electrical models of the 30-inch bow-ties.

It is apparent from Figures 8 and 9 and the discussion of the near-field coupling null theory that the antenna separation distance required for equal tangential and radial electric field contributions at the receiving antenna is highly dependent on the relative amplitudes of the E_θ and E_r fields close to the antennas. The latter is a characteristic of the antennas and may be expected to vary somewhat from antenna to antenna of the same design for practical antennas or for frequency scaled antennas.

Having established that only the side walls of the model enclosure are necessary for the existance of a coupling null, it remained to be determined if the elimination of these side walls would eliminate the coupling null. In order to disturb the enclosure setup as little as possible in making this determination, the model bow-ties were rotated 90 degrees and no changes were made in the enclosure. The resulting configuration, shown in Figure 25(B), was equivalent to having two horizontally polarized bow-tie antennas in an enclosure having a conducting floor and ceiling but having no side walls.

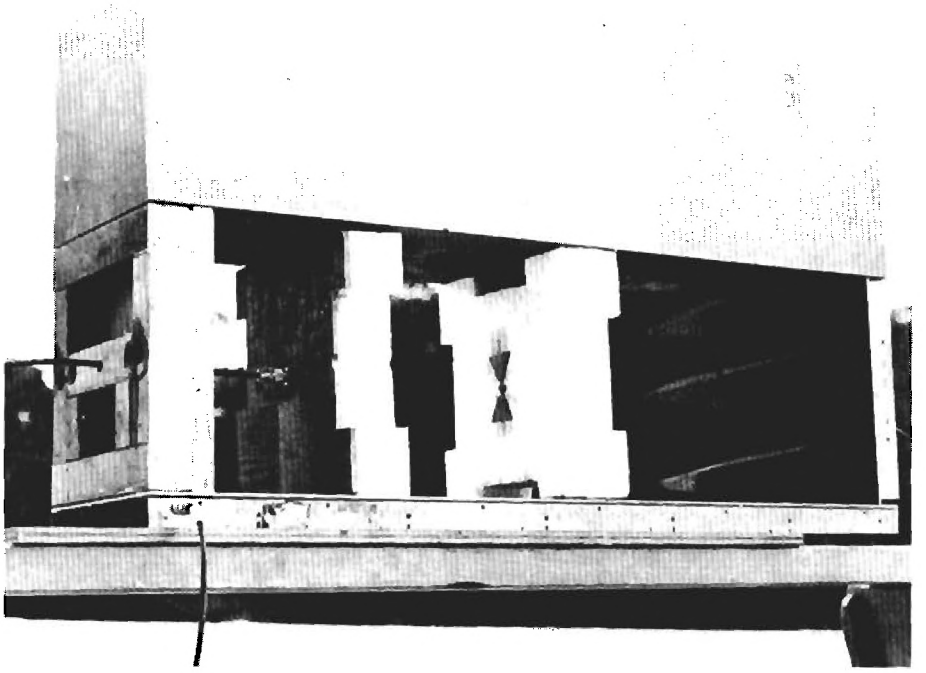

(a)

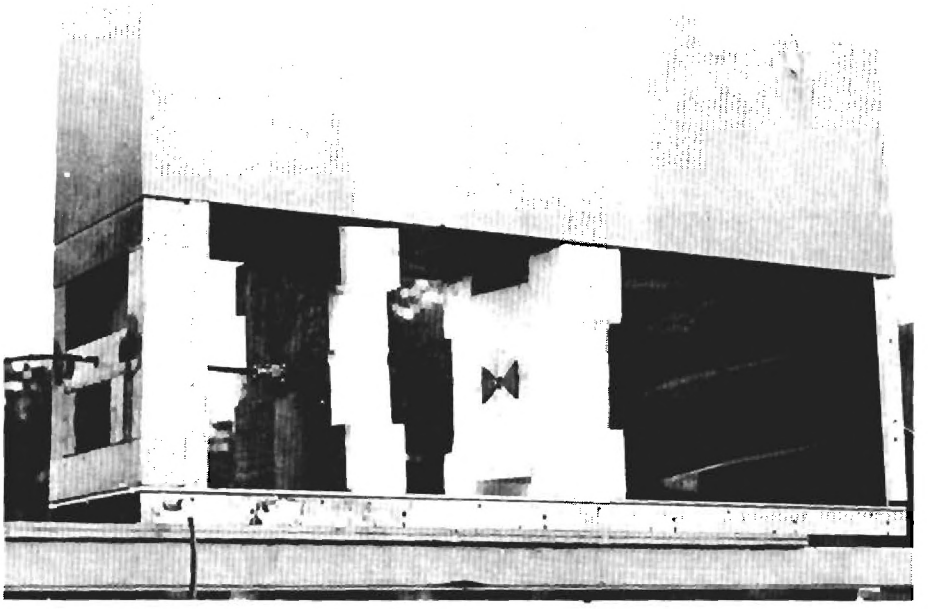

(b)

Figure 25. Views of a Model Enclosure Equivalent to (A) Horizontal Dipoles in an Enclosure With Sidewalls Only and (B) Horizontal Dipoles in an Enclosure With Floor and Ceiling Only.

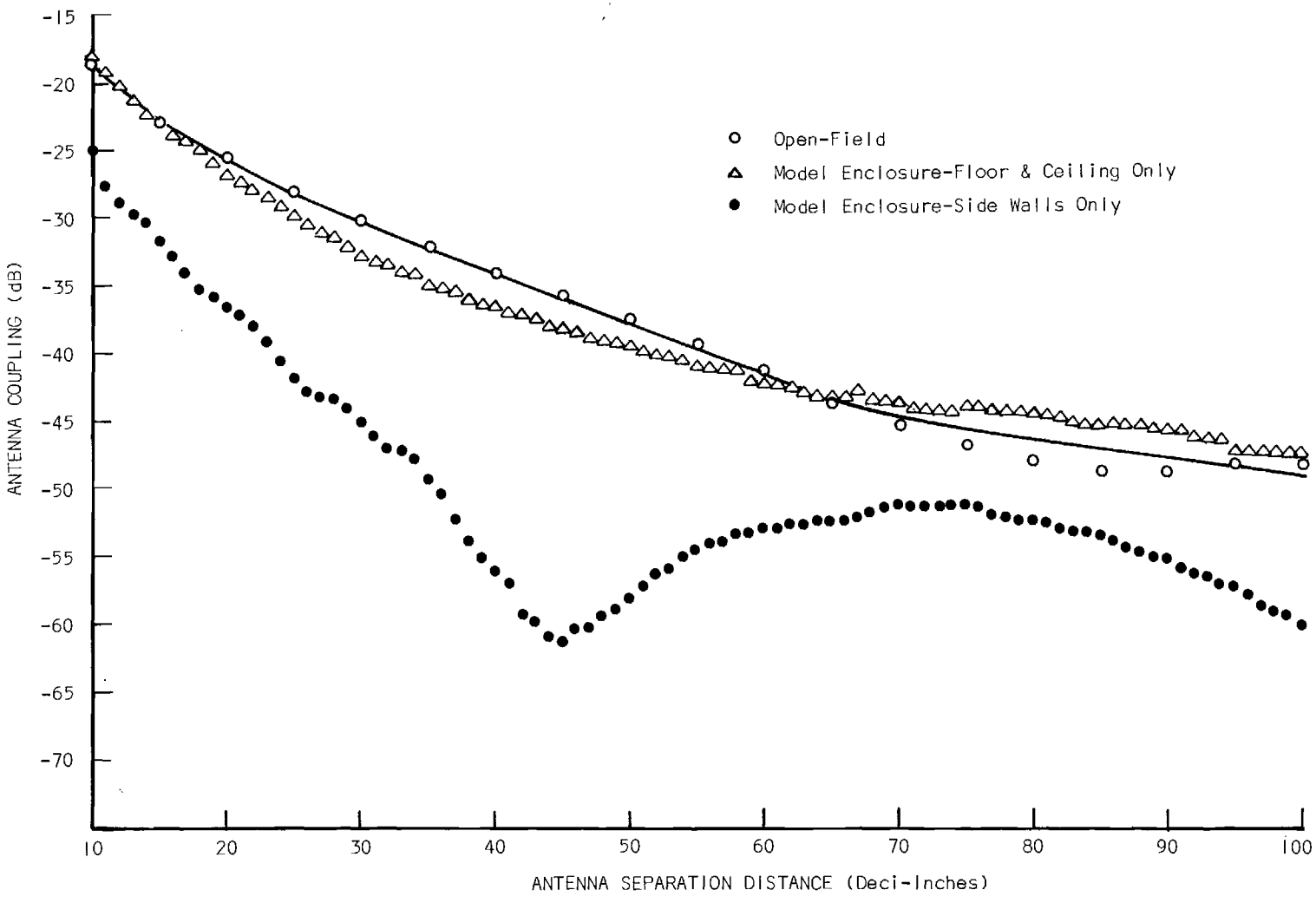

Figure 26. Coupling Between Two Horizontal Bow-Tie Antennas in a Model Enclosure as a Function of Separation at 400 MHz.

Again the non-movable antenna was placed 9.3 inches from the back wall and the coupling measurements were made at 0.1 inch increments at separation distances of from 1.0 to 10.0 inches. The results are shown in Figure 26. As shown in this figure, the removal of the side walls resulted in the complete elimination of the coupling null.

The open-field coupling at 400 MHz between the two model bow-tie antennas was determined using the experimental configuration depicted in Figure 27. Measurements were made at 0.5 inch increments at antenna spacings of from 1.0 to 10.0 inches. The resulting open-field coupling curve is also shown in Figure 26. Since, in the open-field, no path is available by which the radial field component may be coupled between the antennas, it is proper to view this coupling curve as the coupling curve of the tangential electric field component only.

The model chamber coupling curve made with the floor and ceiling, but without the side walls, agrees quite well with the open-field coupling between the two antennas. It should be recognized that the tangential electric field component was equally incident upon both the conducting floor and ceiling of the model enclosure as well as the receiving antenna. The fact that no evidence of multipath interference can be seen in the coupling measurements agrees with the concept that the coupling nulls observed at low frequencies are not due to multipath reflections from the enclosure walls. This is quite important

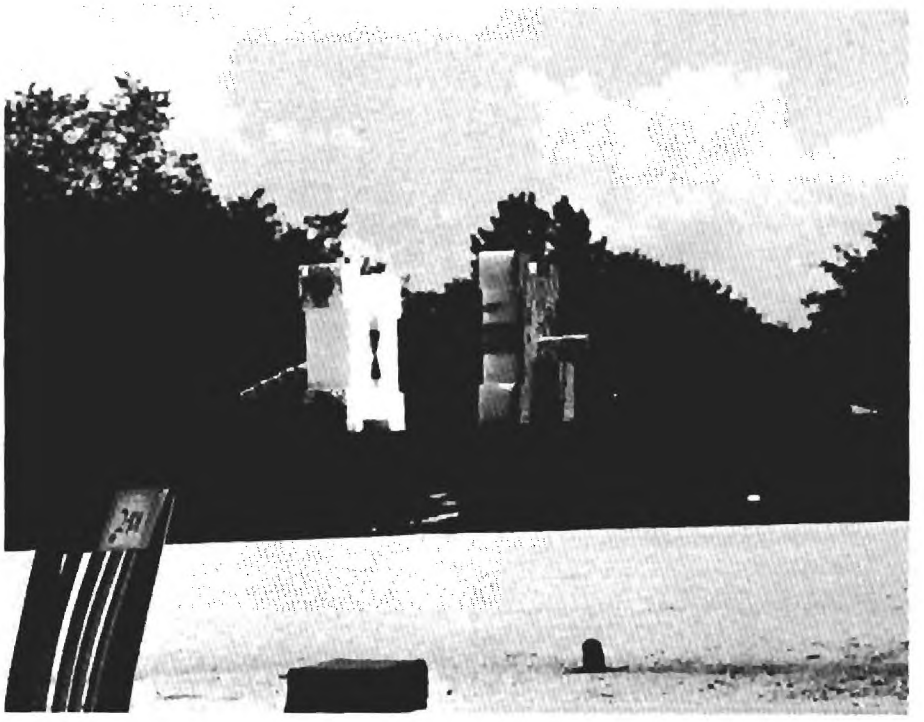

Figure 27. The Open-Field Coupling Measurement Configuration.

to the design of probe antennas at low frequencies because it relaxes the restriction that the beamwidth of the tangential field components be made quite narrow, as is necessary with the higher frequency probe antennas.

All available evidence supports the near-field coupling theory; it appears that with a horizontal dipole or bow-tie probe antenna in a shielded enclosure, the presence of the side walls is a necessary and sufficient condition to cause coupling of the near-field radially polarized field components and hence to cause a coupling null. The exact spacing at which the null will occur in the enclosure is dependent on, among other things, the relative magnitudes of the radially and tangentially polarized electric field components set up by the source, and hence is unpredictable.

5. Low-Frequency Hooded Antenna

One possible antenna configuration having the desired characteristic of minimum response to radially polarized fields incorporates an antenna hood. This is most easily seen by reference to Figure 28. Figure 28(A) pictorially illustrates the response of a dipole probe antenna to the radially polarized field component, E_r, in a shielded enclosure. The E_r field is incident on the enclosure side walls adjacent to the ends of the radiating dipole. Since E_r is orthogonal to the side walls, this field can be coupled via the surface of the walls. As the E_r field is coupled by the side walls adjacent to the ends of the probe dipole, the probe will exhibit maximum response to this field and a portion of the energy will be coupled into the probe antenna. The tangentially polarized electric field, E_θ is propagated as direct radiation from the radiating to the receiving dipole as shown.

Prior to recognition of the near-field coupling theory as the cause of the coupling nulls at low frequencies, the use of conventional hooded antennas at frequencies below 100 MHz was ruled out because of two major considerations. First, to satisfy the aperture-to-wavelength requirements to obtain the directivity necessary to prevent multipath influences on measured field strengths, a low frequency conventional hood would be too large to be accommodated in shielded enclosures. Fortunately, all available data as well as calculations indicate that the dimensions of the enclosure are not large enough to permit any significant multipath interference at low frequencies. Hence, there is apparently little need for obtaining tangentially polarized field directivity with a hood. The other major objection to the use of hoods at low frequencies was that no suitable absorbing material is available with which to line the inside of the hood.

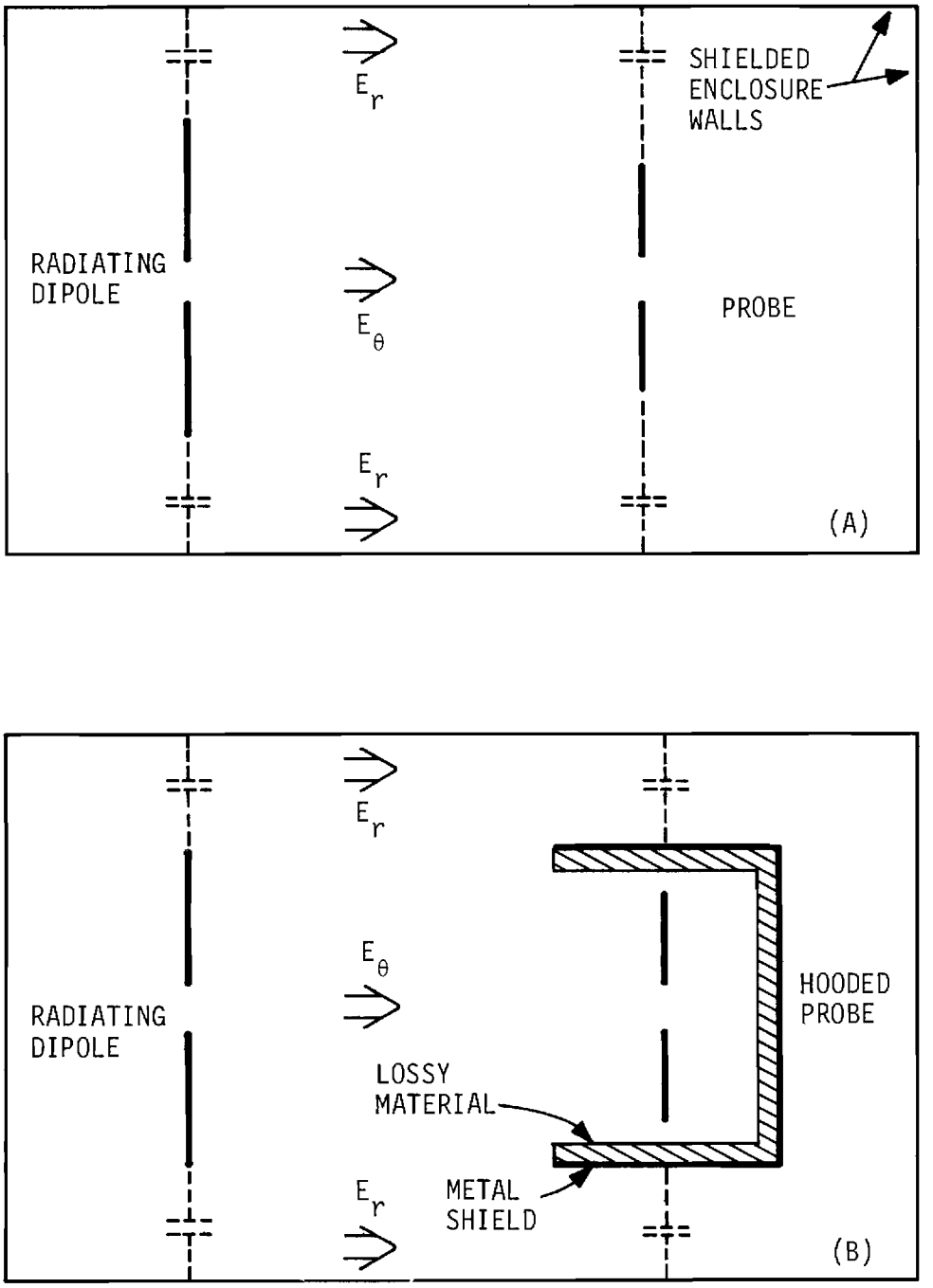

Figure 28. Illustration of the Use of an Antenna Hood to Minimize Probe Response to Radially Polarized Fields.

Since the problem at low frequencies is the wall-coupled, radial field effect and not conventional multipath, it was considered possible to line the inside of a low frequency hood with lossy material and, through the use of an effective balun, isolate the probe antenna from the near-field side wall coupled components as indicated in Figure 28(B).

It should be emphasized that there are distinct conceptual differences between the conventional hooded antennas employed at high frequencies and the low frequency hood depicted in Figure 28(B). In the conventional high frequency hooded antenna, the hood is used to achieve antenna directivity with respect to the tangentially polarized electric field component, E_θ. This increased directivity is utilized to minimize the effects of multipath interference (stray radiation) inside a shielded enclosure by allowing probe illumination of the radiating source while simultaneously minimizing side wall, back wall, floor and ceiling illumination. The inside of a conventional high frequency hood is lined with RF absorbing material and the probe antenna is isolated by a balun from the outside metal shield. In the open-field or free-space environment, measurements made at a given frequency with the probe antenna unhooded differ from measurements made with the same probe hooded by a constant factor at all far-field measurement ranges of interest. This constant factor is the insertion loss (or gain) associated with the hood. After correcting for this insertion loss, the hooded and unhooded measurements are identical at each measurement range of interest.

The concept of the low frequency hood shown in Figure 28(B) is completely different from that of the conventional high frequency hood. In the low frequency hood no increased directivity with respect to the tangentially polarized electric field component, E_θ, is sought or achieved. Rather, the low frequency hood is used solely to isolate the antenna from the radially polarized electric field component, E_r, coupled along the side walls. Although the probe antenna is isolated from the outside metal shield of the hood by a balun as is the case with conventional high frequency hoods, the inside of the metal shield is lined with a lossy material (for isolation from the inside of the metal shield) rather than an absorber. This can be done since the dimensions involved preclude significant effects from multipath reflections inside the hood itself.

The most important conceptual difference between the conventional high frequency hooded antenna and the low frequency hooded antenna is that the latter is intended for use at ranges of from a few wavelengths down to a fraction of a wavelength from the radiating source. Thus, when the low frequency probe antenna is hooded, not only is a far-field insertion loss factor present in the measured results, but the mutual coupling between the source and the probe is appreciably altered by the presence of the hood. Therefore, at longer wavelengths, it is

no longer possible to correct hooded probe measurements to agree with unhooded probe measurements by a range-independent far-field insertion loss factor. It is indeed difficult and more than a little misleading to describe the low frequency probe as either hooded or unhooded in the conventional sense in which this concept is used to describe probes intended for use at higher frequencies. The hooded low-frequency probe operating very close (in terms of wavelength) to a radiating source should and, as is shown in the measurement results section of this report, does exhibit electrical characteristics quite different from those of the same probe unhooded. Instead of being described as hooded and unhooded, it may be clearer to view the two antenna configurations as two distinctly different antennas, just as differentiation is made between dipoles and horn antennas. However, in order to be consistant with previous reports, the low frequency probe antenna will be referred to herein as either hooded or unhooded.

6. Low-Frequency Hooded Antenna Experiments

In order to experimentally test the concept that an antenna hood could be used successfully in shielded enclosures at frequencies below 100 MHz to isolate a probe antenna from the near-field radially polarized components coupled along the side walls, a probe antenna and antenna hood were fabricated. An 18-inch bow-tie antenna with a 38-degree flare angle was built to serve as a probe antenna. An Anzac Model H-1 hybrid junction was used as the probe antenna feed and balun. The hood was constructed from an aluminum cylinder two feet in diameter and four feet long; the wall thickness was 1/8 inch. The hood end plate (back wall) was made from ½ inch sheet aluminum. The cylinder and end plate were lined with Emerson and Cuming NZ-1 ferrite material. While it is documented[5] that this material is a very poor absorber at frequencies appreciably below 300 MHz, it has been found to be an adequate lossy material in the frequency range of interest. Figure 29 shows a view of the bow-tie probe antenna inside the antenna hood.

Antenna coupling measurements were made in an 8 x 8 x 20 foot shielded enclosure. A 30-inch bow-tie antenna was used as the source antenna for all of the coupling measurements. Initially, antenna coupling as a function of separation distance was determined between the source antenna and the unhooded 18-inch bow-tie probe antenna. The source antenna was centered in the shielded enclosure 93 inches from the end wall to correspond with previous experiments in the 20 foot chamber. Coupling measurements were made at frequencies of 50, 40 and 30 MHz. The measurements were made at 2-inch spacing increments at antenna separation distances of from 10 inches to 100 inches. The results of these measurements are shown in Figures 30, 31, and 32.

The coupling data for the unhooded probe antenna clearly show the typical low frequency coupling nulls resulting from the out-of-phase summation of the tangentially and radially polarized field components. Consistant with previously reported coupling measurements in shielded enclosures, at low frequencies, the null occurs further from the source as the frequency is decreased.

To verify that the probe antenna could be isolated from the radially polarized near-field component propagated along the enclosure wall by the use of an antenna hood, the experiment described above was repeated with the 18-inch bow-tie probe antenna hooded as shown in Figure 29. Again the coupling measurements were made at 2-inch spacing increments at each of the three test frequencies. Measurements were made with the probe antenna located at hood depths of 3, 9 and 18 inches. It was found that the 3-inch hood depth did not provide sufficient probe antenna isolation to completely eliminate the coupling nulls. No significant differences were observed between the data recorded at a 9-inch hood depth and that recorded at an 18-inch hood depth.

The results of the coupling measurements made in the shielded enclosure with the probe antenna hooded for a 9-inch hood depth are shown in Figures 30, 31 and 32. As shown in these curves, sufficient isolation

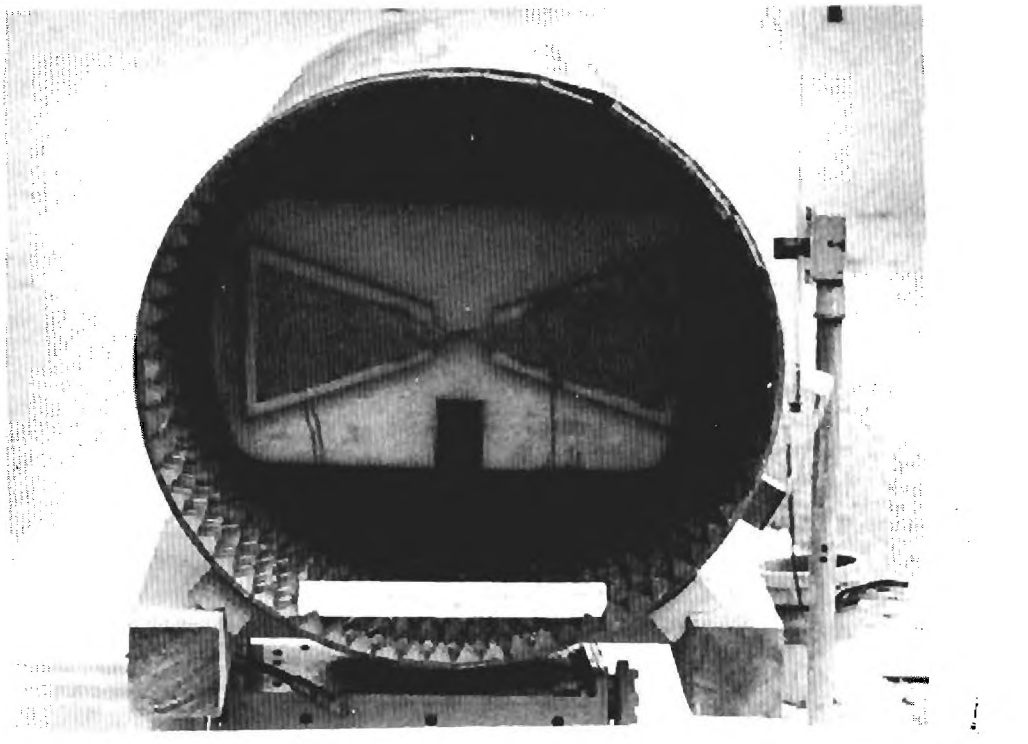

Figure 29. View of the Hooded 18-Inch Bow-Tie Probe Antenna.

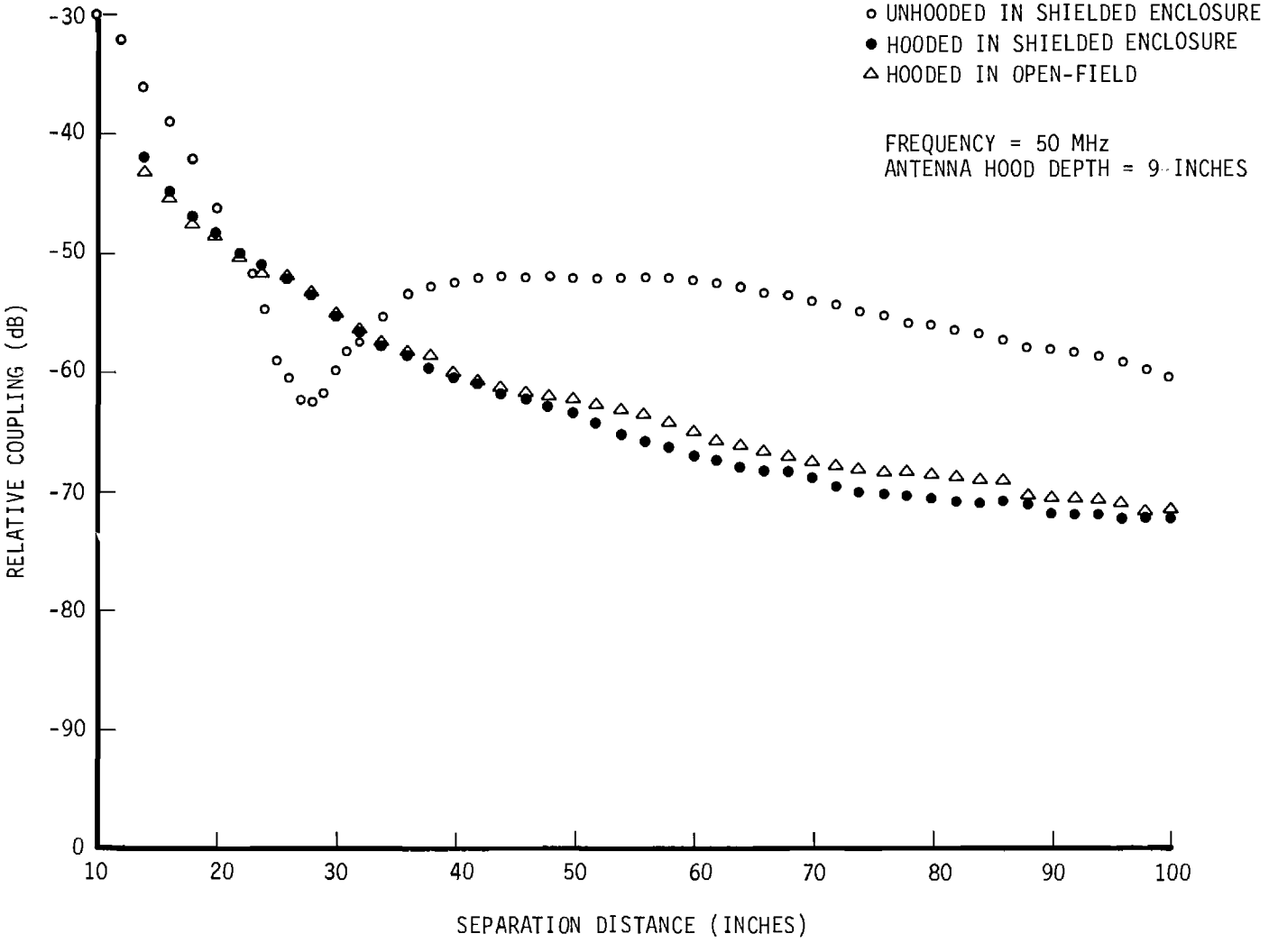

Figure 30. Relative Coupling as a Function of Antenna Separation Distance at a Frequency of 50 MHz.

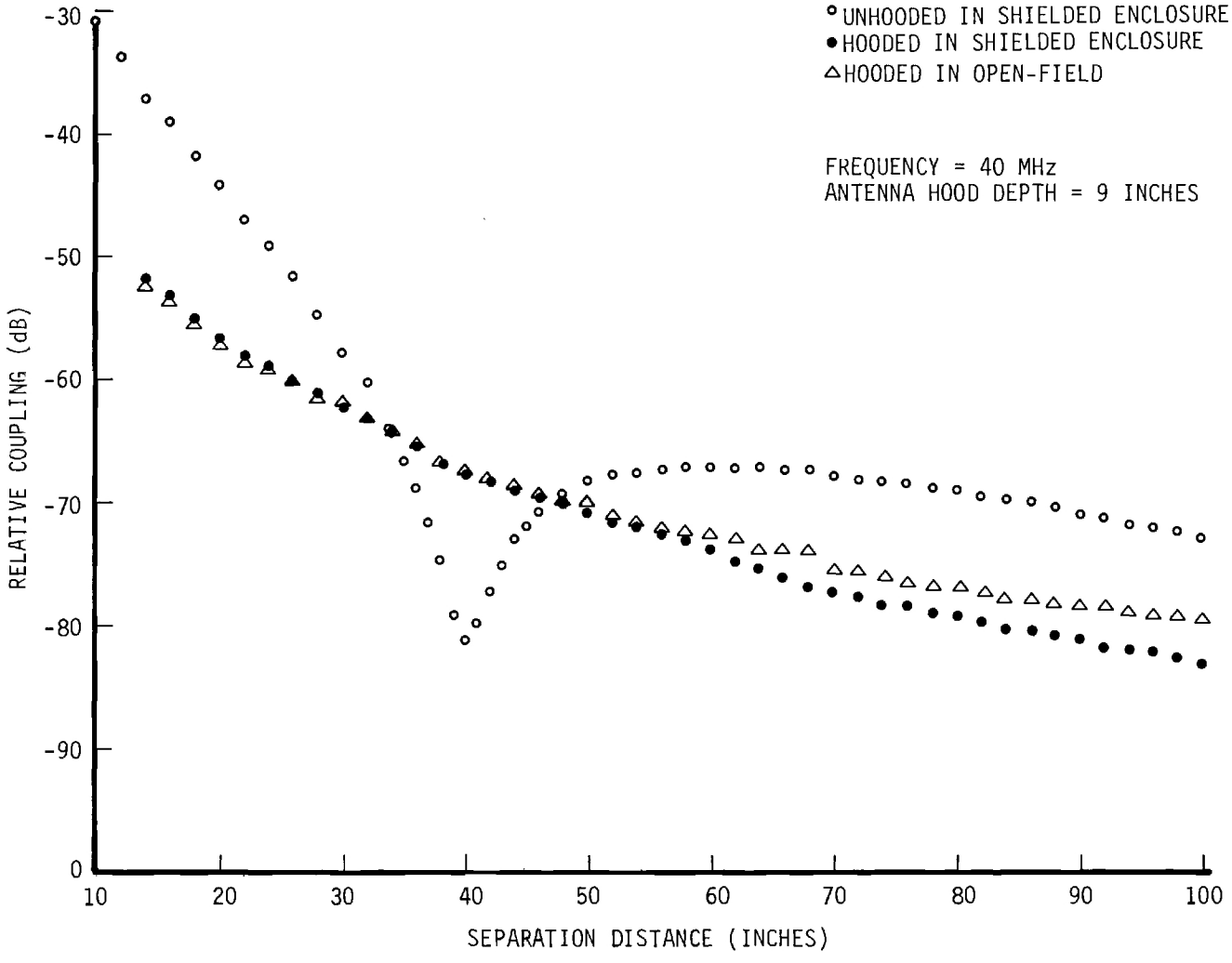

Figure 31. Relative Coupling as a Function of Antenna Separation Distance at a Frequency of 40 MHz.

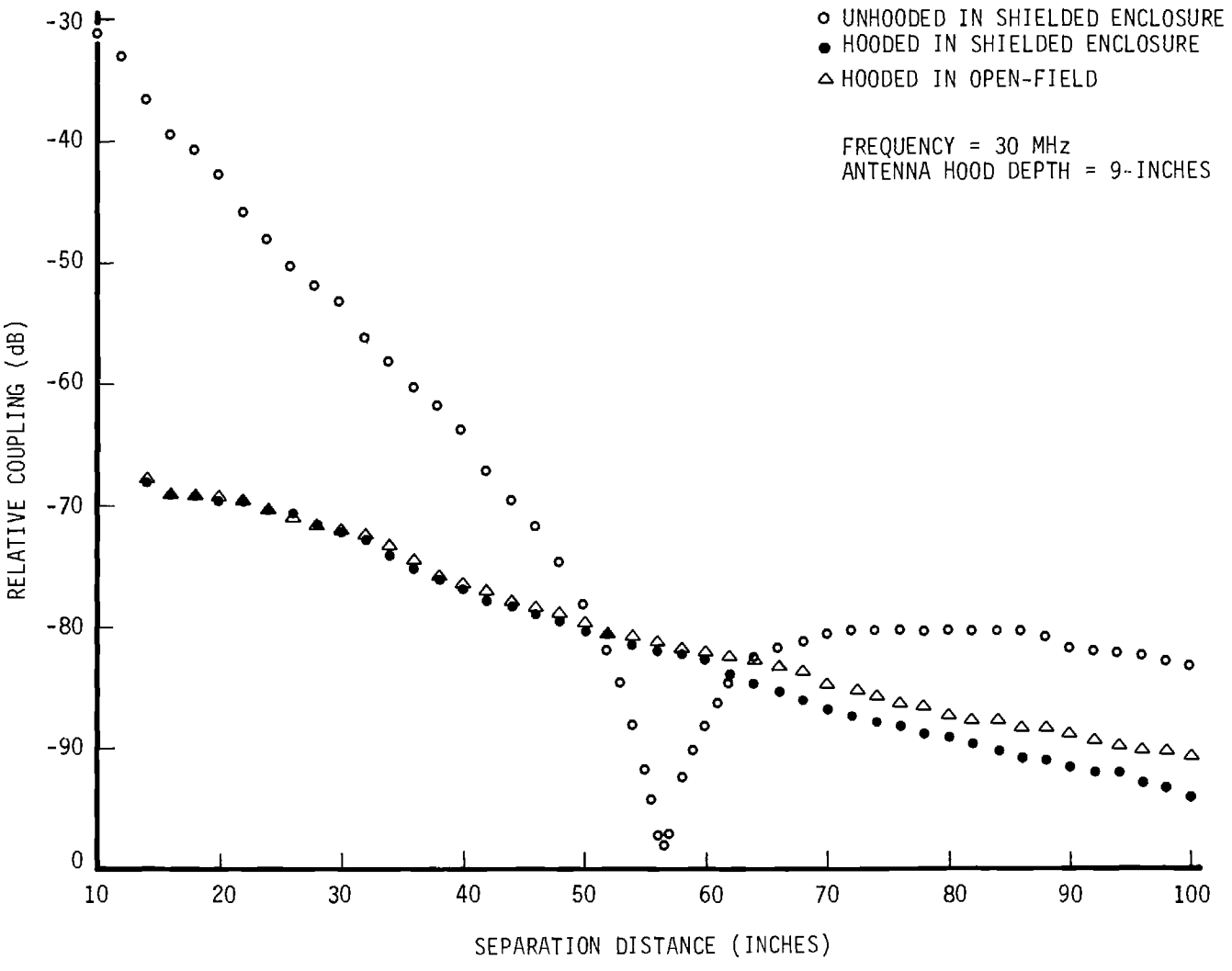

Figure 32. Relative Coupling as a Function of Antenna Separation Distance at a Frequency of 30 MHz.

was provided by the antenna hood to prevent coupling of the E_r component into the probe antenna. Hence, no coupling nulls are evident in the hooded antenna data.

To compare the hooded antenna coupling measured in the shielded enclosure with corresponding data from open-field measurements, the shielded enclosure experiments described above were repeated on the roof antenna range. The open-field coupling data obtained with the hooded antenna are also shown in Figures 30, 31 and 32. The agreement between the hooded antenna measurements in the shielded enclosure and corresponding measurements in the open-field is quite good. Out to a separation distance of just over one meter, the two sets of measurements are identical to within the accuracy of the measurement equipment. At separation distances in excess of 50 inches, a detectable difference in coupling is seen. The coupling in the open-field falls off more slowly with distance than it does in the shielded enclosure. At a separation distance of 100 inches, the difference between the open-field and shielded enclosure measurements is approximately 3 dB.

While the low frequency hooded antenna exhibits little or no response to radially polarized fields, Figures 30, 31 and 32 indicate that this antenna does exhibit less gain than unhooded bow-tie antennas. Open-field coupling measurements were made as a function of the separation distance of the 30-inch bow-tie antenna and the unhooded 18-inch bow-tie antenna. The results of these measurements are shown in Figures 33, 34 and 35. The corresponding open-field coupling curves between the 30-inch bow-tie antenna and the hooded 18-inch bow-tie antenna are included in these figures for comparison.

As expected, the near-field mutual coupling between the source and probe antennas was found to be considerably altered when the probe antenna was hooded. As can be seen from Figures 33, 34 and 35, the additional coupling losses associated with the hooded probe are dependent both on separation distance and frequency. To further document the range dependence of mutual coupling in the near-field, azimuth antenna patterns were made of the response of the hooded probe antenna to the tangentially polarized electric field, E_θ. For these patterns a short dipole antenna was used as a radiating source. Figure 36 shows the test setup used in obtaining the patterns.

Azimuth antenna patterns of the hooded probe antenna were made at source-to-probe separation distances of 28, 36, 48, 60, 72 and 84 inches. The patterns were made at a frequency of 40 MHz with the bow-tie probe located at a 24-inch hood depth. The resulting patterns are shown in Figures 37 and 38. In order to obtain the clearest possible patterns, it was necessary to increase the power delivered to the source antenna

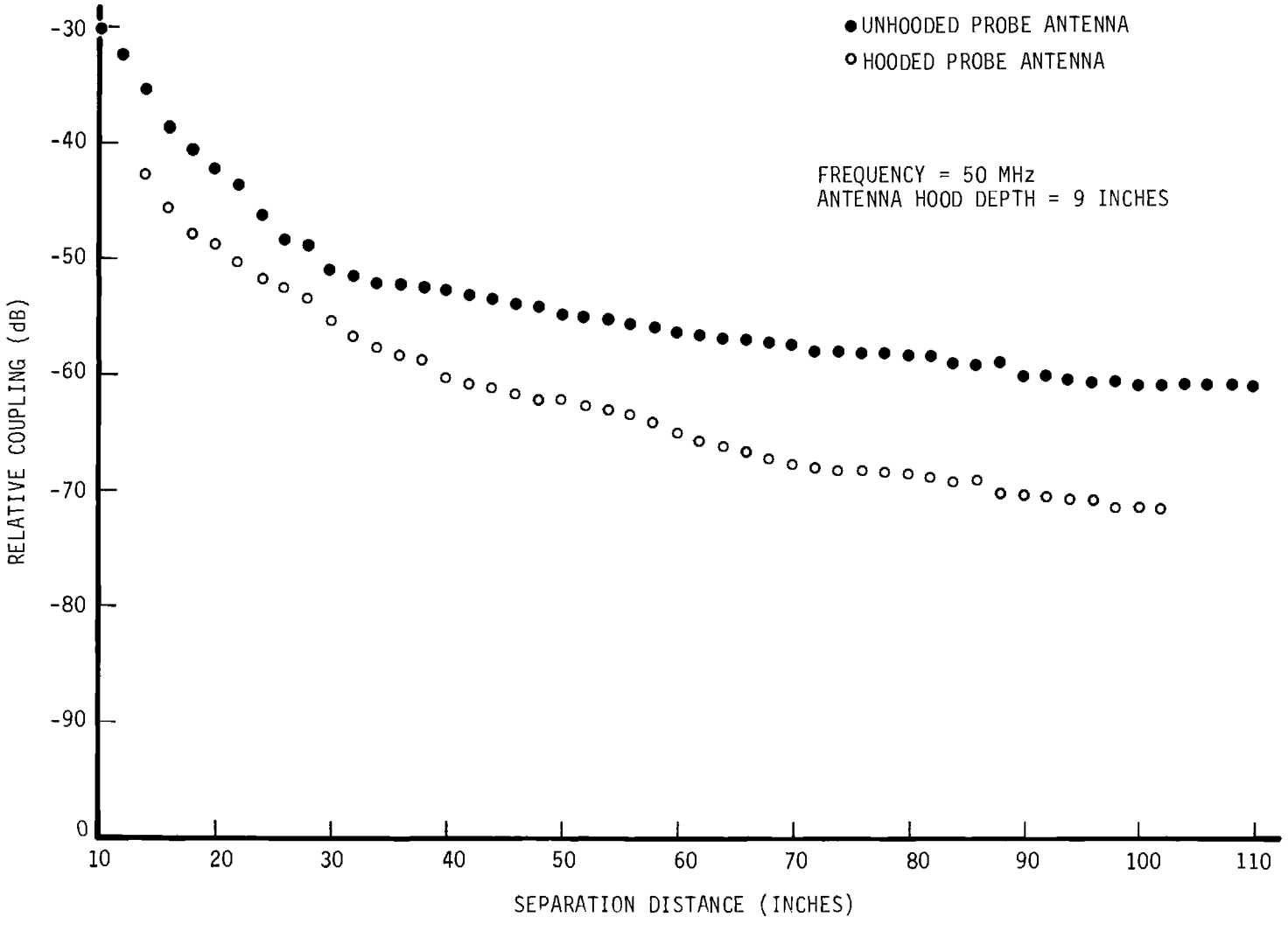

Figure 33. Open-Field Relative Coupling at 50 MHz.

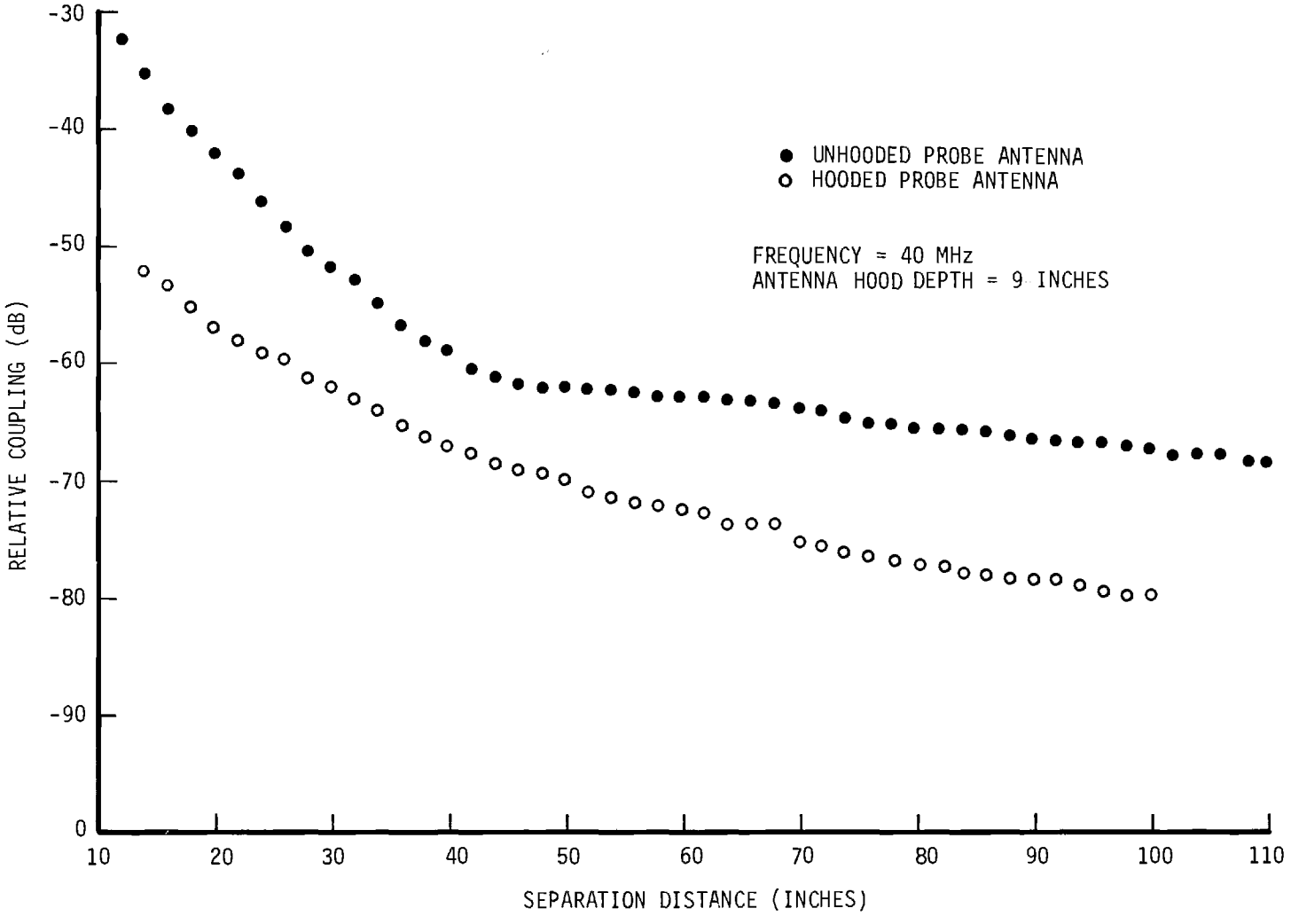

Figure 34. Open-Field Relative Coupling at 40 MHz.

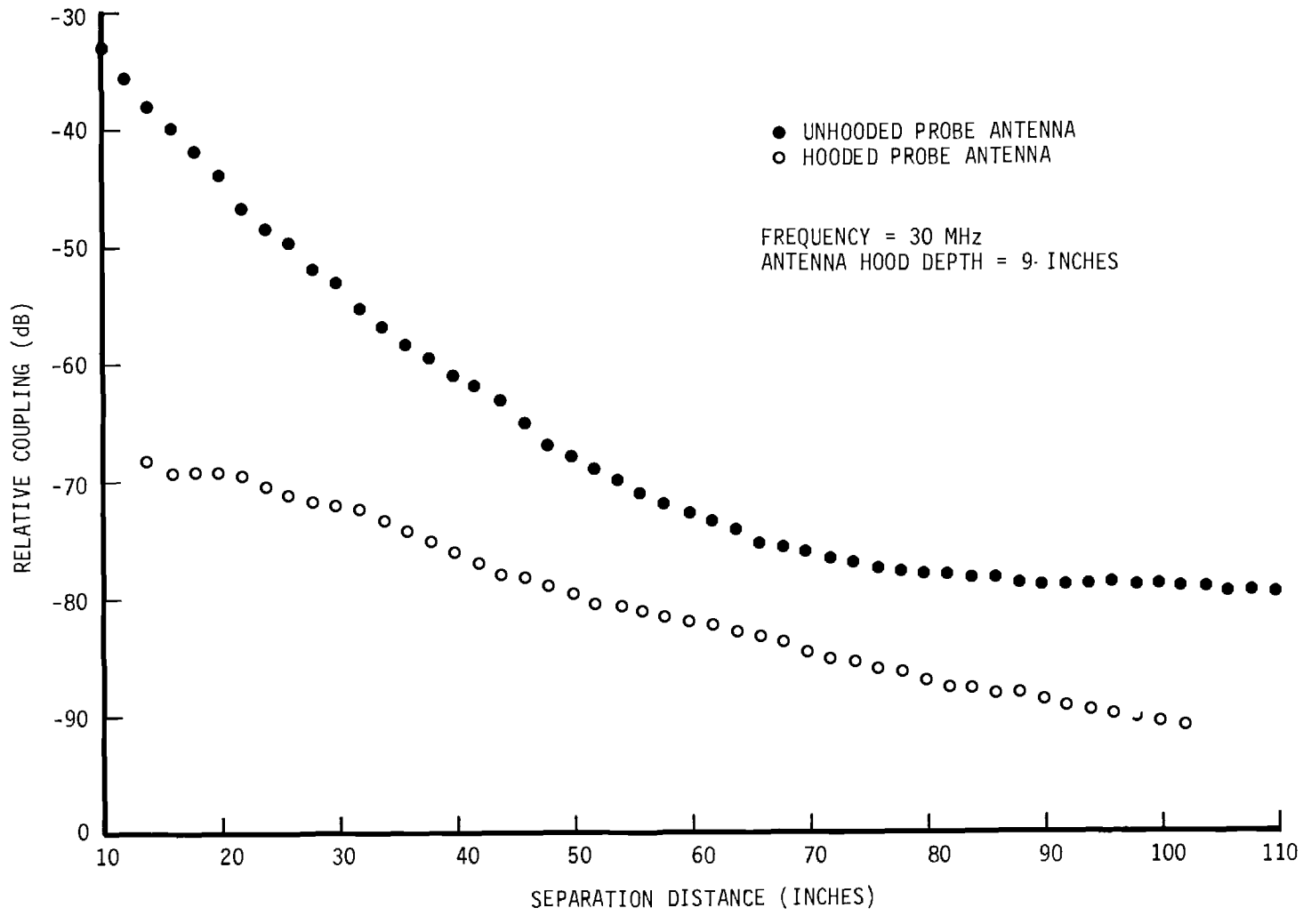

Figure 35. Open-Field Relative Coupling at 30 MHz.

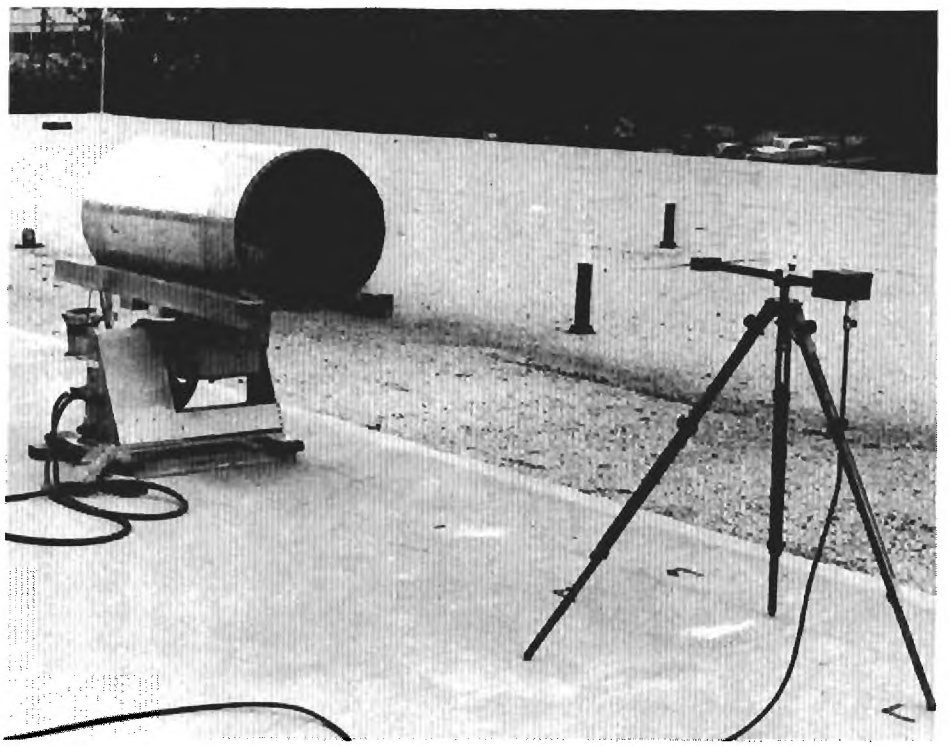

Figure 36. View of the Test Setup for Measuring Near-Field Mutual Coupling Patterns.

as the source-to-probe separation distance was increased. The response level on boresight is indicated on the pattern at each separation distance. All levels are referenced to 0 dB at a 28-inch separation distance.

As Figures 37 and 38 indicate, there are several dramatic effects of separation distance on the hooded probe antenna patterns as a result of near-field mutual coupling changes between the source and hooded probe antenna. The apparent front-to-back ratio is seen to change from about 32 dB at a 28-inch separation distance to about 10 dB at 84 inches. The apparent 3 dB beamwidth changes from approximately 36 degrees at 28 inches to approximately 84 degrees at 84 inches. The word "apparent" is used advisedly in describing the front-to-back ratio and beamwidth changes. It should be recognized that the "patterns" shown in Figures 37 and 38 actually depict the near-field mutual coupling of the dipole source and the hooded probe as a function of the azimuth position of the latter. The near-field as used here implies the region less than a few wavelengths from the antenna where the induction-field and electrostatic-field are significant with respect to the radiated field. In this region the coupling between two antennas includes inductive coupling and capacitive coupling as well as the normal coupling involving

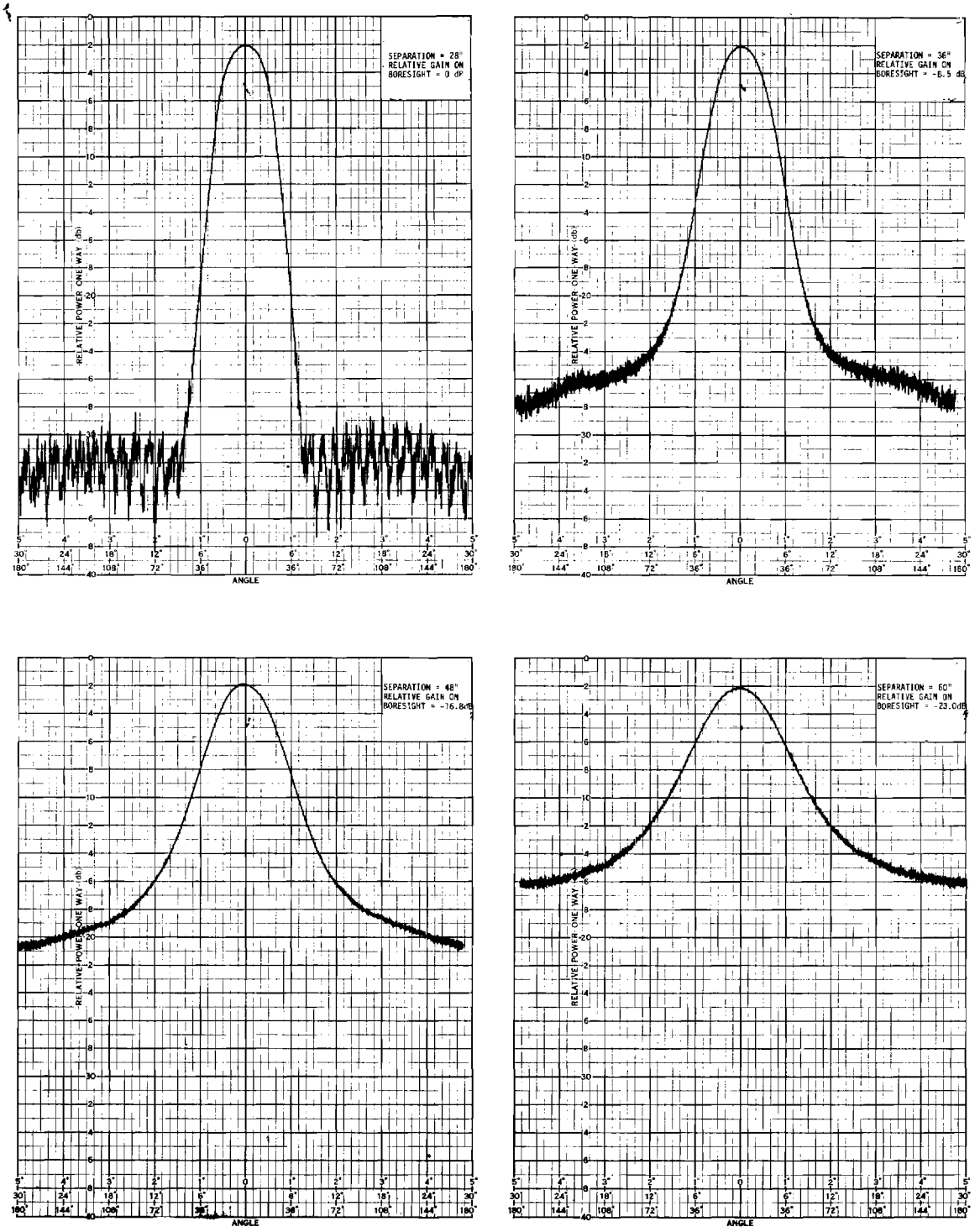

Figure 37. Near-Field Mutual Coupling Between a Dipole and Hooded Probe Antenna at Separation Distances of 28, 36, 48 and 60 Inches.

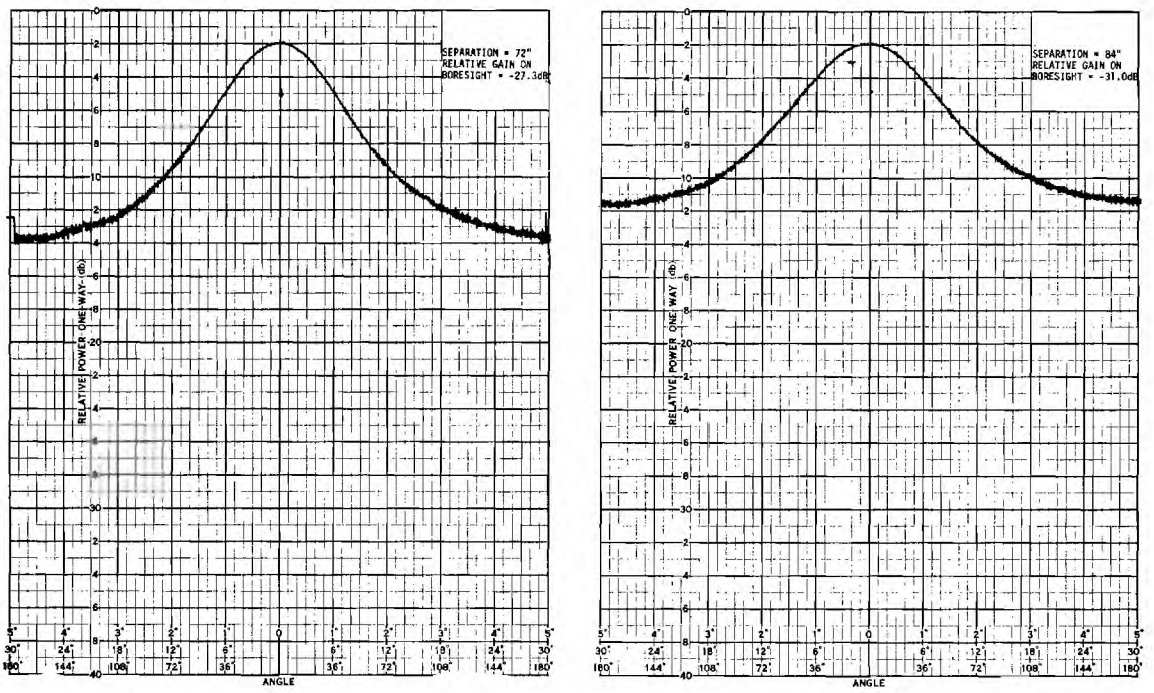

Figure 38. Near-Field Mutual Coupling Between a Dipole and Hooded Probe Antenna at Separation Distances of 72 and 84 Inches.

the radiated field. The inductive coupling and capacitive coupling are extremely sensitive to the configurations of the two antennas involved, to the spacing between the antennas and to the orientation of the two antennas with respect to each other. Hence, it is to be expected that patterns made in this region will be significantly different from far-field patterns and will be a function of the distance at which they are measured. The mutual coupling patterns shown in Figures 37 and 38 would be expected to change, for example, if a different source antenna were used in place of the short dipole shown in Figure 36.

It has been shown that a low frequency antenna hood can be used to effectively isolate the probe antenna from the radially polarized field component coupled by a shielded enclosure wall. Low frequency hooded antenna coupling measurements in a shielded enclosure agree quite well with corresponding hooded measurements made in the open-field. However, coupling losses associated with the low frequency hooded antenna are appreciable and the mutual coupling between the source and probe antenna is significantly affected by the antenna hood. The strong dependence of mutual coupling on the probe antenna hood could further complicate calibration of this type of antenna. Thus, while the low frequency hooded antenna does offer a solution to some of the near-field measurement problems in shielded enclosures, this solution is not without some disadvantages.

7. Baffle Plate Techniques

The low frequency antenna hood was shown to be capable of providing sufficient isolation between the enclosure side walls and the ends of the antenna to prevent side wall coupling of the radially polarized field component. However, as the experiments discussed in the preceeding section showed, substantial insertion losses as well as significant near-field mutual coupling influences are associated with the low frequency hooded antenna technique. An investigation was begun on the use of baffle plates to provide isolation between an antenna and the enclosure side walls. It was hoped that such a technique would have the isolation advantages of the low frequency hooded antenna, but would have smaller insertion losses and mutual coupling influences.

The baffle plate concept is shown in Figure 39. The baffle plates are metal plates lined with lossy material and placed opposite the ends of an antenna in a shielded enclosure. The plates are, in effect, sections of the low frequency hood. The concept is that if coupling between the ends of the antenna and the enclosure side walls can be greatly reduced or prevented, the coupling null can be eliminated. Under such conditions, it is probable that the probe antenna could be accurately calibrated for shielded enclosure measurements. The absorbing material shown on the end wall is not relevant to the baffle plate technique, but since it will normally be in the shielded enclosure for hooded antenna measurements at higher frequencies, it is shown in the figure.

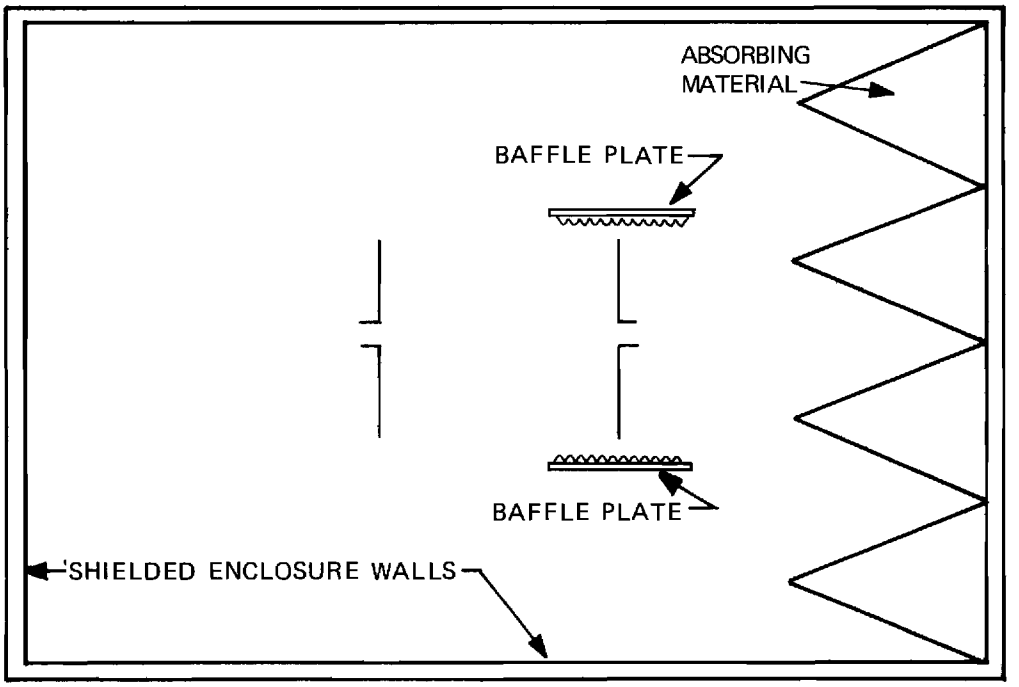

Figure 39. Diagram of Shielded Enclosure Measurement Setup Incorporating Baffle Plates.

A brief discussion of the difference between absorbing materials and lossy materials appears to be in order at this point. Absorbing materials have the characteristic of matching an absorbing medium with a normal propagating medium (usually free space) so that an incident wave is absorbed and dissipated in the material. The specular reflection from the surface of absorbing materials is normally reduced by 20 dB or more below the level of the incident wave. A lossy material does not necessarily match the lossy medium to the propagating medium, it does however, significantly attenuate surface currents which are set up by a wave which is incident on the surface of the lossy material. Hence, while a lossy material does not necessarily significantly reduce the specular reflection of a wave incident on its surface, it does prevent the effect of this wave from being transferred to other parts of its surface.

Since the present concern is not reflections, but rather, the transfer of energy along the enclosure walls, the use of lossy material on the baffle plates should prevent any surface currents on the plates. With no surface currents on the baffle plates, there should be no coupling between the plates and the enclosure walls, and hence, the plates lined with lossy material should provide appreciable isolation between the ends of the antenna and the enclosure walls.

Two baffle plates, as shown in Figure 40(A), were prepared. A section of aluminum plate 24 x 24 inches was covered with NZ-1 ferrite material. This material has been shown to be a lossy material at frequencies below 70 MHz.[5] The two baffle plates were placed opposite the ends of one dipole antenna in a shielded enclosure as shown in Figure 41(A) and (B). Coupling measurements were made for the two dipole antennas as a function of separation distance at a frequency of 40 MHz. The overall dipole antenna lengths were set at 60 inches.

Initially the measurements were made with the baffle plates floating. The measurements using the baffle plates in this manner were quite similar to coupling measurements made in the shielded enclosure without baffle plates. The spacing at which the coupling null occurred when the baffle plates were used was unchanged from the spacing at which it occurred when no baffle plates were used, indicating that no effective side wall isolation was provided by the baffle plates.

The baffle plates then were grounded to the enclosure side walls and antenna baluns by a length of braided wire visible in Figure 41. The antenna coupling measurements were repeated. Again a coupling null was measured; however, the null was found to occur at an antenna spacing of 43 inches, as compared to a spacing of 32 inches when no baffles were used. Based on the side wall coupling theory, these data indicate that the grounded baffle plates provide partial isolation between the ends of the antenna and the enclosure side walls.

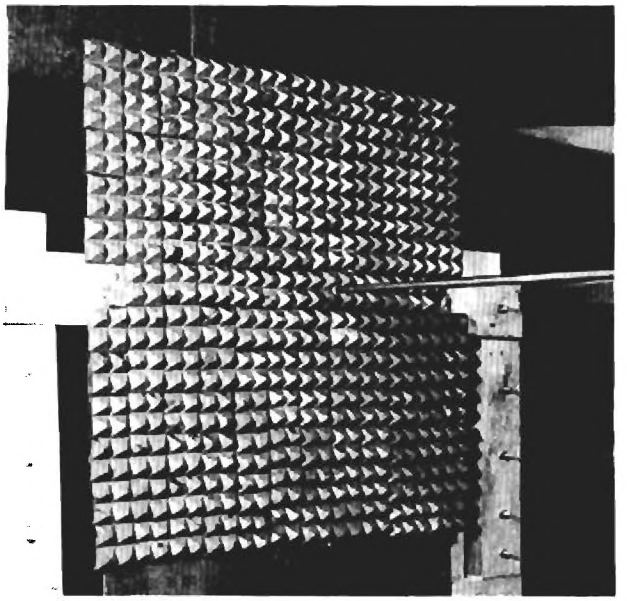

(a)

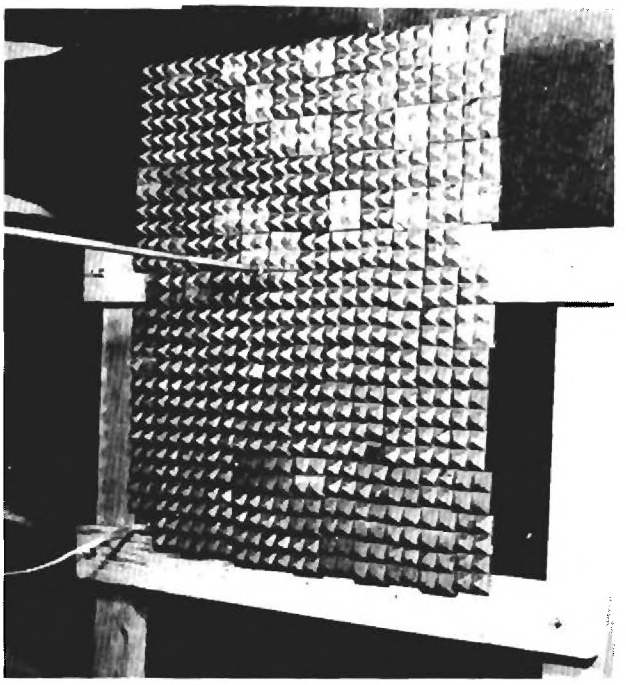

(b)

Figure 40. Two Views of Baffle Plates.

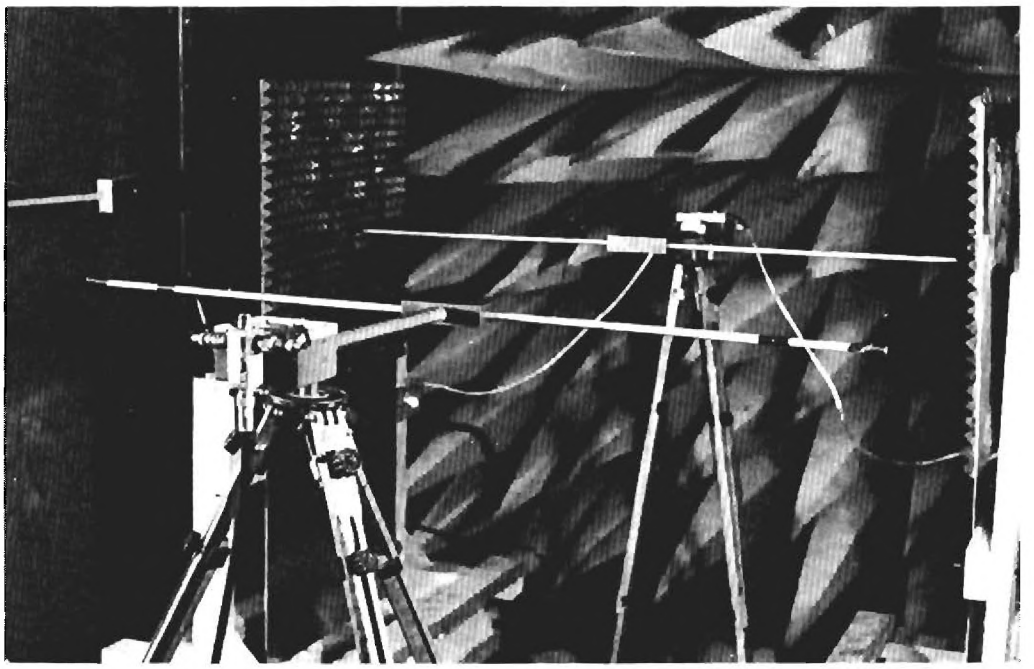

(a)

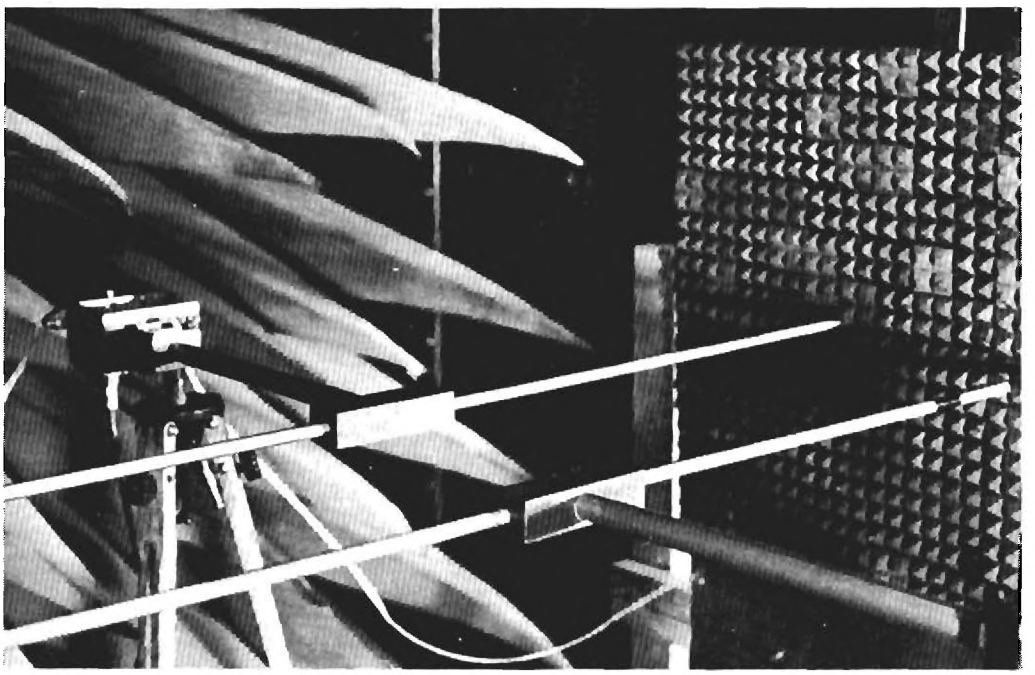

(b)

Figure 41. Two Views of the Baffle Plate Measurement Setup in a Shielded Enclosure.

In order to reduce any "fringing" effects, the baffle plates were modified by removing the exposed plate at the bottom of the baffle. The resulting baffle plates are shown in Figure 40(B). The experiment described above was repeated for the modified baffle plates. The plates were grounded to both the enclosure wall and the antenna balun. A coupling null was measured at an antenna separation distance of 55 inches, indicating more isolation was obtained than in the previous baffle plate experiments.

The braided wire used as a ground strap may not provide adequate grounding at 40 MHz. In addition, there is evidence of "fringing" around the 24 x 24 inch lossy baffle. Larger baffle plates, together with better grounding techniques, may lead to the complete elimination of the coupling nulls observed in the shielded enclosure. Results of the preliminary experiments described in this section justify a more complete future investigation of baffle plate techniques.

8. Summary and Conclusions

Large differences in corresponding open-field and shielded enclosure measurements have been observed at frequencies well below 100 MHz, where the dimensions of most conventional enclosures are small enough, compared to wavelength, to preclude any significant multipath interference effects. In this frequency range the coupling between two antennas in a shielded enclosure is typically characterized by the existance of a single coupling null which is not present in the corresponding measurements made in the open-field.

It has been hypothesized that the coupling nulls in shielded enclosures are caused by the near-field components of the antennas. A near-field coupling theory has been presented which indicates that these nulls are the result of the out-of-phase summation of the tangentially polarized direct radiation and a near-field, radially polarized, electric field component.

The results of a number of experiments to test the validity of the near-field coupling theory have been reported. All available evidence supports the near-field coupling theory.

It has been shown that a low frequency antenna hood can be used to effectively isolate the probe antenna from the radially polarized field component propagated along a shielded enclosure wall. Low frequency hooded antenna coupling measurements in a shielded enclosure agree quite well with corresponding hooded measurements made in the open-field. However, coupling losses associated with the low frequency hooded antenna are appreciable and the mutual coupling between the source and probe antenna is significantly affected by the antenna hood. The strong dependence of mutual coupling on the probe antenna

hood could further complicate the calibration of this type of antenna. Thus, while the low frequency hooded antenna does offer a solution to some of the near-field measurement problems in shielded enclosures, additional investigation of near-field coupling phenomena is indicated.

The concept of reducing the coupling between the ends of an antenna and the enclosure side walls through the use of baffle plates has been tested with only partial success. Results of preliminary experiments justify a more complete future investigation of baffle plate techniques.

C. Short Hooded Antennas

1. Background

A major objective of this program was to improve the design of hooded antennas. The evaluation of the hooded antennas on previous programs revealed that the relatively long hoods utilized with these antennas were yielding more directivity than was required. In fact, at the higher frequency limits, the beamwidths of the antennas were narrower than desired. It was hypothesized that the absorber-lined hood was producing a secondary field pattern which closely approximated the field that would be obtained from a plane wave radiating through a circular aperture in an infinite absorbing screen.

The normalized field pattern of a uniformly illuminated circular aperture in a perfectly absorbing screen of infinite extent is given by

$$F = (1 + \text{Cos } \theta) \frac{J_1(\frac{\pi A}{\lambda} \text{ Sin } \theta)}{\frac{\pi A}{\lambda} \text{ Sin } \theta} \qquad (4)$$

where

A = aperture diameter,

λ = free-space wavelength,

θ = angle with respect to the normal to the aperture,

J_1 = first-order Bessel function.

This equation was programmed for a digital computer and field patterns were calculated for the two hooded antennas at each of the test frequencies. The calculated and measured patterns were compared,

good correlation between the two sets of patterns was observed, and it was concluded that the pattern of the hooded antenna is primarily determined by the ratio of the aperture diameter to the wavelength of interest. Thus, the aperture equation can be used as a tool to design hooded antennas to meet specified beamwidth and sidelobe characteristics.

Considering the typical operation of the hooded antennas inside conventional shielded enclosures, it appeared desirable to limit the half-power beamwidth of the hooded antenna to the range from 20 to 60 degrees. A curve (based on circular aperture field pattern calculations) showing the half-power beamwidth of a hooded antenna as a function of the aperture-to-wavelength ratio is shown in Figure 42. It is apparent from this curve that to maintain the beamwidth within the 20 to 60 degree range, it is necessary to restrict the aperture-to-wavelength ratio to the range between 1.0 and 3.0. To meet these requirements, a minimum of three hooded antennas would be required to cover the 200 MHz to 12 GHz frequency range.

An initial step in reducing the length of hooded antennas was to substitute cavity-backed spiral antennas for conical log-helix antennas as the primary feeds for hooded antennas. The cavity-backed spirals appear to exhibit all the desirable characteristics of the log-conical antennas, and in addition, are planar structures. In previous hooded

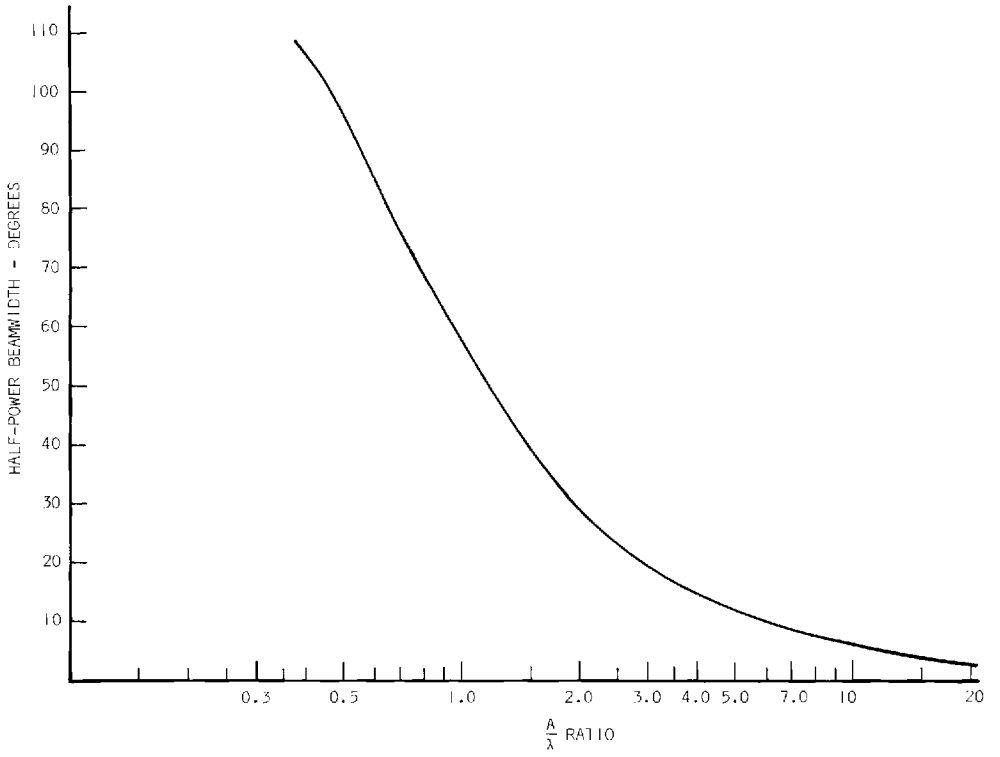

Figure 42. Theoretical Beamwidth of Hooded Antenna Vs. Aperture Size.

antennas utilizing log-conical antennas as primary feeds, an appreciable part of the hood length was required to accomodate the length of the log-conical antenna. The substitution of cavity-backed spiral antennas allowed practically all of this hood length to be eliminated.

2. Hood Length Vs. Beamwidth Study

The discussion of the hooded antenna beamwidth as a function of aperture size in the previous section assumed a planar wavefront at the hood aperture. In order to maintain the phase error over the aperture to a maximum of $\lambda/16$ (22.5 degrees), the distance from the probe antenna to the aperture of the hood (ℓ) must satisfy the condition:

$$\ell = \frac{2A^2}{\lambda} \quad . \tag{5}$$

If it is assumed that the hooded antenna is to operate over a frequency range such that the aperture is 1λ at the lower frequency limit and 3λ at the upper frequency limit, a simple calculation reveals that the probe antenna must be located at least 18λ from the aperture at the upper frequency limit in order to satisfy the phase condition specified by (5). This would require that the length of the hood be somewhat greater than six times the diameter of the hood.

Since it is important from the standpoint of size, weight and cost to minimize the length of the antenna hoods, a study to determine the performance of hooded antennas as a function of hood length was conducted. An adjustable-length hooded antenna was fabricated for this study. A diagram of the adjustable-length hooded antenna is shown in Figure 43. The basic hood structure is the hood of the microwave hooded antenna. This hood is a metal cylinder lined with Eccosorb NZ-1 absorbing material. The outside diameter is 8 inches, the inside diameter is $6\frac{1}{4}$ inches and the length is 19 inches. A metal end-plate, lined with absorbing material and with a type N feed-through connector in the center, was mounted on one end of the cylinder. An AEL Model ASN 118A cavity-backed spiral antenna and a false metal end-plate lined with absorbing material was mounted on a circular piece of expanded polyethylene foam as shown in the figure. The diameter of the foam was made so that it was a tight sliding fit to the inside of the hood, and hence, was capable of supporting the antenna and false end-plate at any location along the length of the basic hood. This configuration made it possible to vary the distance (ℓ) between the aperture of the hood and the aperture of the cavity-backed spiral antenna from zero to $15\frac{1}{2}$ inches. Antenna patterns were made at three frequencies, 2 GHz ($A \approx \lambda$), 4 GHz ($A \approx 2\lambda$) and 6 GHz ($A \approx 3\lambda$), for seven values of ℓ over the range from $1\frac{1}{2}$ inches to $15\frac{1}{2}$ inches. Typical patterns obtained for ℓ values of $1\frac{1}{2}$, $4\frac{1}{2}$, $7\frac{1}{2}$ and $15\frac{1}{2}$ inches

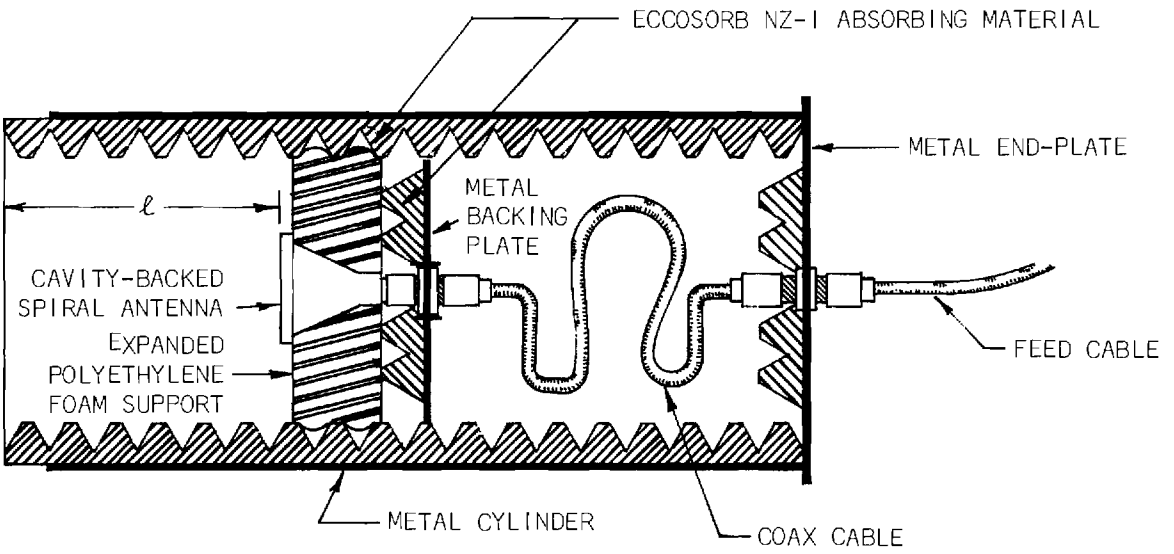

Figure 43. Diagram of Adjustable-Length Hooded Antenna.

at the three frequencies are shown in Figures 44, 45 and 46. It is apparent from Figure 44 that reducing the hood length from 15½ to 1½ inches (approximately 2.5λ to ¼λ) had no significant effect on the antenna pattern when the hood aperture was approximately 1λ. The patterns show that the half-power beamwidth increased from 45 degrees to 49 degrees and the maximum sidelobe levels increased by less than 1 dB.

The patterns in Figure 45 show that at 4 GHz, where the hood aperture was approximately 2λ, reducing the hood length had an appreciable effect on the antenna pattern. The half-power beamwidth was increased from 27 degrees to 43 degrees and the maximum sidelobe levels increased by more than 8 dB. The most significant effect was obtained when the hood length was decreased from 4½ to 1½ inches. For this relatively small change in hood length, the 3 dB beamwidth increased by approximately 13 degrees and the sidelobes increased approximately 6 dB.

Some unexpected results were obtained at 6 GHz. It is apparent from the patterns in Figure 46 that the minimum half-power beamwidth was obtained at a hood length of 7½ inches rather than at the maximum

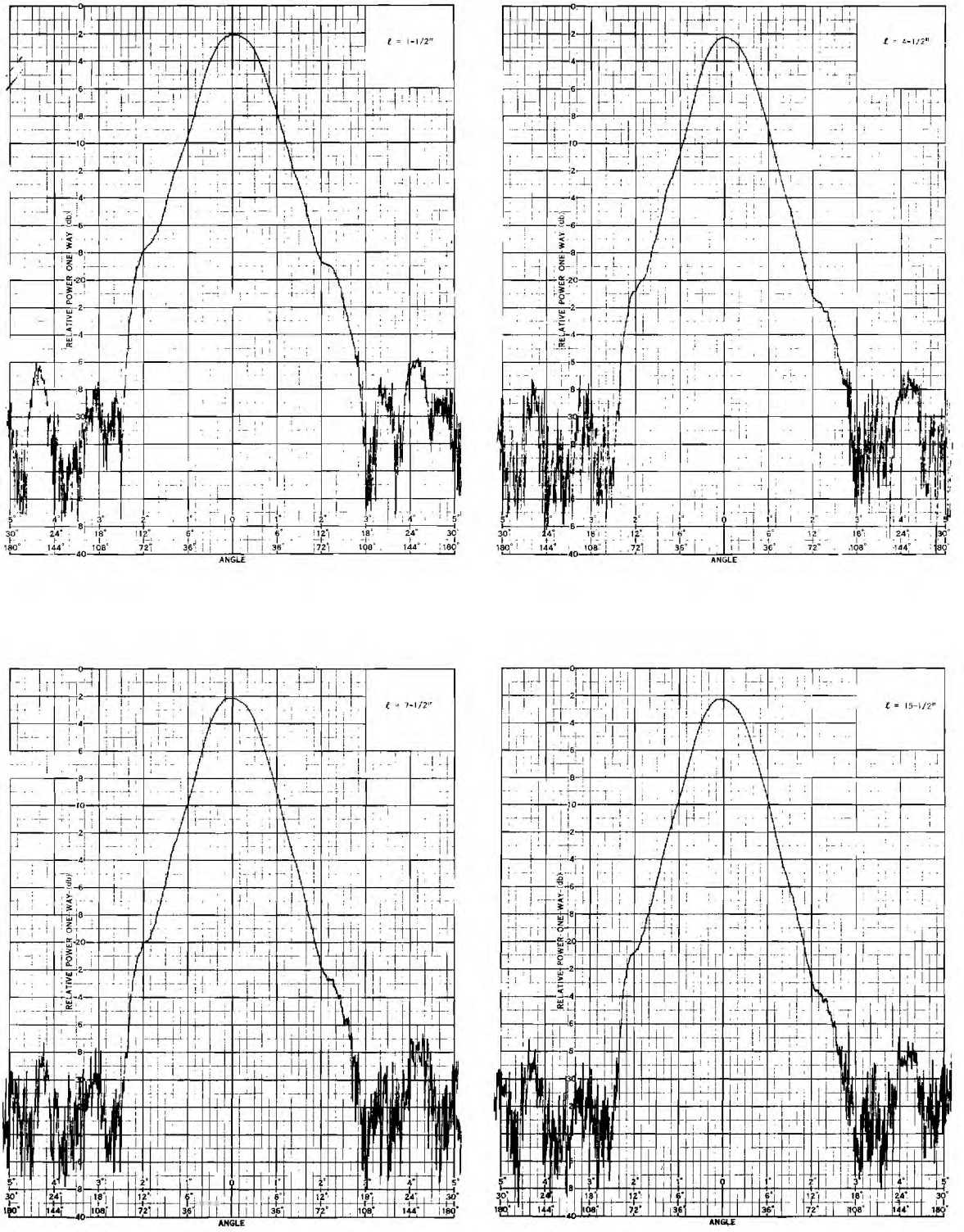

Figure 44. Patterns of Hooded Antenna as a Function of Hood Length at 2 GHz.

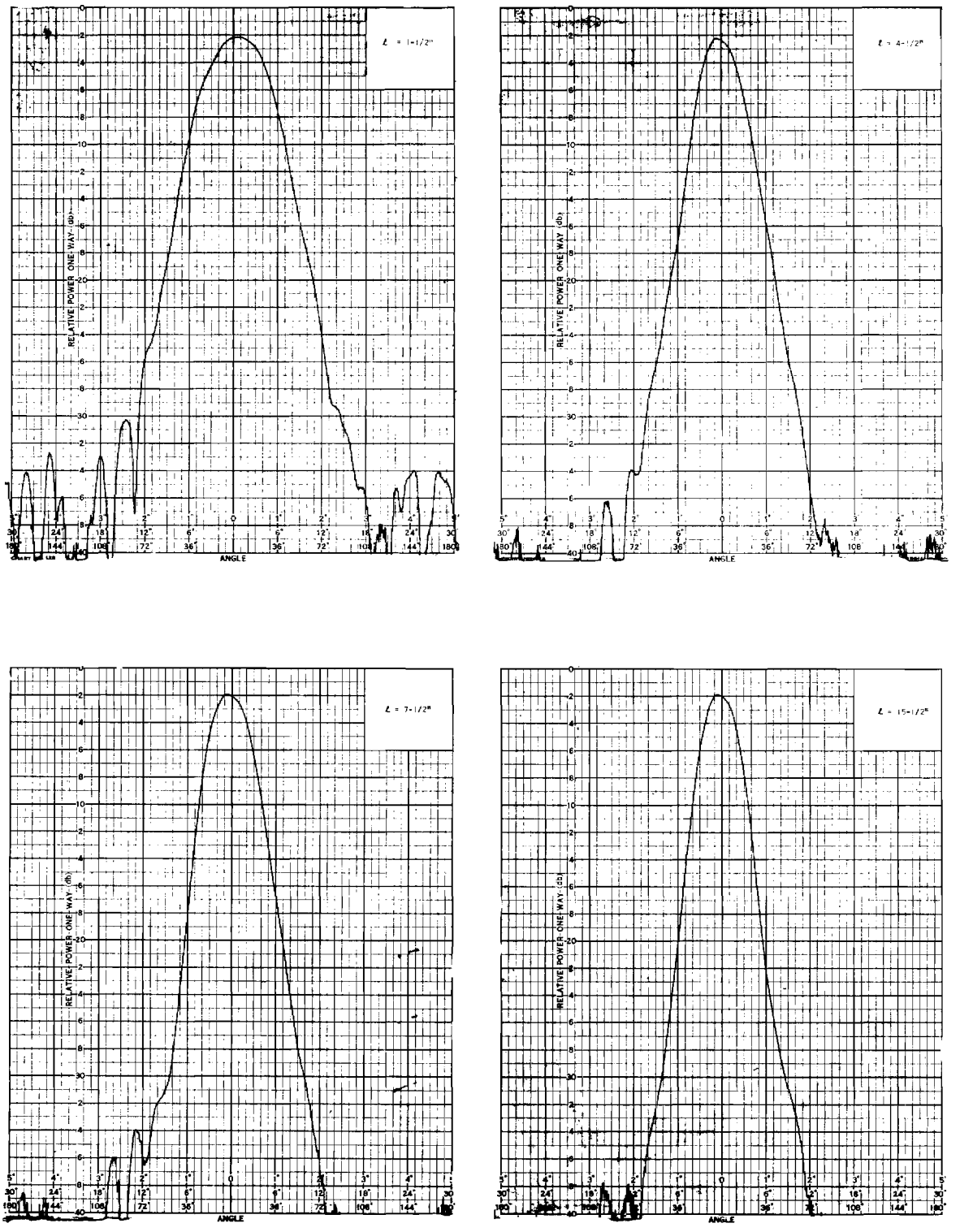

Figure 45. Patterns of Hooded Antenna as a Function of Hood Length at 4 GHz.

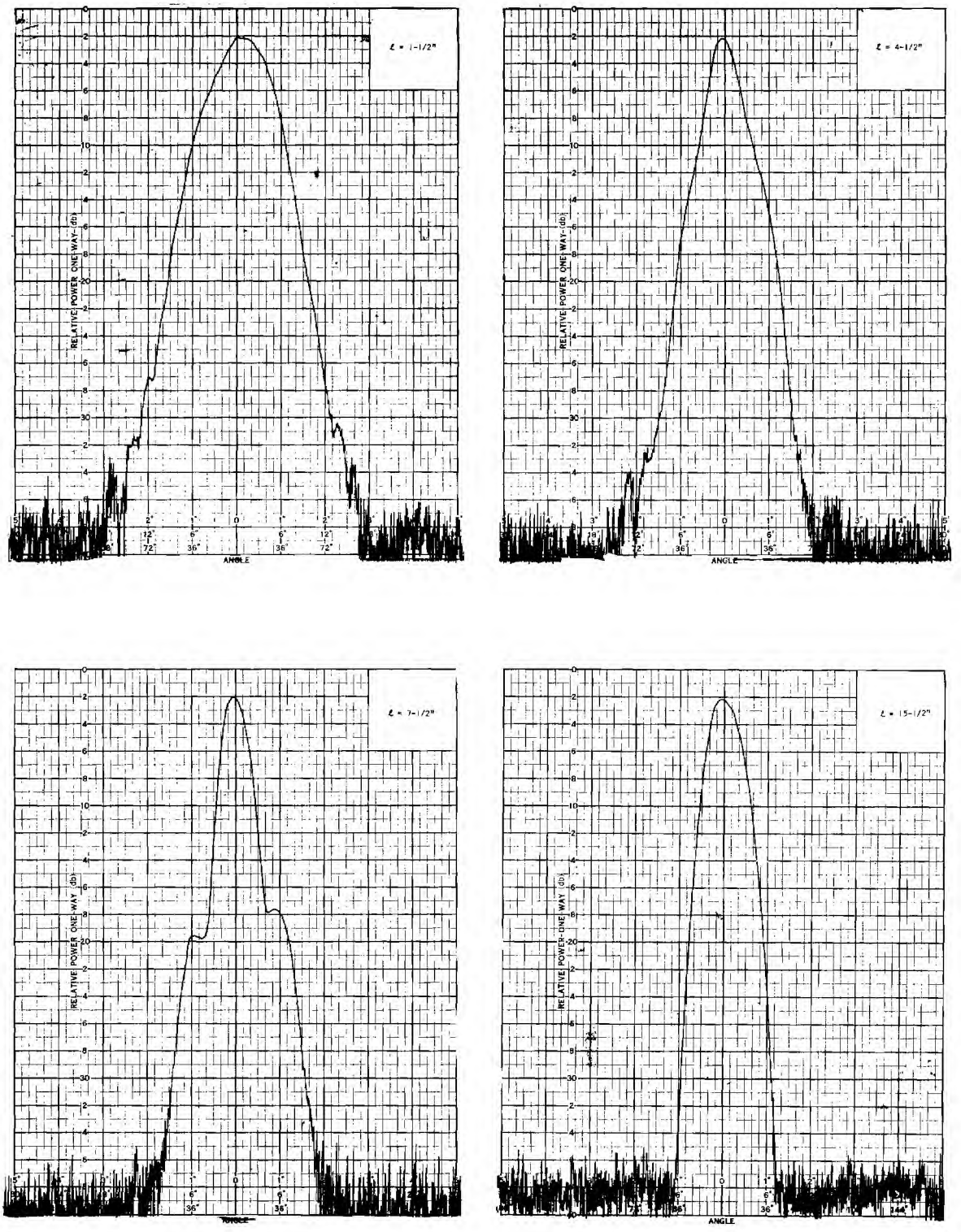

Figure 46. Patterns of Hooded Antenna as a Function of Hood Length at 6 GHz.

hood length of 15½ inches. The beamwidth was 20 degrees at 7½ inches and 27 degrees at 15½ inches. Apparently there is an optimum hood length in terms of wavelengths (in this case 3.75λ), and if the hood length exceeds this optimum length, an additional mode is set up along the walls of the hood which causes a phase error at the aperture which degrades the directivity characteristics of the aperture. At 2 GHz and 4 GHz the maximum hood lengths were 2.58λ and 3.87λ respectively, and hence, this phenomena was not apparent. At 6 GHz, the most significant effect was again obtained when the hood was decreased from 4½ to 1½ inches. The half-power beamwidth increased by approximately 20 degrees. It is interesting to note that for a hood length of 15½ inches at 2 and 4 GHz and 7½ inches at 6 GHz, the measured half-power beamwidths agree quite well with the theoretical beamwidth curve in Figure 42.

The half-power beamwidth data from all of the hooded antenna measurements are shown in Figure 47. Two important conclusions can be made based on the curves shown in this figure. First, the hood of the antenna can be made quite short relative to the diameter and the half-power beamwidth will remain less than 60 degrees from the frequency at which the aperture is one wavelength to at least three times this frequency. Secondly, if the hood length is made short relative to the diameter, the beamwidth of the hooded antenna will be considerably less sensitive to the frequency of operation. For the example shown in Figure 47, if the hood is made 2 inches long

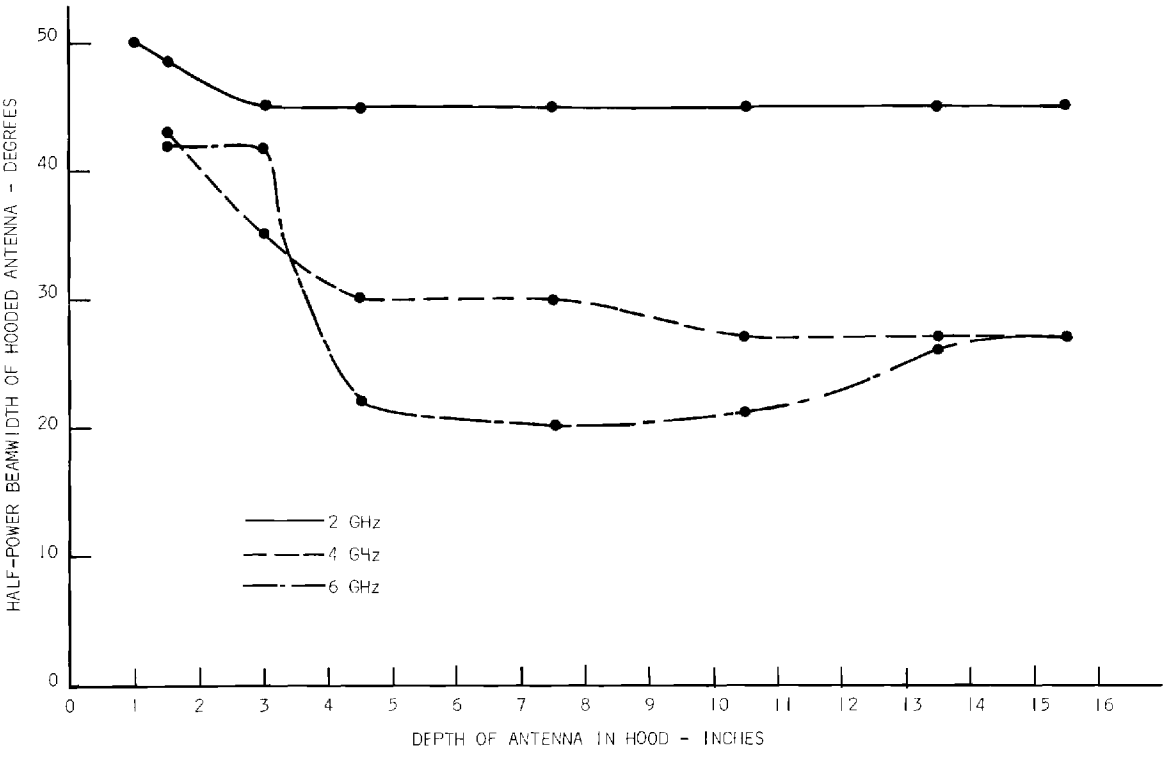

Figure 47. Measured Beamwidth of Hooded Antenna as a Function of Hood Length.

(or $\lambda/3$ at the lower frequency limit), then the beamwidth at the lowest frequency will be 47 degrees, and over a 3:1 frequency range the beamwidth will vary from 47 degrees to 40 degrees (based on the three test frequencies).

To verify these results and determine the beamwidth characteristics of short hooded antennas, two experimental short hooded antennas were designed to cover the frequency ranges of 1 to 4 GHz and 3 to 12 GHz and to yield an essentially constant 50 degree beamwidth over the 1 to 12 GHz range. Details of the design, fabrication and evaluation of these antennas were presented in the second quarterly report.

The results obtained with the two experimental short hooded antennas were not as good as anticipated. The patterns obtained were considerably wider and more sensitive to frequency than expected. It was hypothesized that the lack of success could be due to the fact that the short hooded antenna designs were based on data obtained with an adjustable-length hooded antenna in which the aperture dimension and the primary feed antenna (and hence the primary antenna pattern) were different from the final short hooded antenna configurations. In order to obtain experimental data which are more directly applicable to the short hooded antenna designs, two additional adjustable-length hooded antennas were fabricated. The dimensions and configurations of these antennas were made as near as possible identical to the planned short hooded antennas. In addition, the same cavity-backed spiral antennas planned for use in the final short hooded antennas were utilized in these adjustable-length hooded antennas.

3. Adjustable-Length Hooded ASN 116A Antenna

An adjustable-length hooded antenna for a lower frequency limit of 1 GHz was designed and fabricated. The objective of this antenna was to cover the frequency range from 1 GHz to as high a frequency as possible, and over its useable frequency range, to provide a half-power beamwidth in the range from 20 to 60 degrees. A photograph of this hooded antenna is shown in Figure 48. The hood is a metal cylinder lined with Emerson and Cuming Eccosorb NZ-1 absorbing material. The outside diameter is 12 inches and the inside diameter is 10 inches. An AEL Model ASN 116A cavity-backed spiral antenna was used as the primary feed antenna for this hooded configuration. The ASN 116A antenna is designed to cover the 1 to 10 GHz frequency range. Antenna patterns for the basic unhooded antenna at 2, 3, 4, 6, 7, 8, 9 and 10 GHz are shown in Figures 49 and 50. It is apparent from the figures that the 3 dB beamwidths at the 8 test frequencies vary from 48 degrees to 103 degrees with an average half-power beamwidth of 77.6 degrees. The ASN 116A antenna and a false metal end-plate lined with NZ-1 absorbing material were mounted on a circular piece of expanded polyethylene foam. The diameter of the foam was made

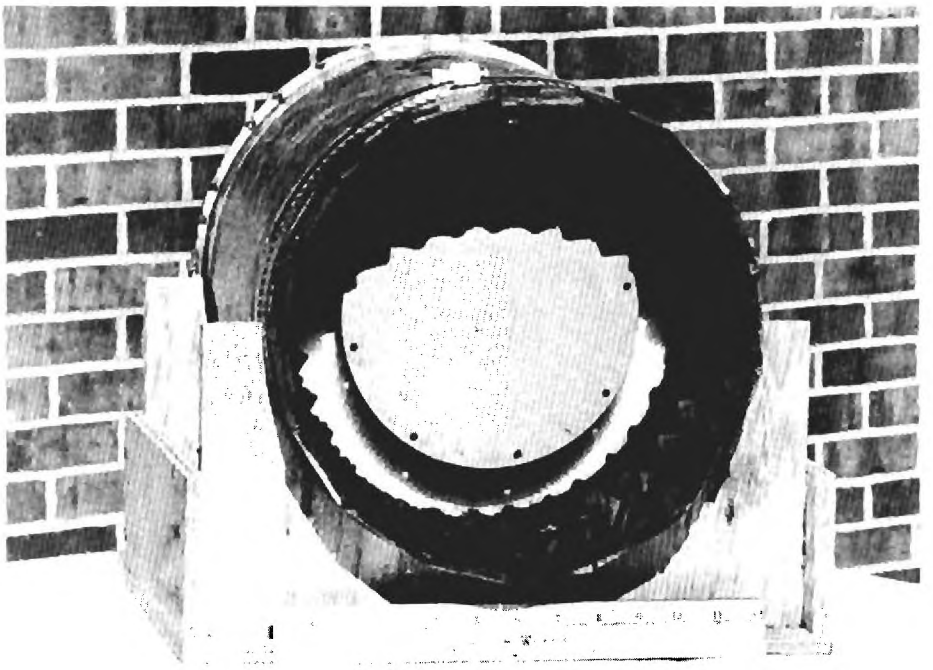

Figure 48. Adjustable-Length Hooded ASN 116A Antenna.

so that it was a tight sliding fit to the inside of the hood, and hence, was capable of supporting the antenna and false end-plate at any location along the length of the hood. The length of the hood was made 13 inches long so that this configuration made it possible to vary the distance between the aperture of the hood and the aperture of the ASN 116A antenna from zero to 4 inches.

Antenna patterns for the hooded antenna were made at five frequencies (1, 2, 3, 4 and 5 GHz) for hood lengths of 0, 1, 2, 3, and 4 inches. The best results were obtained for a hood length of 4 inches and the antenna patterns obtained with this hood length at 1, 2, 3, and 4 GHz are shown in Figure 51. The figure shows that the half-power beamwidth obtained at 1 GHz is 72 degrees. Since an objective of the hooded antenna development program is to obtain half-power beamwidths of less than 60 degrees, this beamwidth is excessive. However, a 72-degree beamwidth was obtained for all hood lengths from zero to 4 inches at 1 GHz indicating that the beamwidth is independent of hood length at this frequency. Thus it was concluded that the aperture of the hood is not sufficiently large to provide the desired directivity at this frequency. Half-power beamwidths of 42 degrees and 45 degrees were obtained at 2 and 3 GHz, respectively. These are well within the desired beamwidth

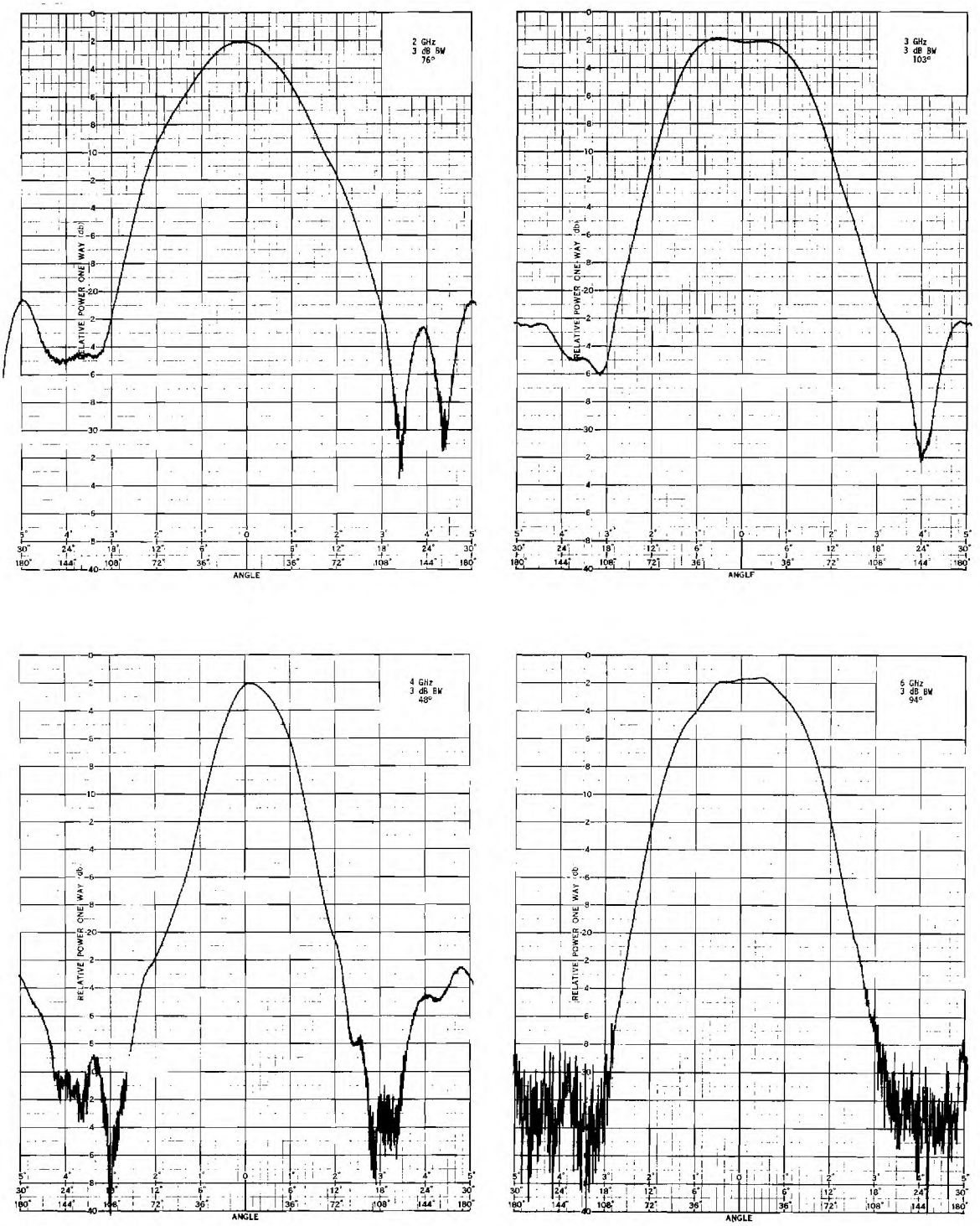

Figure 49. Antenna Patterns for Unhooded ASN 116A Antenna at 2, 3, 4 and 6 GHz.

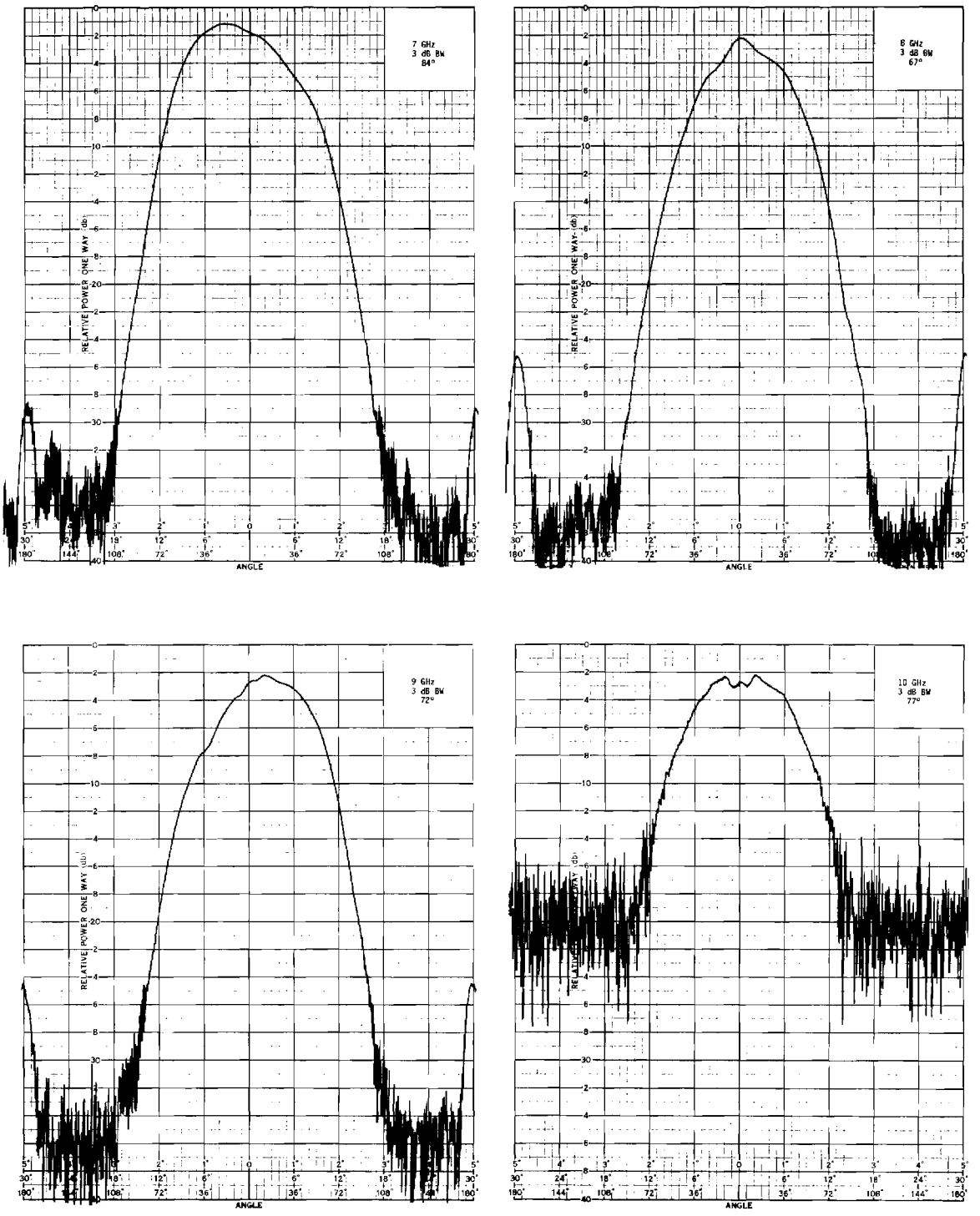

Figure 50. Antenna Patterns for Unhooded ASN 116A Antenna at 7, 8, 9 and 10 GHz.

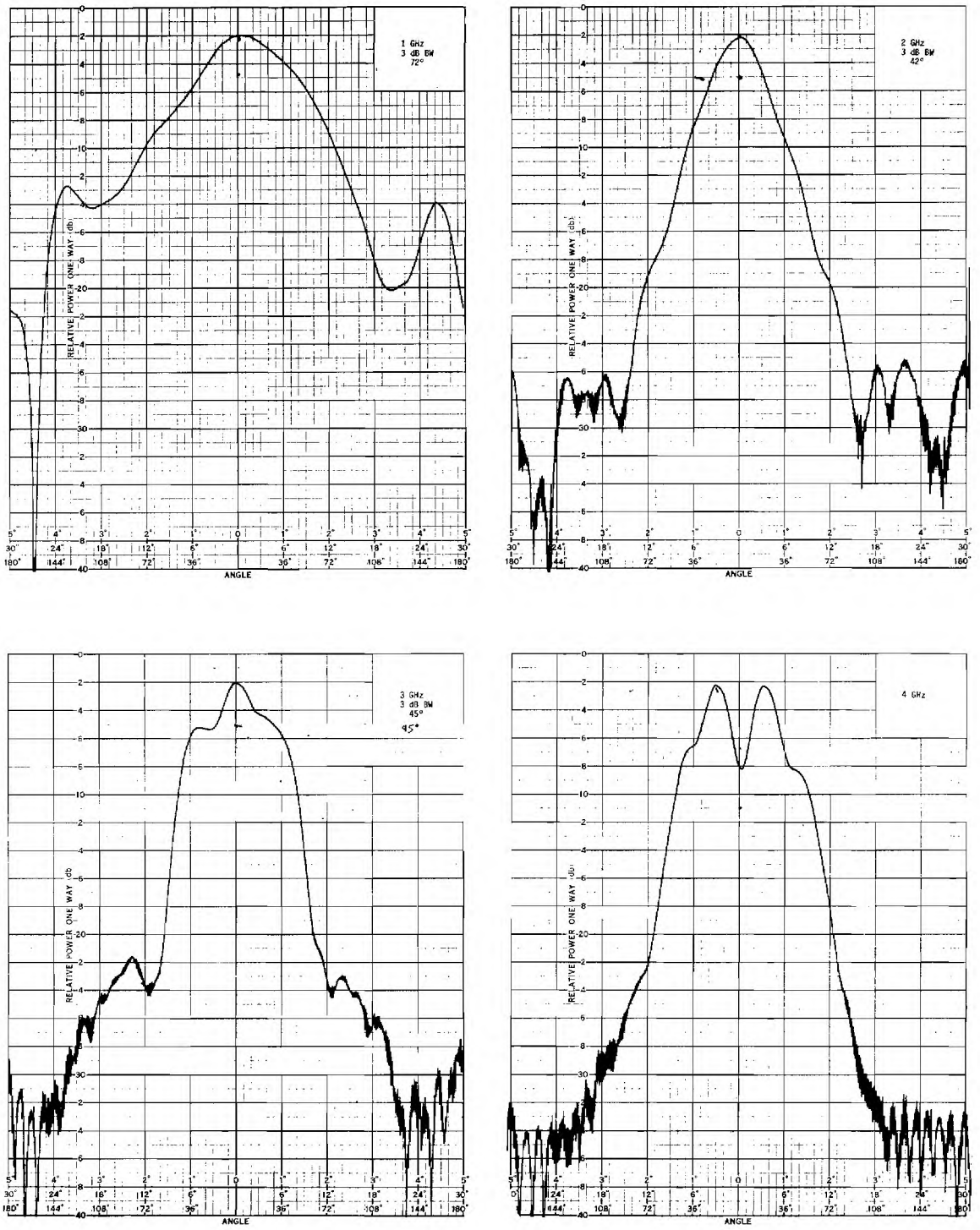

Figure 51. Antenna Patterns for Hooded ASN 116A Antenna at 1, 2, 3 and 4 GHz.

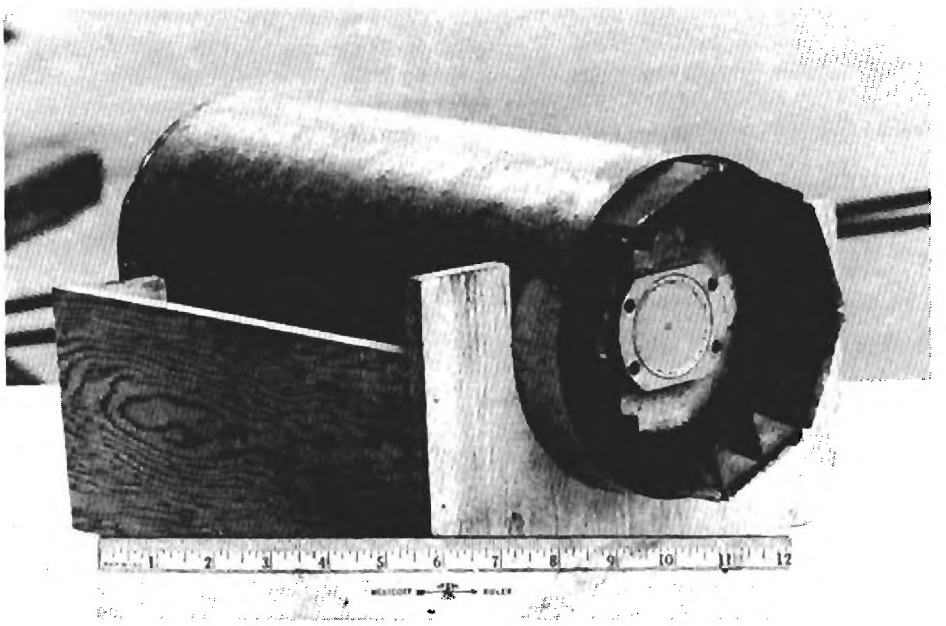

Figure 52. Adjustable-Length Hooded ASN 111A Antenna.

range of 20 to 60 degrees, and hence, indicate that the performance of the short hooded antenna is satisfactory in this frequency range. The antenna pattern obtained at 4 GHz shows that significant beam-splitting occurs at this frequency. Patterns at higher frequencies indicate that the beam-splitting becomes more severe with increasing frequency.

The results from this study indicate that (1) in order to operate down to 1 GHz, the aperture of the short hooded antenna will have to be increased slightly, possibly to an inside diameter of 12 inches, (2) the useable frequency range of a short hooded ASN 116A hooded antenna will probably cover the 1 to 3 GHz range and (3) the optimum hood length for a 1 to 3 GHz short hooded antenna is 4 inches.

4. Adjustable-Length Hooded ASN 111A Antenna

An adjustable-length hooded antenna for a lower frequency limit of 3 GHz was designed and fabricated. The objective for this antenna is to cover the frequency range from 3 GHz to as high a frequency as possible, and over its useable frequency range, to provide a half-power beamwidth in the range from 20 to 60 degrees. A photograph of this hooded antenna is shown in Figure 52. The hood is the same configuration as the ASN 116A hooded antenna, the difference being the outside diameter of this hood is 6 inches and the inside diameter is

4 inches. An AEL Model ASN 111A cavity-backed spiral antenna was used as the primary feed antenna for this hooded configuration. The ASN 111A antenna is designed to cover the 3 to 12 GHz frequency range. Antenna patterns for the basic unhooded antenna at 4, 6, 8 and 10 GHz are shown in Figure 53. It is apparent from the figure that the 3 dB beamwidths at the four test frequencies vary from 54 degrees to 84 degrees. The ASN 111A antenna and a false end-plate covered with NZ-1 material were mounted in the hood in the same manner as the ASN 116A antenna so that the antenna could be positioned at any location along the length of the hood. The length of the hood was made 13.5 inches so that the aperture of the ASN 111A antenna could be located at any distance from zero to 4 inches from the aperture of the hood.

Antenna patterns for the hooded antenna were made at six frequencies (3, 4, 5, 6, 7 and 8.5 GHz) for hood lengths of 0, 1, 2, 3 and 4 inches. The best results were obtained for a hood length of 2 inches, and the antenna patterns obtained with this hood length at the six test frequencies are shown in Figures 54 and 55. It is apparent from the antenna patterns that the half-power beamwidth of the hooded antenna over the frequency range from 3 to 8.5 GHz remains in the range from 28 to 60 degrees.

The results from this study indicate that a short hooded antenna with a 4-inch aperture and 2-inch hood length will operate satisfactorily over the frequency range from 3 to 8 GHz.

5. Final Short Hooded Probe Antennas

Results from the programs described above indicate that the 1 to 12 GHz frequency range can be covered with three short hooded antennas. The measured data indicate that a 4-inch long hooded antenna with a 12-inch inside diameter aperture will operate satisfactorily over the 1 to 3 GHz frequency range and a 2-inch long hooded antenna with a 4-inch inside diameter aperture will operate satisfactorily over the 3 to 8 GHz range. It was anticipated that a 1-inch long hooded antenna with a 2-inch inside diameter aperture will operate satisfactorily over the 8 to 12 GHz frequency range. A set of three short hooded antennas having these parameters were fabricated and tested.

Two views of the short hooded antenna designed for use over the 1 to 3 GHz frequency range are shown in Figure 56. The hood for this antenna configuration is a metal cylinder enclosed on one end and lined with Eccosorb NZ-1 ferrite absorbing material. The outside diameter of the hood is 14 inches, the inside diameter is 12 inches, and the length is 4 inches. An AEL Model ASN 116A cavity-backed spiral antenna is mounted in the center of the hood end wall.

Antenna patterns for this short hooded configuration were made over the frequency range from 600 MHz to 3 GHz. The patterns obtained

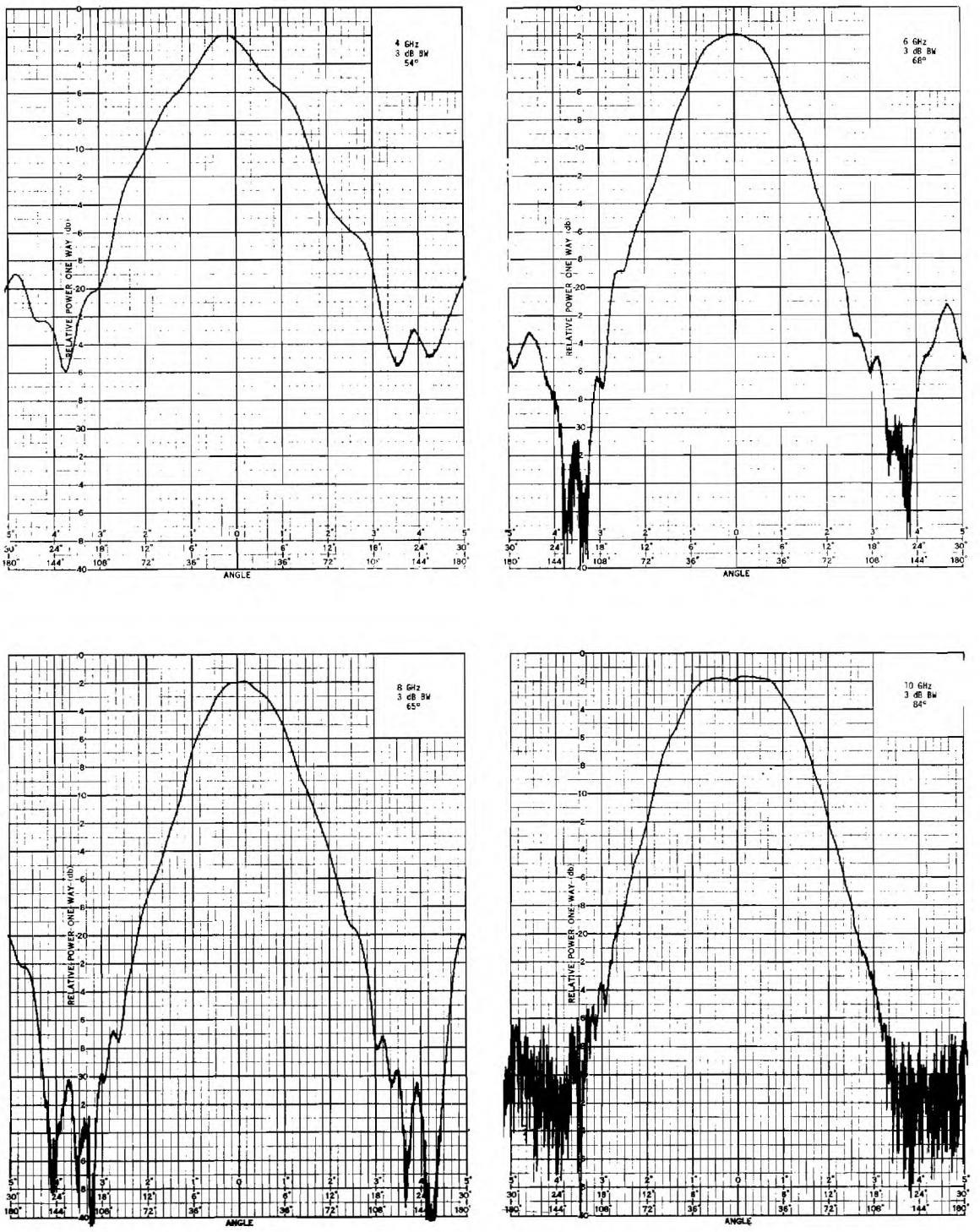

Figure 53. Antenna Patterns for Unhooded ASN 111A Antenna at 4, 6, 8 and 10 GHz.

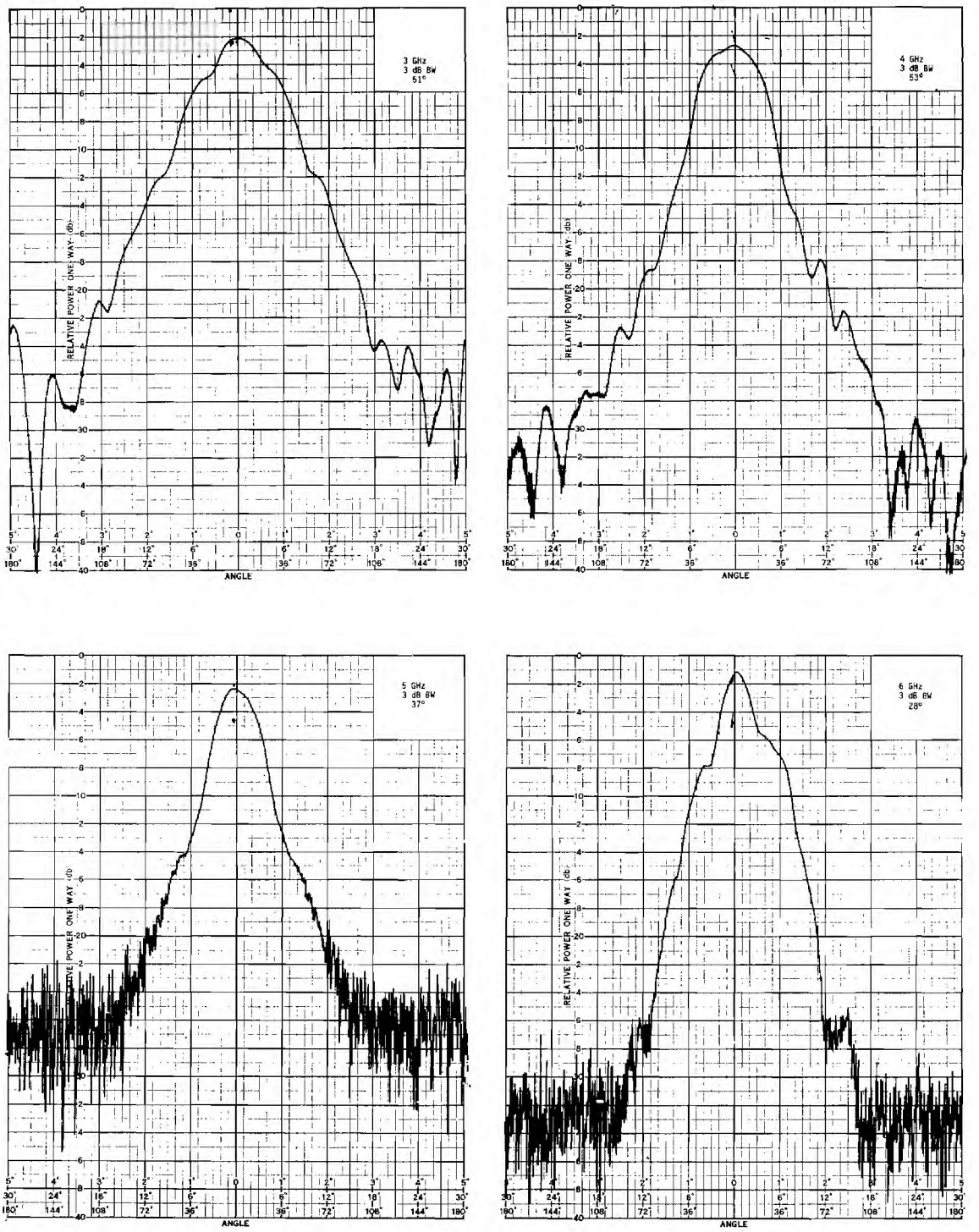

Figure 54. Antenna Patterns for Hooded ASN 111A Antenna at 3, 4, 5 and 6 GHz.

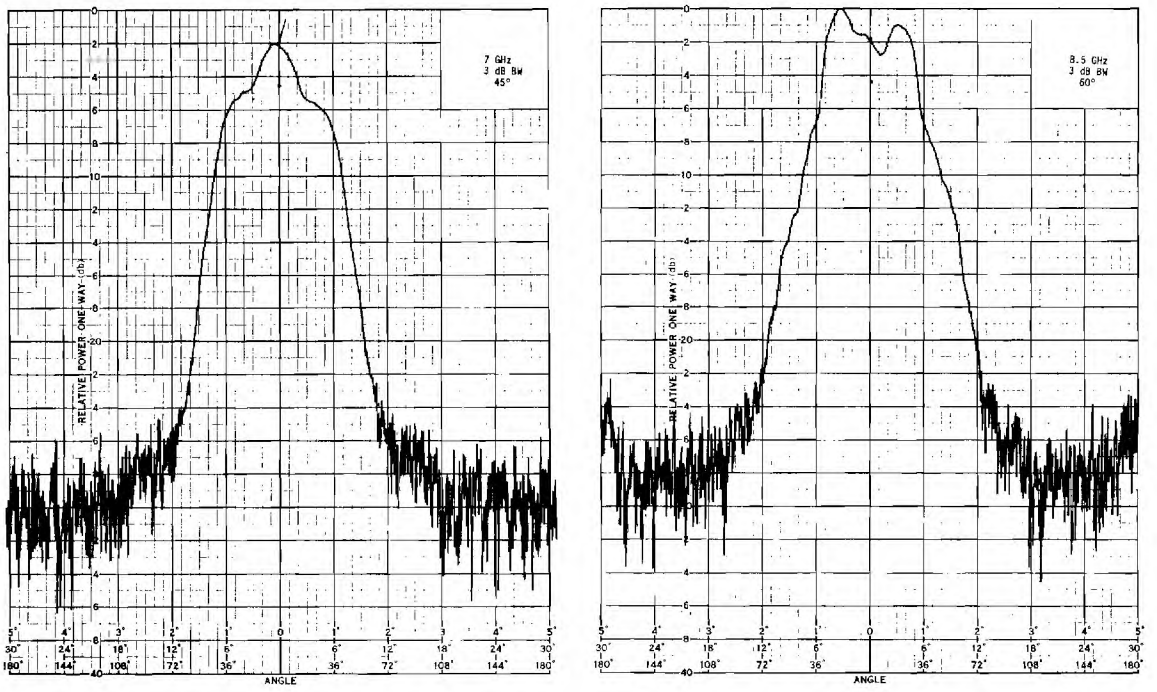

Figure 55. Antenna Patterns for Hooded ASN 111A Antenna at 7 and 8.5 GHz.

at 1, 1.5, 2 and 2.5 GHz are shown in Figure 57. At 1, 1.5 and 2 GHz the half-power beamwidths of the short hooded antenna are 60 degrees. At 2.5 GHz serious beam-splitting is apparent in the main lobe of the pattern and hence it must be concluded that this antenna is not useable above 2 GHz. At 800 and 900 MHz, the half-power beamwidths were 66 degrees which is considered excessive for use in shielded enclosures. The useable bandwidth of this hooded antenna is therefore considered to be 1 to 2 GHz.

Two views of a short hooded antenna designed for use over the 3 to 8 GHz range are shown in Figure 58. The construction of the hood for this antenna was similar to the previous antenna with the exceptions that the outside diameter is 6 inches, the inside diameter is 4 inches and the length is 2 inches. An AEL Model ASN 118A cavity-backed spiral antenna was used as the primary antenna for this hooded configuration.

Antenna patterns were made over the frequency range from 1.5 to 12 GHz. The patterns obtained at 2, 4, 6 and 8 GHz are shown in Figure 59. The half-power beamwidth at 2 GHz is 60 degrees, at 4 GHz

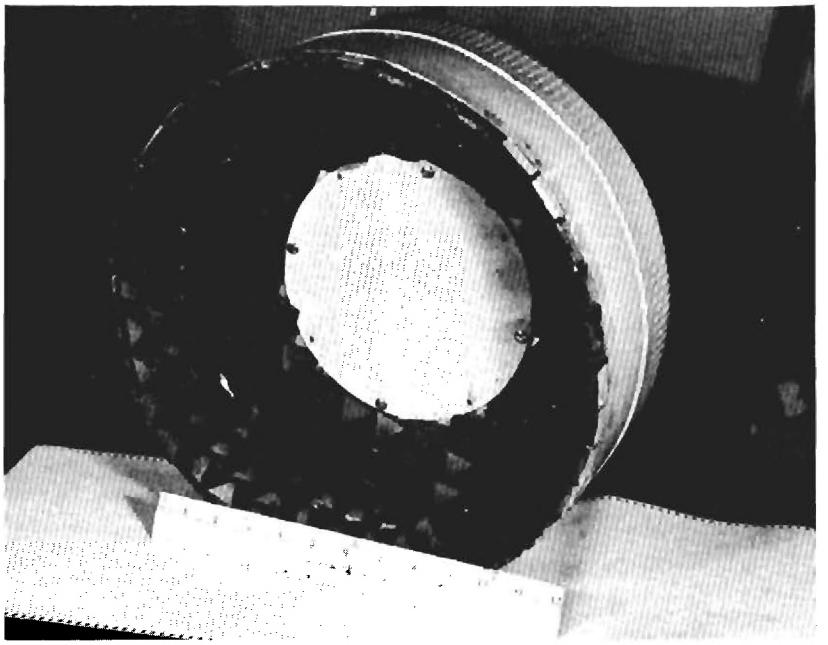

(a)

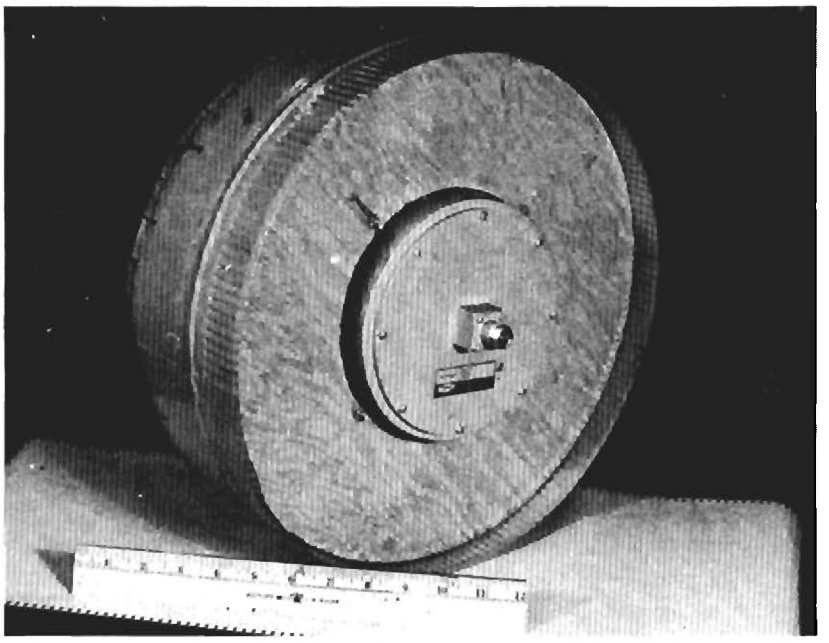

(b)

Figure 56. Two views of the 1 to 2 GHz Short Hooded Antenna.

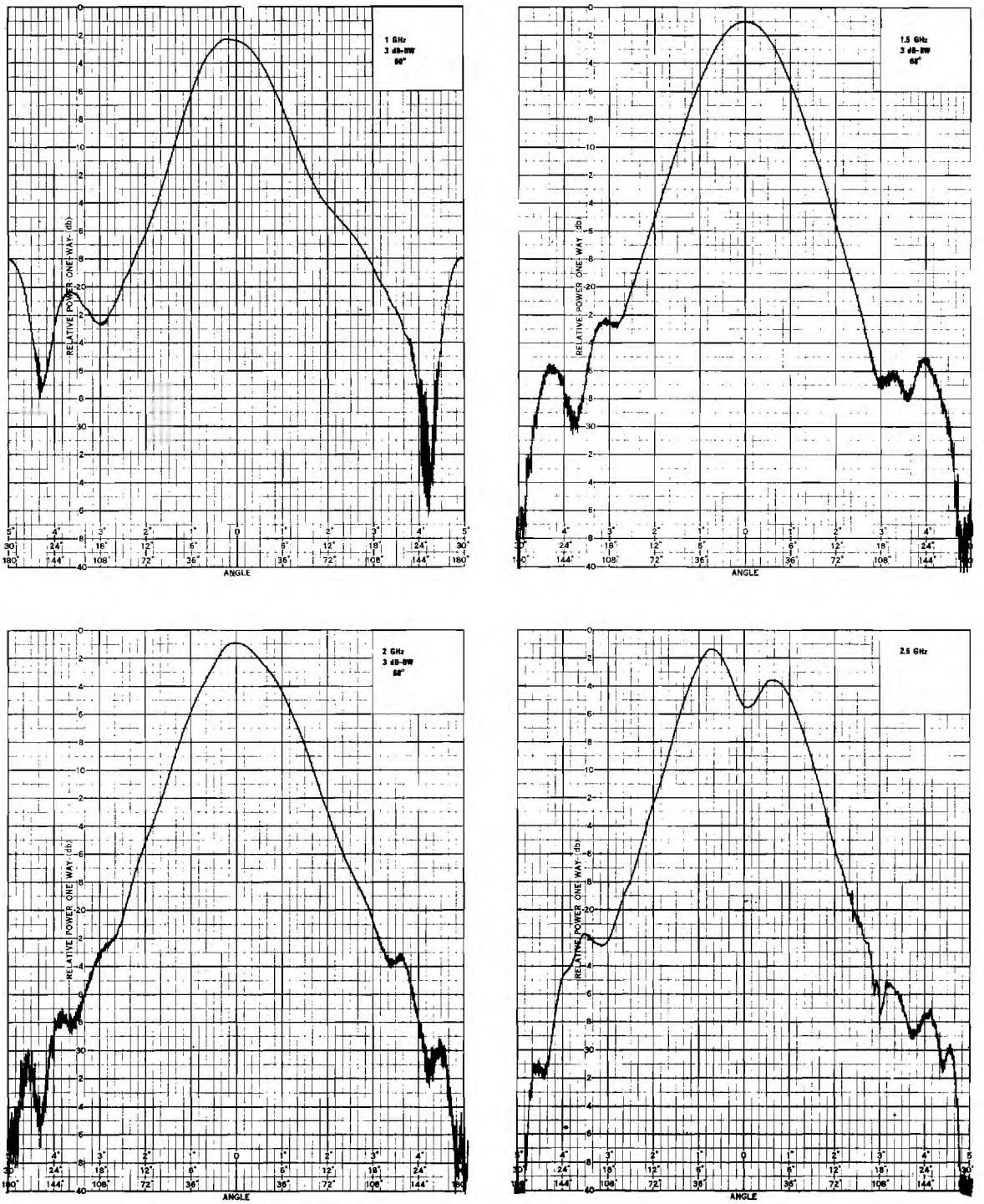

Figure 57. Antenna Patterns for the 1 to 2 GHz Short Hooded Antenna at 1, 1.5, 2 and 2.5 GHz.

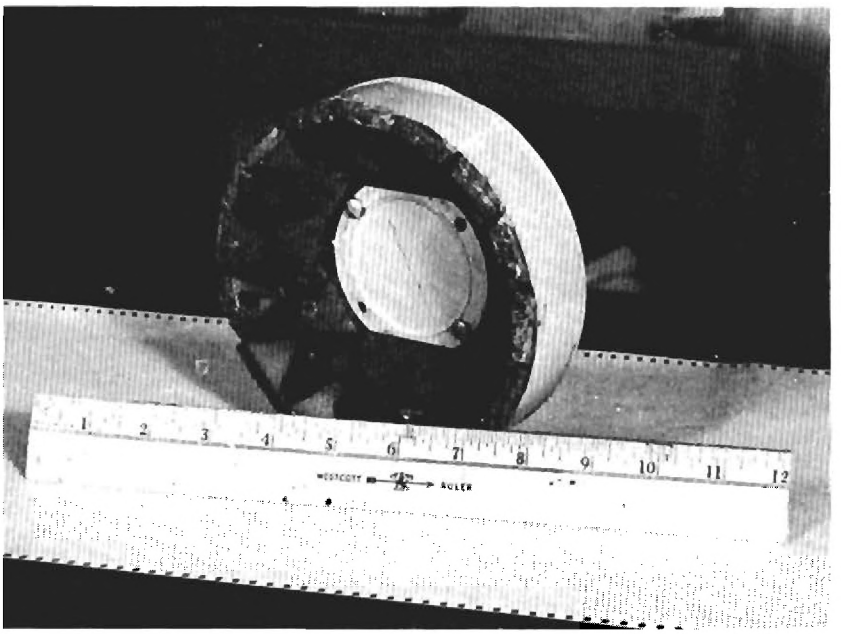

(a)

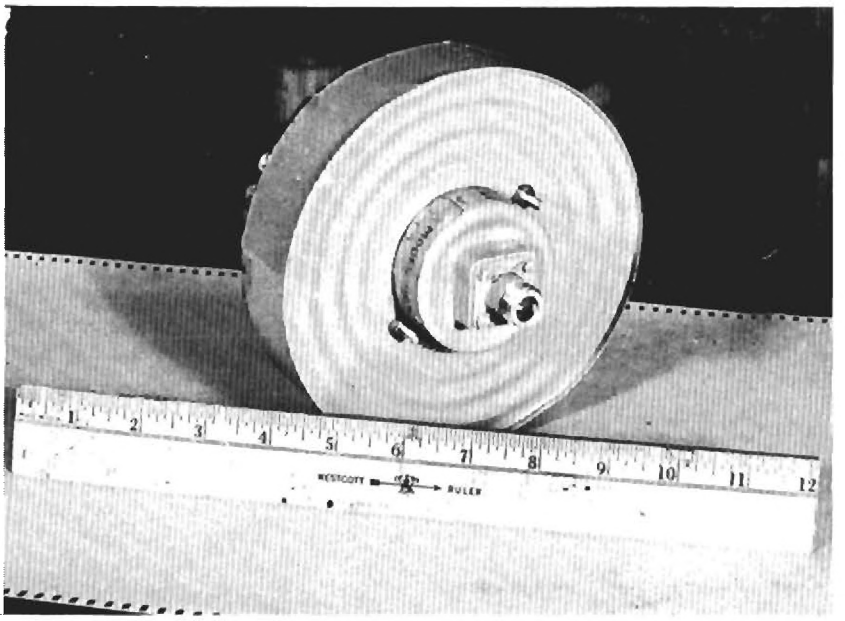

(b)

Figure 58. Two Views of the 2 to 6 GHz Short Hooded Antenna.

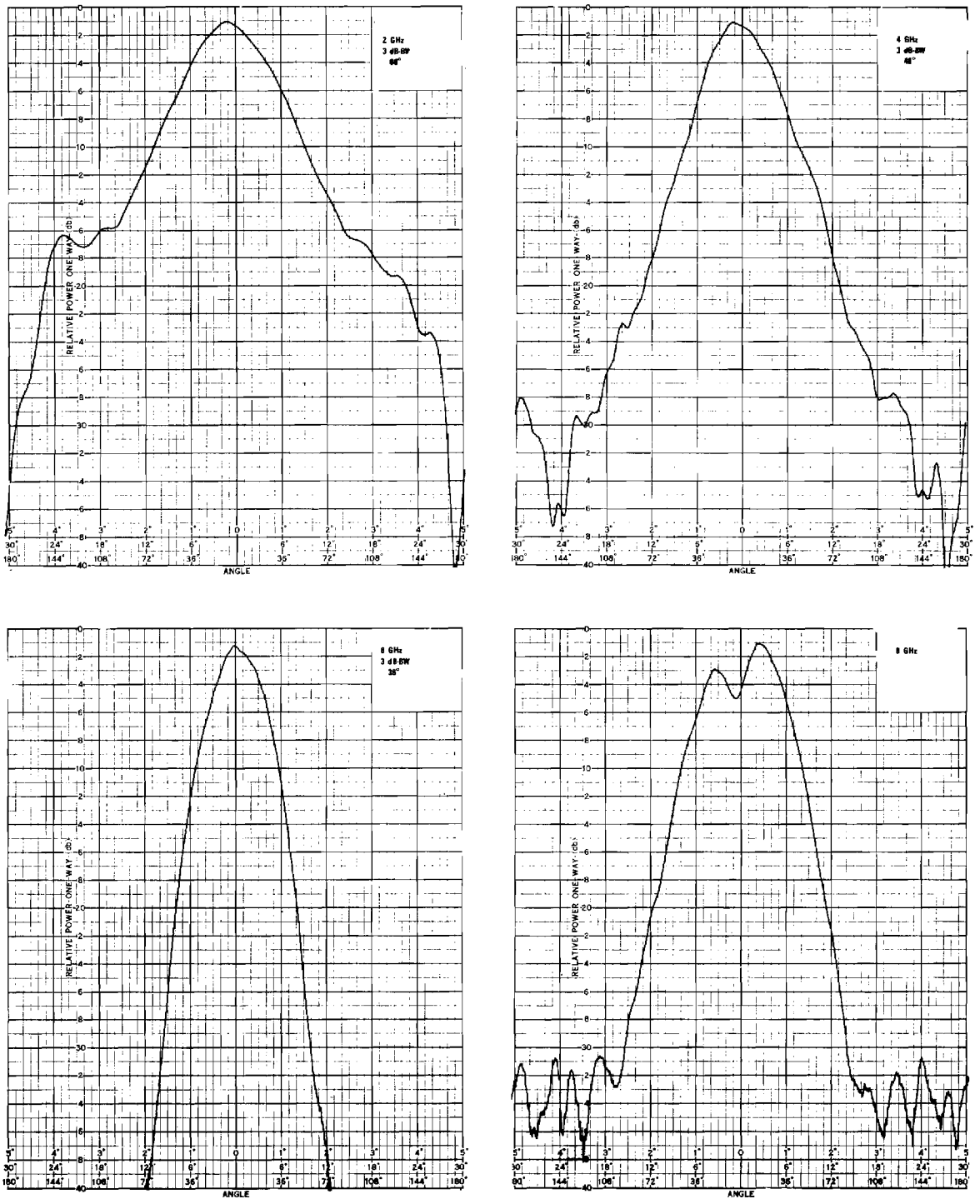

Figure 59. Antenna Patterns for the 2 to 6 GHz Short Hooded Antenna at 2, 4, 6 and 8 GHz.

it is 48 degrees and at 6 GHz it is 36 degrees. At 8 GHz beam-splitting is apparent in the main lobe of the pattern and 6 GHz is considered the upper useable frequency limit for this probe antenna. The useable bandwidth of this hooded antenna is therefore considered to be 2 to 6 GHz.

Two views of a short hooded antenna designed to cover the 8 to 12 GHz frequency range are shown in Figure 60. The hood is similar to the other two hoods with the exceptions that the outside diameter is 4 inches, the inside diameter is 2 inches, and the length is 1 inch. An AEL Model ASN 111A cavity-backed spiral antenna was used as the primary antenna.

Antenna patterns were made over the frequency range from 4 to 12 GHz. The patterns obtained at 5, 7, 10 and 12 GHz are shown in Figure 61. The half-power beamwidth is 54 degrees at 5 GHz, 38 degrees at 7 GHz, 30 degrees at 10 GHz and 32 degrees at 12 GHz. Hence, the antenna meets the 20 to 60 degree beamwidth criteria over the entire range and the useable bandwidth of this antenna is considered to be from 5 to 12 GHz.

6. Summary and Conclusions

A set of three short hooded probe antennas were developed to cover the 1 to 12 GHz frequency range. The evaluation of these antennas reveals that the half-power beamwidths of these antennas are maintained within the limits of 20 to 60 degrees over the entire frequency range. This beamwidth range provides sufficient direcitivity to reject the multipath reflections from the enclosure sidewalls, floor and ceiling, and at the same time, provides adequate beamwidth to illuminate most test specimens at reasonably short ranges.

While short hooded probe antennas for use below 1 GHz were not developed on this program, it is not expected that any appreciable difficulty would be encountered in extending the short hooded antenna coverage down to 200 MHz with two additional hooded antennas. Experience with long hooded antennas on previous programs has demonstrated that the hooded antenna technique works quite well down to approximately 200 MHz.

On the basis of results from this short hooded antenna program, it is concluded that reliable radiated measurements, which can be correlated with open-field measurements, can be made in shielded enclosures over the frequency range from 200 MHz to 12 GHz. Results from this program also indicate that in addition to being smaller, lighter and less costly, the short antenna hood yields a more constant beamwidth as a function of frequency than a long antenna hood.

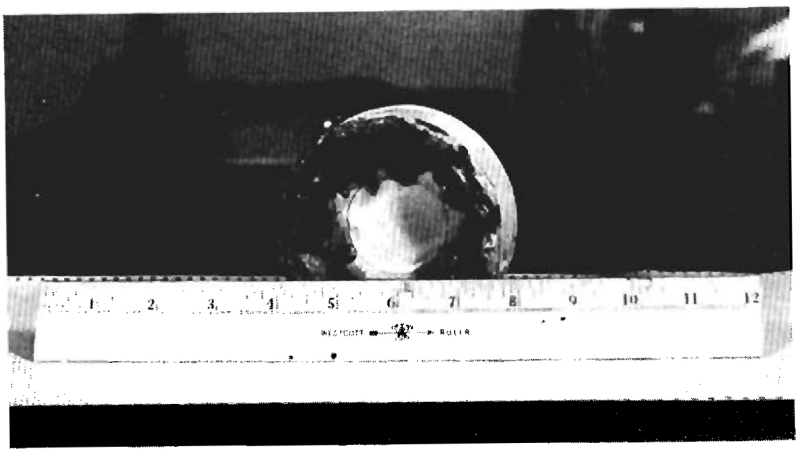

(a)

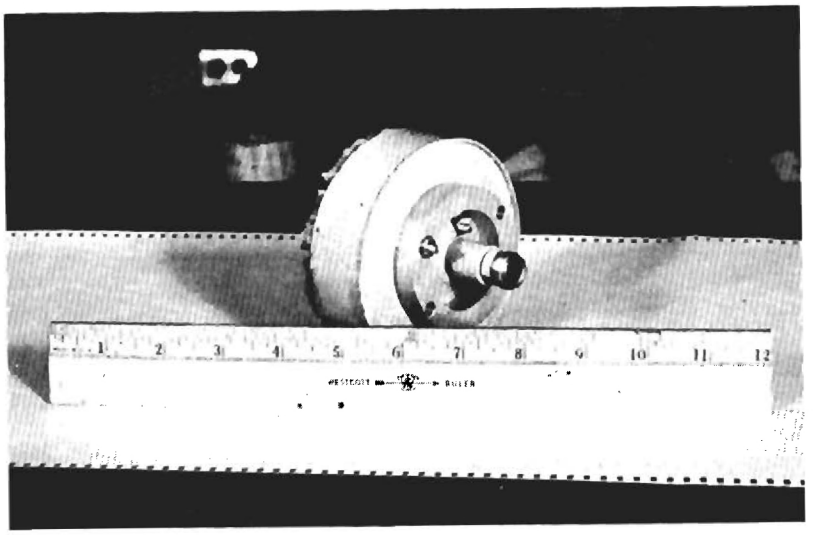

(b)

Figure 60. Two Views of the 5 to 12 GHz Short Hooded Antenna.

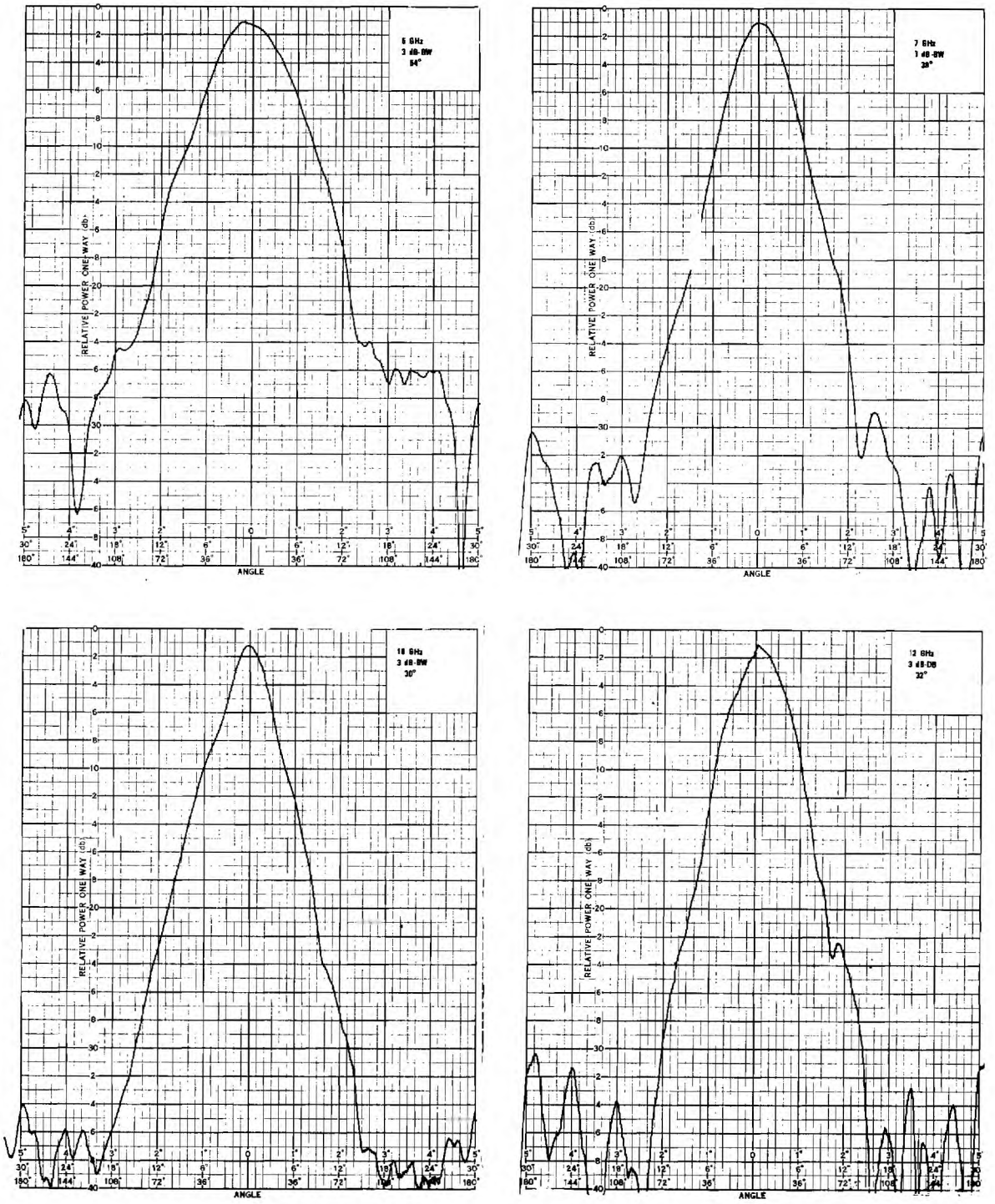

Figure 61. Antenna Patterns for the 5 to 12 GHz Short Hooded Antenna at 5, 7, 10 and 12 GHz.

D. Low Frequency Measurements

1. General

In the frequency range below 20 MHz there is apparently good correlation between radiated measurements made in shielded enclosures and the equivalent measurements made in the open-field. This is apparently due to the fact that (1) the dimensions of most shielded enclosures are too short to support significant multipath effects at the long wavelengths involved and (2) the side wall coupling is so small that there is no significant effect on the boresight coupling of the probe antenna.

However, there are some measurement problem areas in this frequency range which apply to both shielded enclosure and open-field measurements. These problems are primarily concerned with the efficiency of probe antennas in this frequency range and the interpretation of measurement results obtained in the near-field of a radiating source. These areas were investigated during this program and are discussed in the sections below.

2. Measurements Below 1 MHz

Extensive measurements of the coupling between two 30-inch bow-tie antennas in an 8 x 8 x 20 foot shielded enclosure were made over the frequency range from 1 to 150 MHz on previous programs. Equivalent coupling measurements were performed over the 200 kHz to 1 MHz frequency range on this program. The configuration used in performing these measurements is shown in Figure 62.

The signal generator used for these measurements was a Hewlett-Packard 606A. The signal generator output was set to +20 dBm to achieve the maximum overall system signal level. While it is recognized that the Emerson and Cumings HPY-72 absorbing material located on the back wall of the 8 x 8 x 20 foot enclosure provided no absorption at the frequencies of interest, the material was left in place as a matter of convenience. The source antenna was located 93 inches from the end wall of the enclosure.

The Empire Devices NF-105 receiver (NFIM) was calibrated by inserting 120 dB of attenuation at the Hewlett-Packard 335-D step attenuator and 20 dB of internal attenuation at the NFIM. The NFIM gain was adjusted for a +10 dB indication on the meter when the antenna cables were connected straight through. As shown in the block diagram, the measuring equipment was located in a separate shielded enclosure to avoid interference from high intensity local radio stations. Double

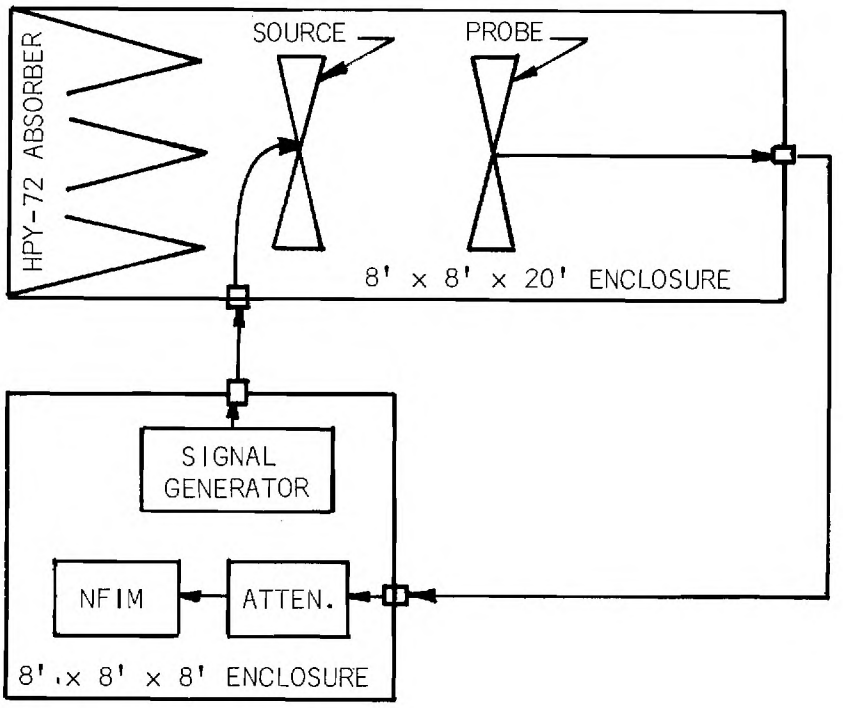

Figure 62. Block Diagram of Low Frequency Coupling Measurement Configuration.

shielded cables were used between the two enclosures. The noise level was found to be over 18 dB below the above indicated reference calibration level; a total system dynamic range of about 150 dB was thus achieved.

Antenna coupling measurements were made in two inch increments at antenna separation distances of from 12 inches out to the point at which the coupling loss exceeded 150 dB relative to the straight through connection between the antenna cables. Figure 63 shows a typical view inside the 8 x 8 x 20 foot enclosure during the low frequency antenna coupling measurements. A complete set of measurements was made at each 100 kHz frequency increment between 200 kHz and 1 MHz.

Figure 64 shows antenna coupling as a function of separation distance for the two 30-inch bow-tie antennas in the shielded enclosure at each measurement frequency. As seen from this figure a family of roughly parallel coupling curves are generated which fall off quite sharply with distance and frequency as a result of being in the near-field of the antennas. An alternate method of viewing the data is shown in Figure 65, which shows coupling as a function of frequency

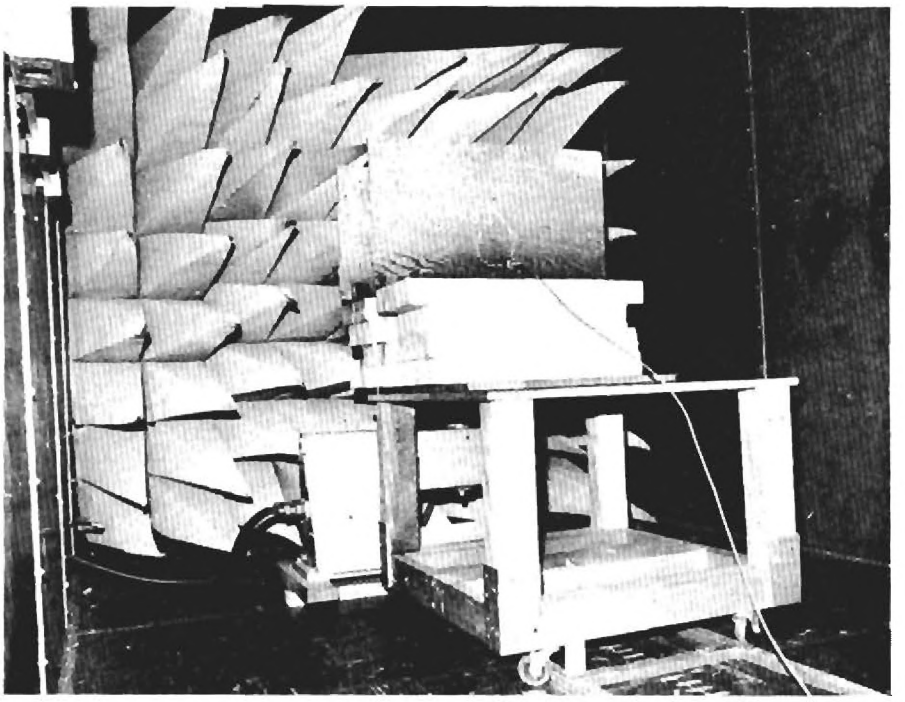

Figure 63. View of Low Frequency Measurement Setup Inside an 8 x 8 x 20 Foot Shielded Enclosure.

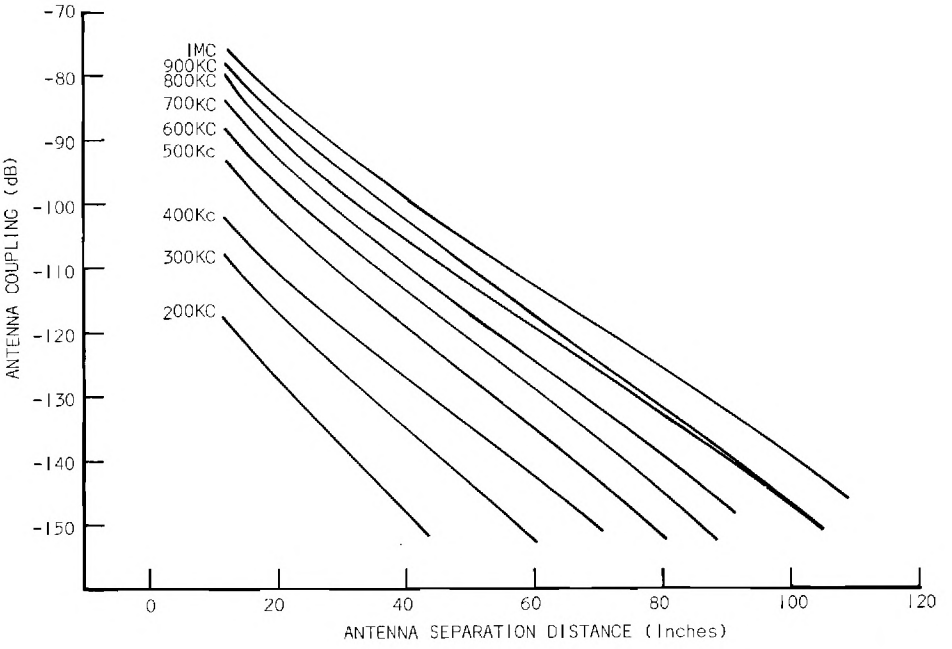

Figure 64. Antenna Coupling as a Function of Separation Distance for Two 30-Inch Bow-Tie Antennas in a Shielded Enclosure.

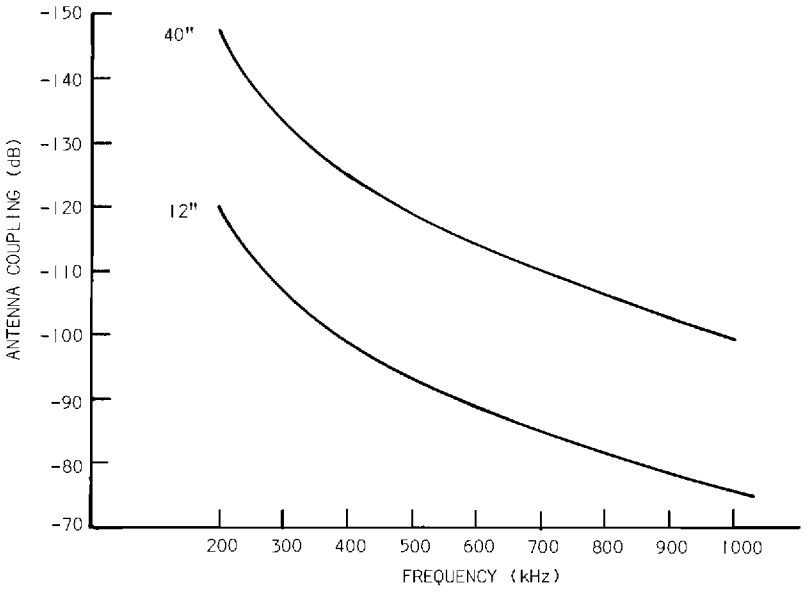

Figure 65. Antenna Coupling as a Function of Frequency for Two 30-Inch Bow-Tie Antennas in a Shielded Enclosure.

at antenna separation distances of 12 and 40 inches. These curves fall off with frequency at a nominal rate of 18 dB per octave as is predicted by the near-field equations for short dipole antennas.

On the basis of these measurement results, it was concluded that radiated measurements performed in shielded enclosures over the 200 kHz to 1 MHz frequency range would yield essentially the same results as equivalent measurements performed in the open-field.

3. Low Frequency Probe Antennas

The majority of the probe antennas currently used to make radiated EMC measurements in the 14 kHz to 20 MHz frequency range are very inefficient. In many cases, no attempt is made to match the antenna impedance to the input impedance of the field intensity meter; in other cases, narrowband matching is provided, but this approach requires frequent switching of matching networks or frequent antenna changes. In still other cases, unbalanced probe antennas are used which significantly effect the repeatibility of the measurement results. With an unbalanced

antenna, the transmission line becomes an integral part of the antenna, and hence, the measurement results are influenced by both the length and routing of the transmission line. In view of these problems, consideration was given to establishing a technique for obtaining a satisfactory broadband matched, balanced probe antenna for use in the 14 kHz to 20 MHz frequency range.

A number of programs concerned with the development of compact efficient antennas are currently in progress. The literature from several of these programs was analyzed. This literature is listed in the bibliography in the appendix. The majority of the programs studied were attempting to improve the efficiencies of small antennas by incorporating active elements into the antenna structure. While the integration of active components into small antenna structures is a valid approach to improving the efficiencies of the antennas, this technique has a number of problems associated with it. First of all, in most cases, it is necessary to provide power to the active elements. This requires additional wiring to the antenna or the use of batteries which necessitates frequent maintenance. If the antenna is made broadband, it is possible that high level undesired signals or very broadband spectrums will (1) burnout the active elements, (2) saturate the active elements, (3) cause intermodulation in the active elements, and/or (4) change the bias on the active elements and hence, change the gain characteristics of the antenna. In addition, integrated antennas are not normally reciprocal and hence the antenna must be designed specifically for either the receiver or radiate mode. For applications requiring the radiation of considerable power, the active element technique is considerably less attractive than for receiving and other very low power applications. One argument for the active element antenna is that it is possible to obtain additional gain from the active elements. It should be pointed out, however, that unless the noise figure of the active elements in the antenna is considerably better than the noise figure of equipment to be used in conjunction with the antenna, the additional gain is of little consequence. Considering all of the disadvantages and possible problem areas associated with the active antenna technique, it was concluded that this approach to obtaining satisfactory, efficient probe antennas for the 14 kHz to 20 MHz frequency range would require considerable improvement in the state-of-the-art of active antennas.

Several of the programs that were studied attempted to improve the efficiencies of small antennas by loading the antenna structures with materials having high permeability and permittivity characteristics. This technique is based on the concept that the velocity of propagation of a wave through a medium is inversely proportional to the square root of the product of the permeability and permittivity of the medium. Hence, if a high permeability, high permittivity material is placed on the surface of an antenna structure, a slow wave mode is established on the surface of the antenna and the effective electrical size of the antenna is increased.

Some success has been obtained in reducing the size of antennas by loading with ferrite materials. Typical reductions that have been obtained are in the order of $\frac{1}{3}$ or $\frac{1}{5}$. Unfortunately, the loading technique does not increase the bandwidth of the antennas and the losses in the loading materials degrade the efficiencies of the antennas to approximately 80 or 90 percent of their unloaded values. It was concluded that at this time the antenna loading technique does not appear to be a useful approach to obtaining satisfactory low frequency probe antennas.

A technique which appears to have considerable potential for obtaining broadband matching in small low frequency antennas is presented in a MSEE thesis by D. E. Gentry.[6] The technique is based on the fact that the impedance of a small antenna is predominately reactive and that the value of the equivalent lumped constant reactive component does not change appreciably over a considerably wide frequency range. Gentry shows that the impedance of a single turn 12-inch diameter loop over the 1 to 30 MHz frequency range can be assumed to be a resistor of less than 1 ohm (including both the radiation and copper resistance) in series with a 1 microhenry inductor. Since the reactive part of the antenna impedance can be assumed to act as a fixed value inductor over this frequency range, it can be incorporated into a synthesized filter network as the leading element in the filter. Once this is accomplished, the only remaining task to match the antenna to the load is to obtain maximum power transfer from the low radiation resistance of the antenna to the load resistance. This can also be accomplished in the filter synthesis. Considering the small radiation resistance of the loop antenna over the 1 to 30 MHz frequency range (less than 1 ohm) and assuming that test equipment used with the antenna will have 50 ohm impedances, the filter could be designed for a zero source impedance and a 50 ohm output impedance.

Gentry designed several Butterworth and Tschebyscheff filter networks from Weinbergs tables[7] and evaluated their performance with a loop antenna to validate the matching technique. Figure 66 shows Gentry's calculated and measured response of an unmatched 12-inch loop antenna with a 50 ohm receiver. The figure shows that the response of the unmatched loop decreases by approximately 12 dB as the frequency is increased from 1 to 30 MHz. Figure 67 shows the calculated and measured response of the same loop antenna matched to the 50 ohm receiver with a simple 3-element low-pass filter. The loop antenna acts as a 1 microhenry inductor in the filter network. The figure shows that the response is essentially flat (within the 1 dB filter ripple) from 1 to 15 MHz. The apparent 6 dB loss in response between Figures 66 and 67 is due to the measurement setup used for the experimental measurements and is not inherent in the matching technique. The insertion loss of the filter matching network is considerably less than 1 dB. Figure 68 illustrates the matching characteristics obtained with a simple 3-element bandpass filter. Figure 69 shows the results obtained with a slightly more complex 5-element bandpass filter.

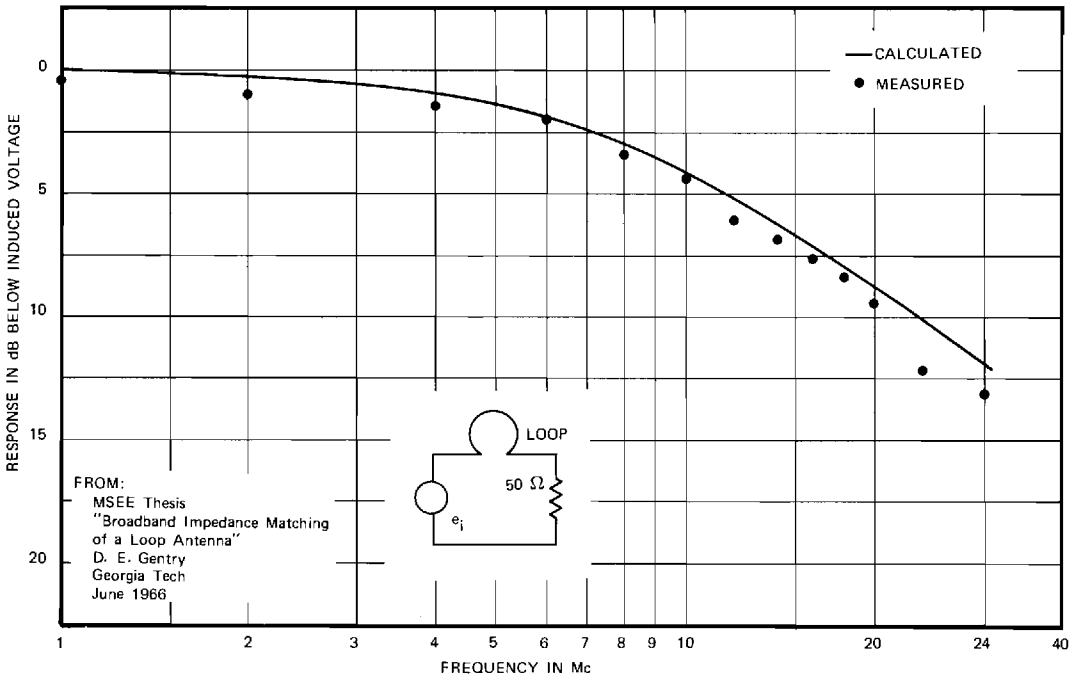

Figure 66. Response of a 12-Inch Loop Antenna.

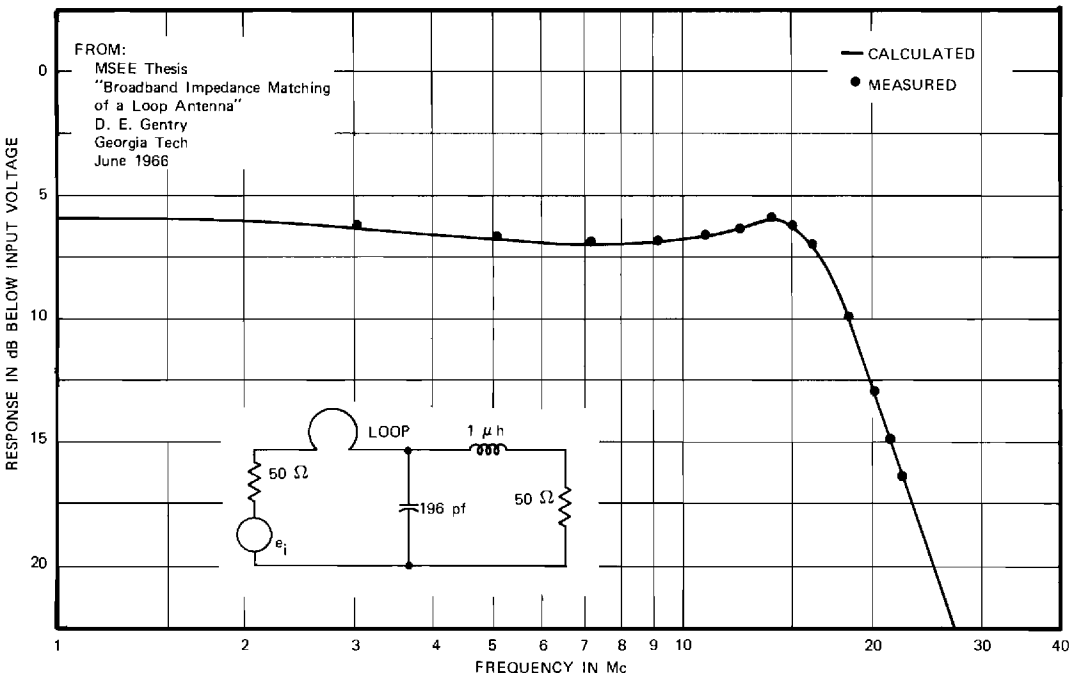

Figure 67. Response of a Three Element Chbychev Lowpass Filter with a 1 dB Ripple (R_S = 50 ohms).

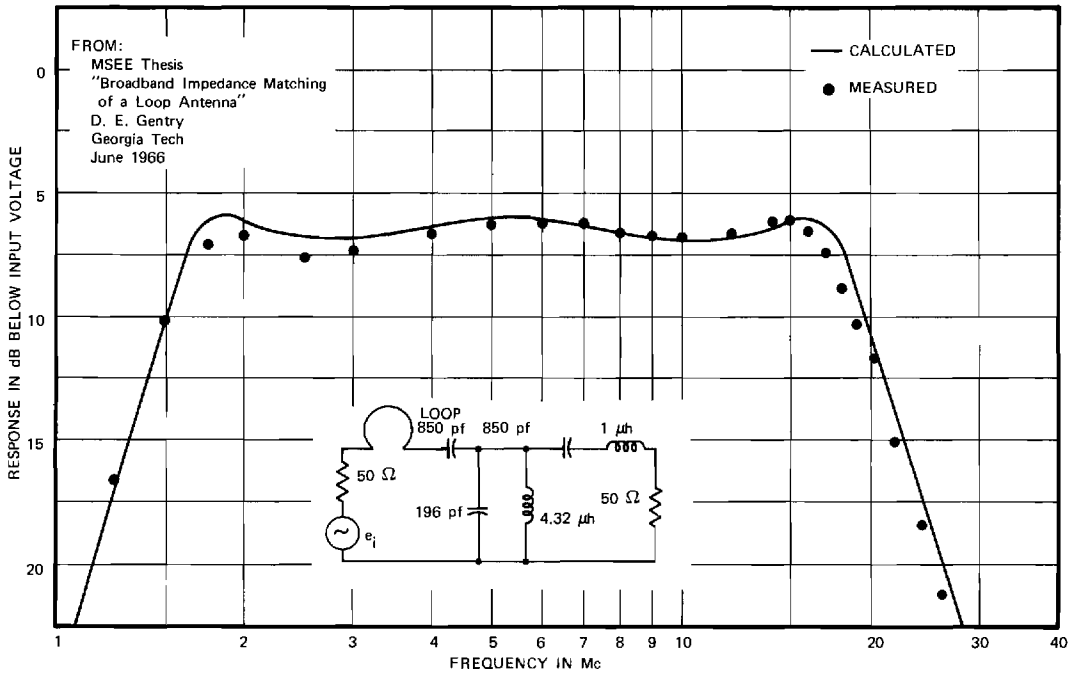

Figure 68. Response of a Three Element Chebychev Bandpass Filter with a 1 dB Ripple (R_s = 50 ohms).

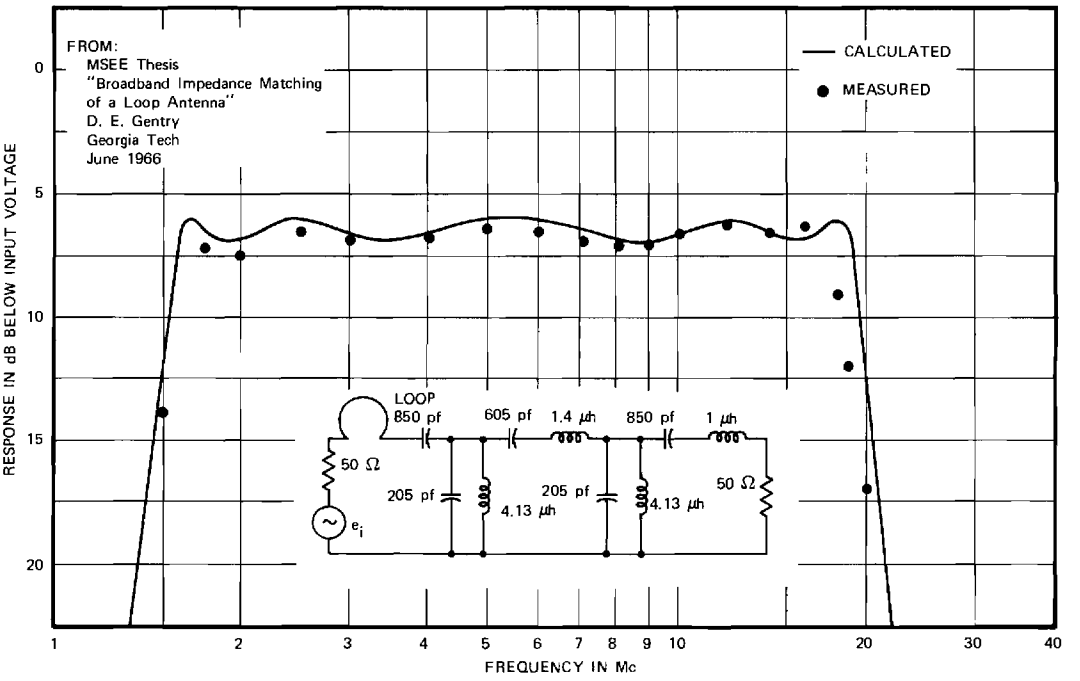

Figure 69. Response of a Five Element Chebychev Bandpass Filter with a 1 dB Ripple (R_s = 50 ohms).

The results obtained with these relatively simple filter networks are quite impressive and tend to indicate considerable potential for this technique in obtaining broadband, low frequency probe antennas. A possible broadband, balanced loop probe configuration incorporating a filter matching network is shown in Figure 70. The upper diagram is a pictorial representation showing how the filter matching network is integrated with the loop antenna. As shown in the diagram, a symmetrical filter network is utilized to obtain a balanced probe. An impedance transformer (T_1) is included in the filter to match the radiation resistance of the loop to the load impedance. The lower diagram is an equivalent circuit schematic of the loop antenna, filter and load. This diagram shows how the equivalent circuit of the loop fits into the filter network.

Figure 71 shows the equivalent configuration for a short dipole antenna. Note that since the reactive part of a short dipole antenna is capacitive, the leading element of the matching filter network must be capacitive. This dictates that the filter network must be either a highpass or bandpass filter, and hence, the lowest frequency at which the dipole probe can be used will be limited. It is concluded that additional study is warrented in applying this technique to the development of low frequency probe antennas.

4. Near-Field Measurements

While it has been concluded that radiated measurements performed in shielded enclosures over the 14 kHz to 20 MHz frequency range will yield essentially the same results as equivalent measurements performed in the open-field, there is considerable question as to the value of measurement results obtained in either location over this frequency range with the measurement techniques currently being utilized. The present measurement procedures specify that the probe antenna be located either one foot or one meter from the unit being tested. This close proximity of probe and source in terms of wavelength greatly increases the probability of measurement error assignable to near-field effects.

Accurate measurements become increasingly more difficult as the distance between a measurement probe and the radiating source is reduced. For purposes of describing some of these measurement difficulties, the space surrounding a radiating source antenna will be considered to be divided into three separate regions. These three regions, the boundaries of which are not precisely defined, are referred to in this discussion as (1) the radiation far-field, (2) the radiation near-field, and (3) the reactive near-field.

The radiation far-field region is generally considered to extend from infinity to a distance of $2D^2/\lambda$ from the source, where D is the

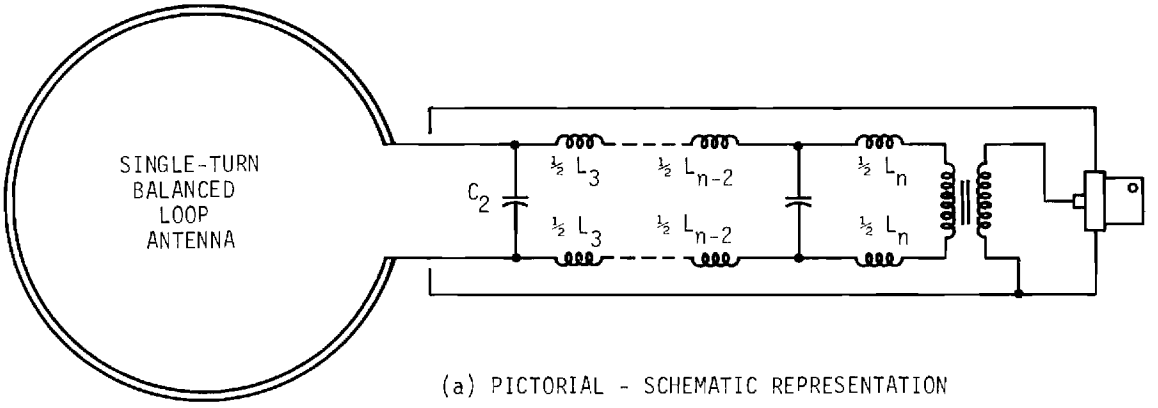

(a) PICTORIAL - SCHEMATIC REPRESENTATION

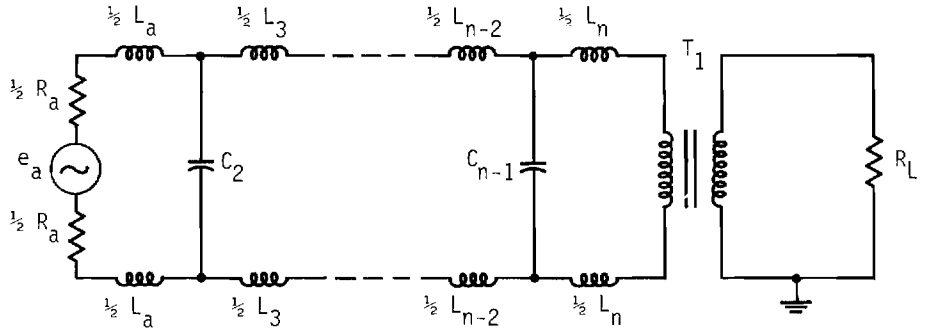

(b) Equivalent Circuit Representation

Figure 70. Broadband Matched, Balanced, Single-Turn Loop Antenna.

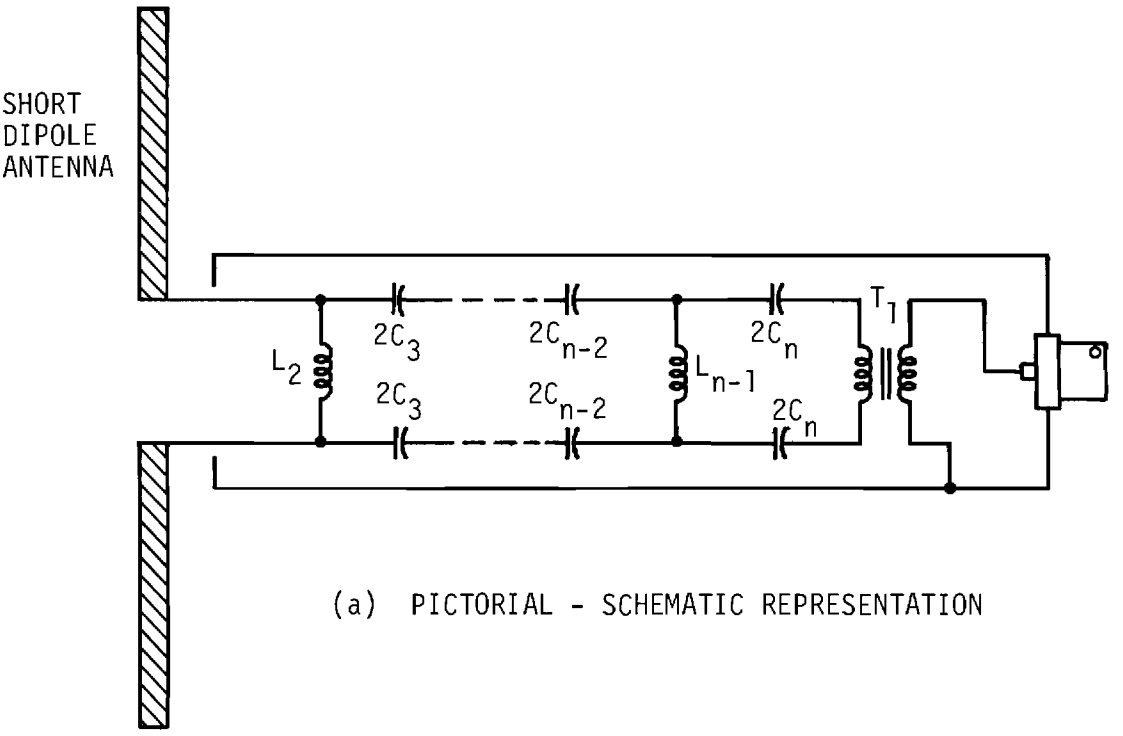

(a) PICTORIAL - SCHEMATIC REPRESENTATION

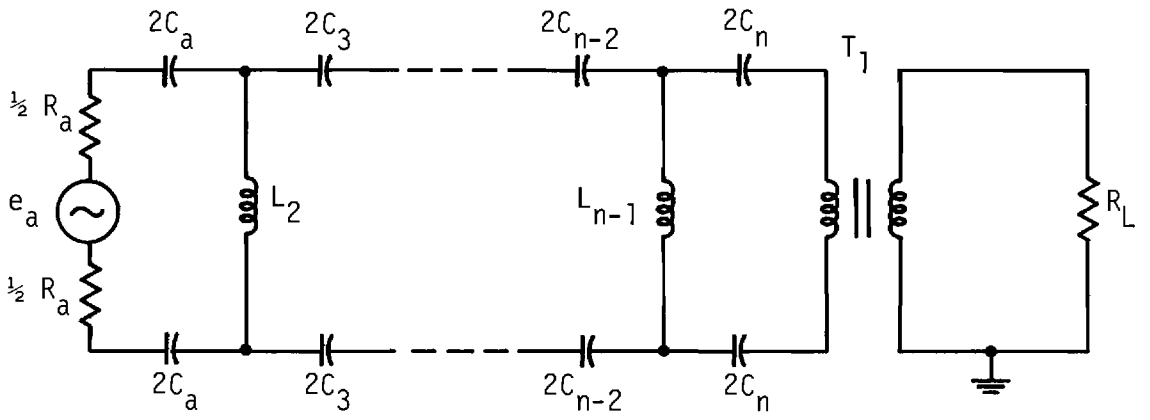

(b) EQUIVALENT CIRCUIT REPRESENTATION

Figure 71. Broadband Matched, Balanced, Short Dipole Antenna.

largest linear dimension of the source antenna aperture and λ is the operating wavelength. It is at this $2D^2/\lambda$ separation distance that measurement inaccuracies introduced by the non-planar nature of the radiated wave begin to become apparent. It should be pointed out that although a source-to-probe separation distance of $2D^2/\lambda$ is generally accepted as the boundary between the radiation far-field region and the radiation near-field region, the effective boundary for a given application is dependent upon the magnitude of the error in measured or calculated power density which is acceptable in the particular situation. In the radiation far-field region, calculations of field patterns with Fourier integral techniques usually yield very satisfactory approximations. Similarly, probe antennas calibrated in a planar field generally yield accurate measurement results anywhere in the radiation far-field.

The radiation near-field region is usually accepted as extending from the far-field boundary to within a few wavelengths of the radiating source. In this region the field pattern of the source is a function of distance from the source; both the relative phase and relative amplitude of field contributions from different elements of the source change appreciably with distance. Thus, the non-planar nature of the radiated wave is more pronounced, and significant power density measurement errors arising from the use of a probe antenna calibrated in a planar field can occur. This fact is particularly important when the power density measurements made with the probe do not include the potentially significant contributions of the radially polarized field components.* In the radiation near-field region, calculations of field patterns usually involve approximations of the fields by integrals of the Fresnel form. These approximations become increasingly inaccurate as distance to the source is decreased.

It should be recognized that the probe antenna also has radiation near-field and far-field regions. The boundary of these regions is also generally accepted to be $2D^2/\lambda$, where D is the largest linear dimension of the probe antenna aperture. If the probe antenna is used for making measurements at source-to-probe separation distances within the radiation near-field region of the probe itself, severe inaccuracies in measured power density can arise from phase variation across the probe aperture. At these separation distances, both the gain of the probe antenna and the source radiation pattern become dependent on source-to-probe separation distance.

---

*It is assumed throughout this discussion that the probe antenna responds equally to all polarizations of plane waves or that the probe can be used to determine the components of a plane wave which can be summed to yield total power density.

That region of space immediately surrounding a source is referred to as the reactive near-field region. In the radiation far-field region and, to a lesser extent, in the radiation near-field region, a propagating or radiating field predominates. The magnitude of this field varies inversely with the distance from the source. In the reactive near-field region the induction and static* fields predominate. The magnitude of the induction field varies inversely with the square of the distance from the source and the magnitude of the static field varies inversely with the cube of the distance. In the region where these reactive fields predominate, relatively little time average energy flow associated with radiated power exists. Instead, most of the energy flows outward and inward in a cyclic manner and these fields may be thought of as alternately expanding and collapsing at the operating frequency. The induction and static fields are normally thought of as "stored energy" fields, as differentiated from the far-field where a time average power flow from the source occurs and there is no appreciable energy storage. It is important to note that energy can be coupled from these "stored energy" fields in the reactive near-field region. The presence of a foreign body such as probe antenna or a person can result in a coupling to these fields. The principal methods of taking energy from these fields involve inductive coupling in the case of the induction field and capacitive coupling in the case of the static field.

Any source or probe antenna has a certain characteristic ability to emit and receive energy. In the case of radiated fields, this ability to emit or receive energy is quantified by the far-field pattern of the antenna, and is usually measured relative to the pattern of some "standard" antenna such as an isotropic source. However, any given probe or source antenna also has a certain characteristic ability to store energy in the reactive fields, which is usually neither known nor specified.

The complete field pattern of an antenna is made up of the far-field, induction, and static fields. The relative contribution of each of these to the complete field pattern is dependent on source-to-probe separation distance. In the radiation far-field region the field pattern is essentially independent of the induction and static fields since the contributions of these to measured field strength is inversely proportional to higher powers of separation distance and hence, negligible. However, to some extent in the radiation near-field region and to a much greater extent in the reactive near-field region, the field pattern of the antenna is highly dependent on induction and static fields. In these regions the field pattern of the antenna becomes a complex function of the source-to-probe separation distance azimuth orientation, and the source and probe configurations of antennas. Interpretations of measurements made in the radiation and reactive near-field regions using probe antennas designed and calibrated for far-field power density measurements involve considerable speculation.

---

*The term static conventionally is used to identify this field because the variation of the amplitude of the field with range is the same as that of the classical static electric dipole.

5. Low Frequency Absorbing Material

The successful measurement techniques for use in shielded enclosures require the use of some absorbing material except at very low frequencies. The requirement extends to sufficiently low frequencies that the absorbing materials become extremely bulky and/or expensive. In an attempt to satisfy the absorption requirements without the attendant space and cost disadvantages, a limited study was conducted to investigate techniques for obtaining compact, inexpensive, low frequency absorbing materials.

Conventional absorbing materials are generally prepared by suspending a lossy material, such as carbon black, in a binder which is transparent to RF energy. Styrofoam, sponge rubber or other similar materials are usually used as a binder. The absorbing material then acts as a continuously distributed transmission medium whose propagation constant has an appreciable real part. The characteristic impedance of this medium is not equal to that of free space and some form of impedance matching must be used if reflections at the absorbing material - air interface are to be avoided. The required impedance match is normally provided by shaping the material in the form of a pyramid whose base is placed flat against the anechoic chamber surface. The incoming RF wave then strikes the point of the pyramid, and sees a gradual tapering off of the terminating impedance from air to that of the absorbing material. The effectiveness of this type of impedance transformer diminishes rapidly when the length of the transformer is less than the wavelength of the incident RF energy. For this reason, absorbing materials which are effective at frequencies below 400-500 MHz are generally quite large and unwieldly.

It is apparent then that the construction of effective low frequency absorbing materials of reasonable dimensions requires some different means for providing the required termination of the incident RF wave at the chamber walls.

One approach to the solution of this problem is to construct a lumped constant approximation to the distributed absorbing material. The most direct application of this idea is to replace the absorbing material with a lumped constant resistive termination such as might be constructed with small carbon resistors. If the resistor network is selected to present a good match to the incident wave, no impedance transformer is required and the necessity of providing a long tapered matching section is avoided. Nevertheless, some coupling structure is still necessary to provide a means of coupling the terminating resistor structure to the incident RF wave. For linearly polarized waves, a short parallel plate transmission line oriented so that the electric field of the incident wave is normal to the planes of the plates can furnish the necessary coupling structure. In general, the spacing of the parallel plate transmission line should be small with

respect to a wavelength to minimize re-radiation of the RF energy by the terminating resistor network. The absorbing material then could be thought of as being constructed of a large number of cells, with each cell composed of a small parallel plate transmission line of appropriate width to obtain a 377 ohm characteristic impedance and terminated in a 377 ohm resistor. Construction is illustrated in the sketch of Figure 72.

To construct a large piece of absorbing material, the cells would be placed side-by-side in the horizontal direction so that the plates of the cells form two continuous sheets. The material can then be extended in the vertical direction by stacking more plates vertically. The resulting appearance of the structure is shown in the sketch of Figure 73.

A piece of absorbing material was constructed using the procedure illustrated in Figure 73. The material was made $2\frac{3}{4}$ inches high by 12 inches deep by about 55 inches long. Single 390 ohm resistors were used to terminate each $2\frac{3}{4}$ inch section. Reflectivity measurements were made on the material by mounting a flat reflecting plate against the back of the material parallel to the plane of the terminating resistors. Reflectivity measurements were made looking directly at the reflector plate and looking at the "BACK" of the reflector plate through the absorbing material. The result of this test is shown by the curve of Figure 74.

The general lack of absorption shown in this curve was attributed to possible fringing of the field at the edges of the material and to the possible interaction effect of the reflector on the field set up by the resistor currents. The configuration of the material was changed to make the material 12 inches high and $2\frac{3}{4}$ inches deep. The 390 ohm resistors were placed $2\frac{3}{4}$ inches apart along the 12 inch dimension of the material to approximate a 377 ohm per square condition.

Results of the tests of this material with the reflecting plate at two different spacings behind the resistors is shown in Figure 75. The material is shown in Figure 76. The better absorption generally achieved with this material indicates that fringing or edge effects play a significant role in the characteristics of this type of absorber. Comparison of the two curves of Figure 75 indicates that the spacing between the resistors and metal plate also influence the absorbing characteristics.

Comparison of Figure 74 with 75 indicates that by reducing the edge effects, significantly better absorption is achieved at lower frequencies. Larger spacings between the terminating resistors and the metal backing plate also is seen (Figure 75) to enhance the absorbing characteristics at lower frequencies. These two results suggest the possibility of further improvement in reducing edge effects and resistor field effects to provide performance comparable to that discussed above at significantly lower frequencies.

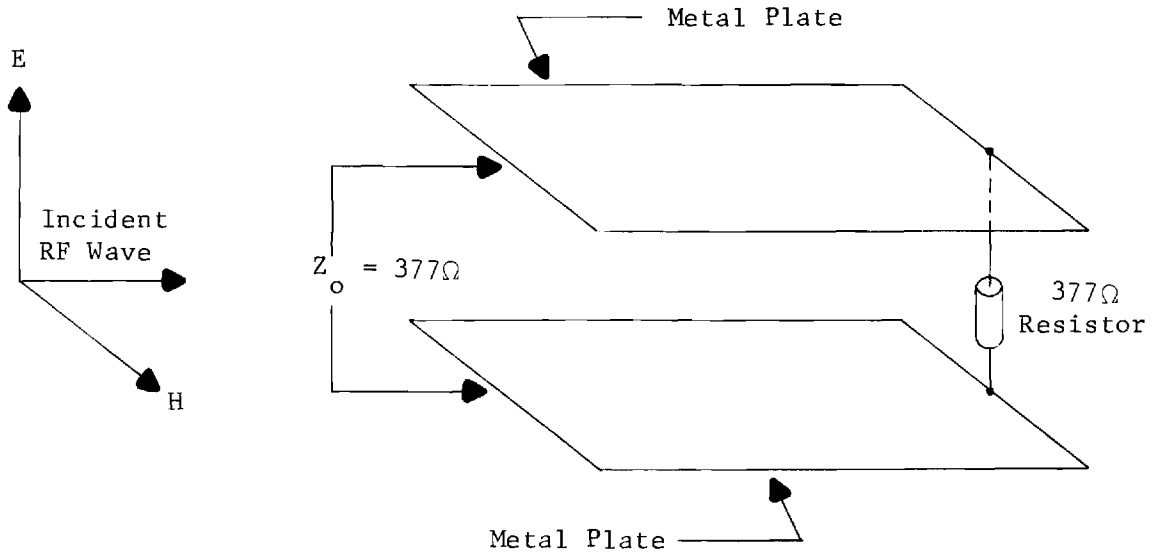

Figure 72. Parallel Plate Absorbing Cell.

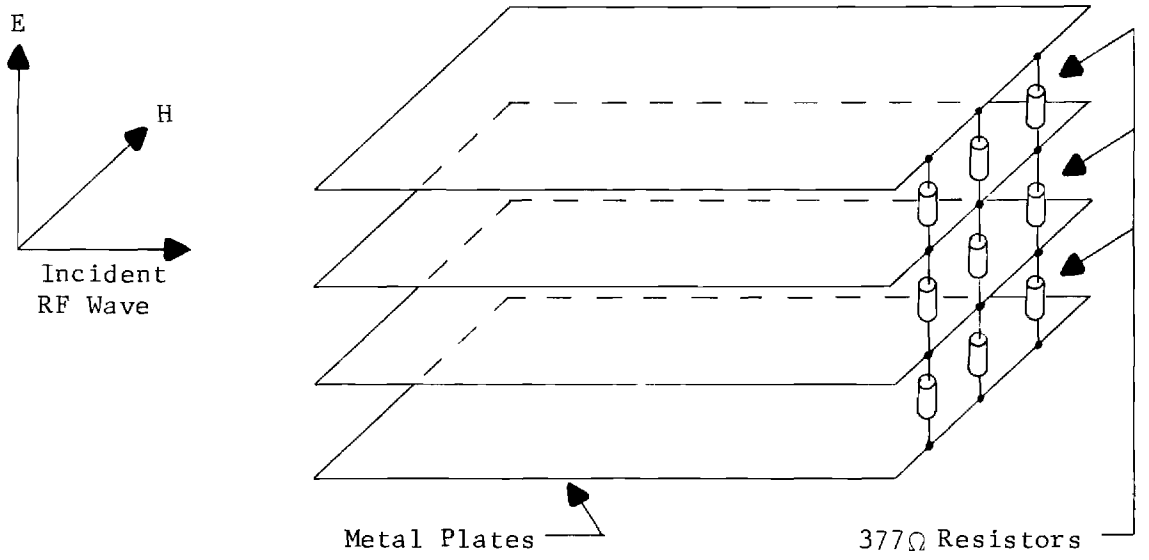

Figure 73. Parallel Plate Absorbing Material

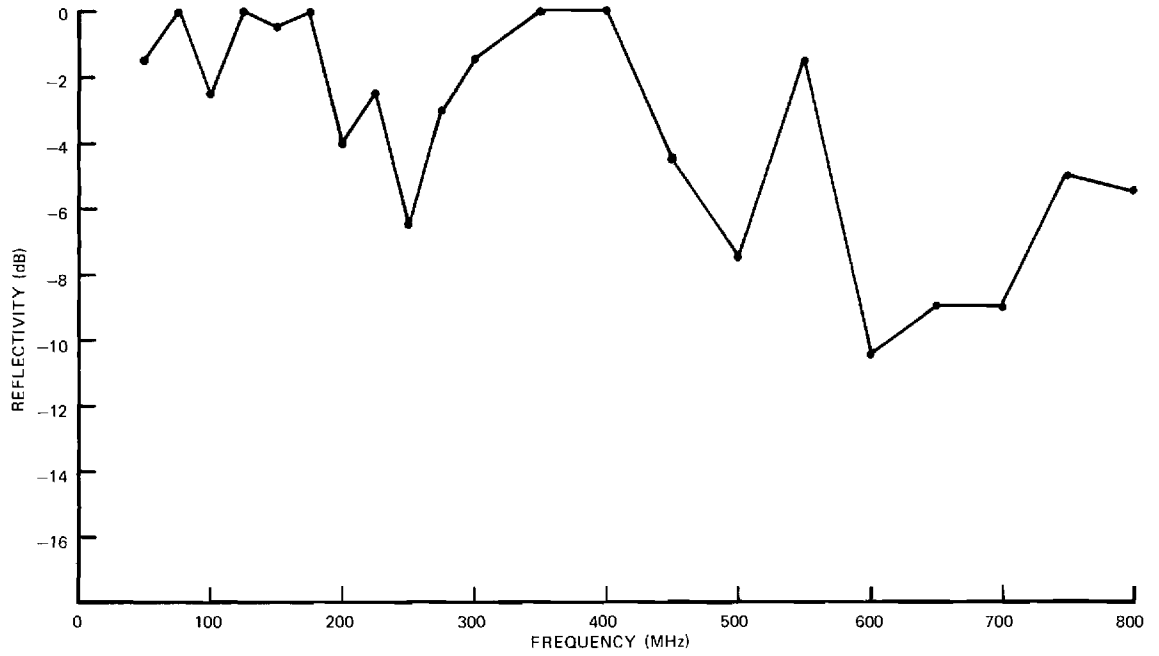

Figure 74. Absorbing Characteristics of Parallel Plate Absorbing Material 2-3/4 Inches High by 12 Inches Deep.

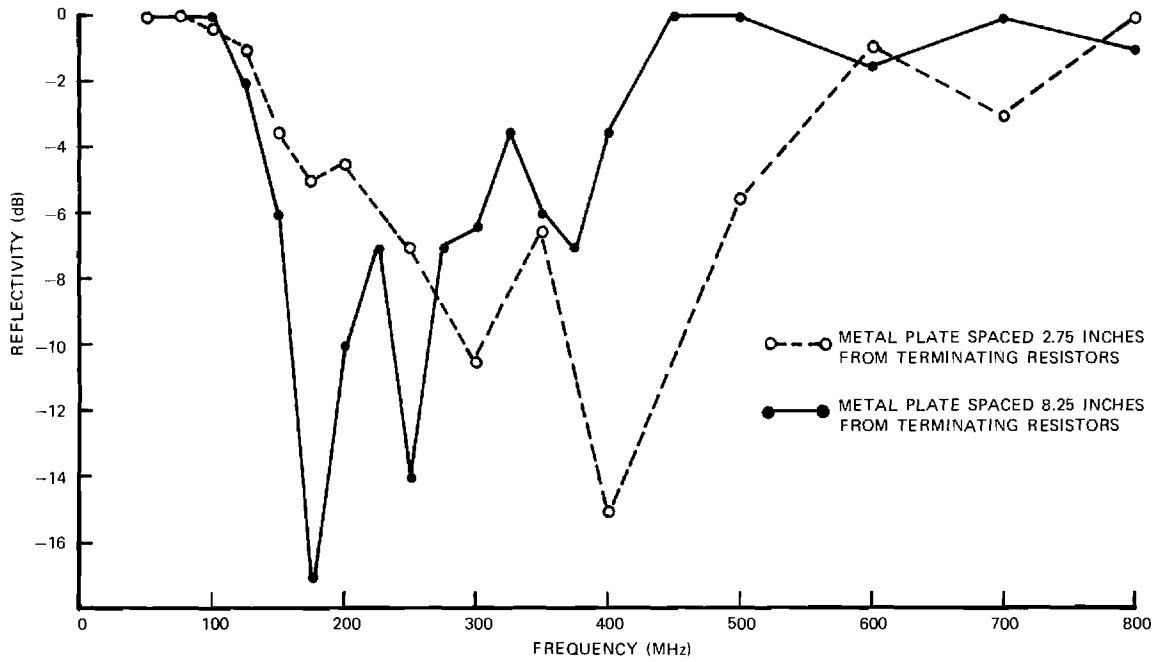

Figure 75. Absorbing Characteristics of Parallel Plate Absorbing Material 12 Inches High by 2-3/4 Inches Deep.

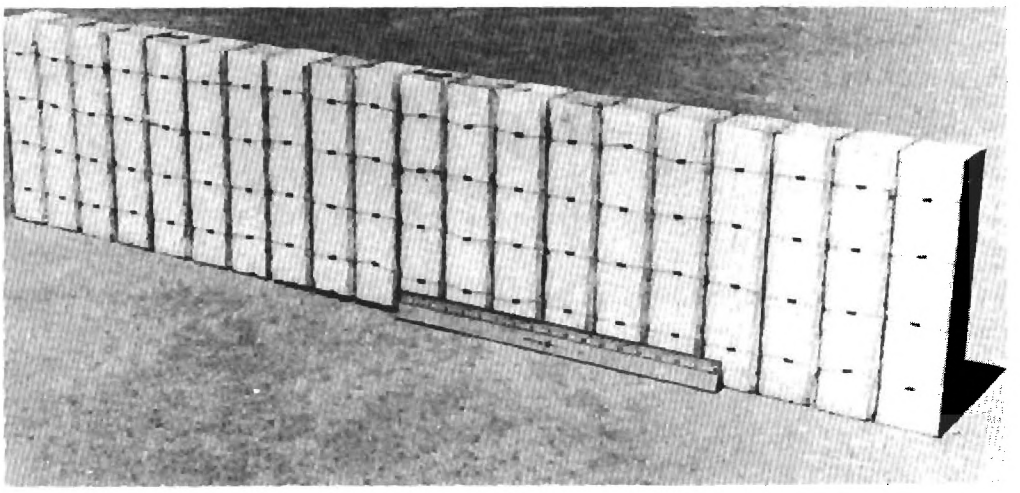

(a)

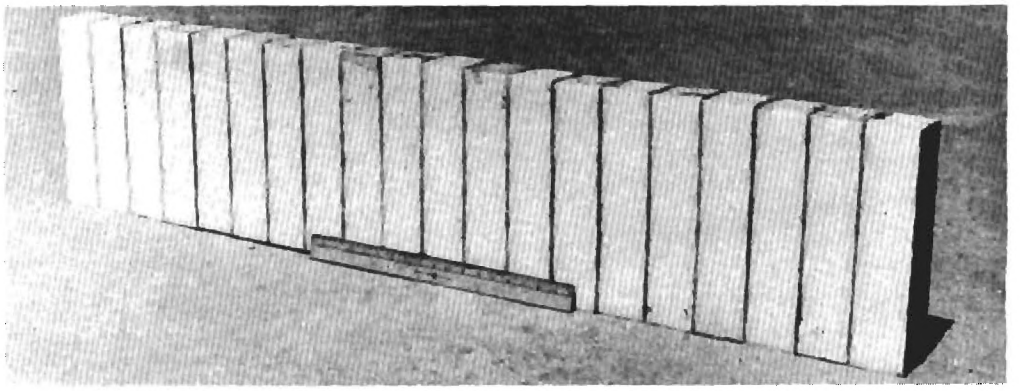

(b)

Figure 76. Two Views of Parallel Plate Absorbing Material 12 Inches High by 2-3/4 Inches Deep.

In summary, the curves of Figure 75 indicate that significant absorption was obtained for the parallel plane material over certain frequency ranges, and that further investigations of this technique should be considered.

II. CONCLUSIONS AND RECOMMENDATIONS

The results from an investigation of radiated measurements over the frequency range from 200 kHz to 20 MHz revealed that essentially the same results are obtained in shielded enclosures and the open-field over this frequency range. This investigation was not extended below 200 kHz to 14 kHz due to lack of sensitivity. The lack of sensitivity was due primarily to the poor efficiency of the low frequency probe antennas. It appears safe to assume however, that the enclosure and open-field results would be the same over the 14 kHz to 200 kHz frequency range. Even though there is correlation between measurement results obtained in shielded enclosures and the open-field over this frequency range, there are two areas which appear to need additional investigation. There is a critical need for more efficient, balanced probe antennas for use over this frequency range. It is recommended that the broadband matching technique utilizing a synthesized filter network be investigated as an approach to realizing improved low frequency probe antennas. The other area of concern is due to the fact that at low frequencies the measurements are made in the near-field of the radiating source. Considering that the near-field distribution is so complex that only the distribution of the most elementary antennas are known and that the distribution is extremely sensitive to both range and azimuth with respect to the radiating source, there is considerable question as to whether a valid interference judgement can be made on the basis of the measurement results. It is suggested that considerably more study of the near-field characteristics of complex radiating sources is necessary before the value of these near-field measurement results can be established.

This study has established the fact that coupling nulls can exist in shielded enclosures well below the lowest resonant frequency of the enclosure (or at frequencies where the dimensions of the enclosure are extremely small relative to a wavelength). The results from extensive experimental measurements supported a theory that these coupling nulls result from near-field coupling between the radiating source and the enclosure walls and between the enclosure walls and the probe antenna. The experimental measurements were made utilizing two bow-tie antennas, one representing the radiating source and the other representing the probe antenna. The bow-tie antenna is a reasonably good representation of the biconical probe antenna (which is the probe which would normally be used over the frequency range of interest, 20 to 100 MHz). In all probability the biconical antenna would exhibit more near-field coupling to the enclosure walls due to its larger size. The question of how realistically the bow-tie antenna represents the case of a typical unit under test is open to considerable conjecture. It could be argued that an equipment case could be represented by a group of randomly oriented dipole antennas. With this concept, it would not be expected that the radially polarized component of the near-field of the case would approach the magnitude of this component off the end of the bow-tie antenna. On the other hand,

it could be argued that the case could be quite large and in close proximity to the enclosure walls so that the near-field coupling between case and walls is greater than with the bow-tie antenna. Considering the extreme latitudes in configuration and size of all possible cases to be tested, it was concluded that the bow-tie antenna is a reasonable representation of a typical equipment case. However, the exact location of the coupling nulls in the shielded enclosure is a complex function of both the ratio of the near-field component to the radiated component and the near-field coupling between the case and the enclosure walls. Hence the null locations are influenced by both the configuration and the size of the case of the equipment under test.

This study has established that the coupling nulls in shielded enclosures over the frequency range from 20 MHz to the lowest resonant frequency of the enclosure are due to near-field coupling via the enclosure walls. The fact that the cause of these low-frequency coupling nulls was significantly different than the normal or multipath coupling mechanism requires that alternate approaches be considered in the development of techniques for eliminating the coupling nulls. The results from very preliminary studies of two techniques, a low-frequency antenna hood and baffle plates, were encouraging, but considerably more study would be required to develop these techniques to the point that they could be utilized in measurement procedures with confidence. Antenna configurations exhibiting inherently low radial field characteristics should also be investigated for possible application as measurement probes in this frequency range.

In the frequency range from the lowest resonant frequency of the shielded enclosure to approximately 200 MHz, coupling variations occur both as a result of near-field coupling to the enclosure walls and as a result of multipath reflections from the enclosure walls. Hence, a satisfactory measurement technique for this frequency range must be capable of eliminating both of these undesired coupling modes.

For rectangular enclosures, the lowest resonant frequency can be determined by the expression

$$f = 150\sqrt{\frac{1}{w^2} + \frac{1}{h^2} + \frac{1}{\ell^2}} \quad \text{MHz}$$

where w, h, and ℓ are the width, height and length of the enclosure in meters. Thus the lowest resonant frequency of a 20' x 20' x 12' enclosure would be approximately 54 MHz and that of a 8' x 8' x 8' enclosure would be approximately 107 MHz.

The results from this program indicate that reliable radiated measurements, which can be correlated with open-field measurements, can be made in shielded enclosures over the frequency range from 200 MHz to

12 GHz by means of the hooded antenna technique and the use of a limited amount of absorbing material on the enclosure walls.

The requirement for a limited amount of absorbing material on the enclosure walls down to the lowest resonant frequency of the enclosure led to an investigation of techniques for obtaining compact, inexpensive, low-frequency absorbing materials. The results from a preliminary study of a lumped constant absorbing material consisting of short sections of parallel-plate transmission lines terminated with resistors were encouraging. The major difficulty was the fact that the absorption was obtained over limited frequency ranges. The difficulty could very well have been due to resonances in the resistor terminations due to the relatively long lead lengths required for these components. It is recommended that further investigation of this technique be performed utilizing distributed resistive terminations. This approach would eliminate any leads and associated resonances from the absorption characteristics.

To make it possible to perform valid radiated measurements in shielded enclosures over the entire 14 kHz to 12 GHz frequency range, it appears the following tasks remain to be accomplished:

(1) A theoretical and experimental study of the near-field characteristics of equipment cases to better define the parameters necessary to determine the interference characteristics at low frequencies.

(2) The development of more efficient, balanced probe antennas for use in the 14 kHz to 20 MHz frequency range.

(3) The development of a satisfactory measurement technique for the 20 to 200 MHz frequency range.

(4) The development of a compact, economical, low-frequency absorbing material.

III. LITERATURE CITED

1. W. R. Free, B. M. Jenkins, and S. L. Robinette, "Electronic Equipment Interference Characteristics - Communication Type," Final Report, Contract DA 36-039 AMC-02294(E), Georgia Tech, (July 1966), AD 486-731.

2. W. R. Free, et.al., "Electromagnetic Interference Measurement Methods - Shielded Enclosure," Final Report, Contract DA 28-043 AMC-02381(E), Georgia Tech, (December 1967).

3. J. D. Kraus, Antennas, McGraw Hill, 1950, pp. 133-135.

4. H. H. Skilling, Fundamentals of Electric Waves, John Wiley and Sons, 1948, pp. 193-198.

5. W. R. Free, et.al., "Compact Chamber for Impedance and Power Testing of VHF Whip Antennas," Final Report, Georgia Tech, Contract DAAB07-67-C-0575, U. S. Army ECOM, October 1968.

6. D. E. Gentry, Broadband Impedance Matching of a Loop Antenna, MSEE Thesis, Georgia Institute of Technology, Atlanta, Georgia, June 1966.

IV. APPENDIX

BIBLIOGRAPHY ON COMPACT AND EFFICIENT ANTENNA TECHNIQUES

1. "Active Aerials," Dr. H. H. Meinke, NTZ. 19, No. 12, 697-705 (1966), Library Translation No. 1242, Royal Aircraft Establishment, August 1967.

2. "A Bibliography of Active Antenna Systems," Bryan A. B. Hodson, Royal Aircraft Establishment, Library Bibliography No. 267, November 1966, AD 807-670.

3. "Broadband Antenna Techniques Study," J. E. Ferris, et.al., University of Michigan, Quarterly Report No. 1, U. S. Army Electronics Command, Contract No. DA 28-043 AMC-01263(E), October 1965, AD 474-493.

4. "Broadband Antenna Techniques Study," J. E. Ferris, et.al., University of Michigan, Quarterly Report No. 2, U. S. Army Electronics Command, Contract No. DA 28-043 AMC-01263(E), 30 November 1965, AD 477-176.

5. "Broadband Antenna Techniques Study," J. E. Ferris, et.al., University of Michigan, Quarterly Report No. 3, U. S. Army Electronics Command, Contract No. DA 28-043 AMC-01263(E), February 1966, AD 480-494.

6. "Broadband Antenna Techniques Study," J. E. Ferris, et.al., University of Michigan, Quarterly Report No. 5, U. S. Army Electronics Command, Contract No. DA 28-043 AMC-01263(E), December 1966, AD 807-406.

7. "Broadband Antenna Techniques Study," J. E. Ferris, et.al., University of Michigan, Interim Report No. 1, U. S. Army Electronics Command, Contract No. DA 28-043 AMC-01263(E), June 1966, AD 488-067.

8. "Broadband HF Antenna Development," J. Killian, et.al., Sylvania Electronics Systems Division, Final Report, RADC, Griffiss Air Force Base, New York, Contract AF 30(602)-3710, May 1966, AD 484-443.

9. Broadband Impedance Matching of a Loop Antenna, D. E. Gentry, MSEE Thesis, Georgia Tech, June 1966.

10. "Description and Results of a Highly-Directive Electrically-Small Antenna," S. B. Pitts, Air Force Avionics Laboratory, Wright-Patterson Air Force Base, Ohio, Report No. AFAL-TR-66-198, Task No. 627803, August 1966, AD 803-749.

11. "Development of Log-Periodic VHF/ECM Antennas," Charles F. Reichert, Chu Associates, First Quarterly Progress Report, U. S. Army Electronics Command, Contract No. DA 28-043 AMC-00258(E), 6 March 1965, AD 468-707.

12. "Development of Probes and Measurement Techniques for Automated Interference Measurements in Shielded Enclosures, 3 to 300 MHz," A. H. Mills, General Dynamics, Interim Technical Report No. 4, Wright-Patterson Air Force Base, Ohio, Contract AF 33(615)-2397, 11 March 1966.

13. "Development of Probes and Measurement Techniques for Automated Interference Measurements in Shielded Enclosures, 3 to 300 MHz," A. H. Mills, General Dynamics, Interim Technical Report No. 5, Wright-Patterson Air Force Base, Ohio, Contract AF 33(615)-2397, 10 June 1966.

14. "Extremely Short Antenna Techniques," S. Czorpita and S. T. Fisher, Philco-Ford Corporation, Final Report, U. S. Army Electronics Command, Contract No. DA 28-043 AMC-02210(E), October 1967.

15. "Improved Performance Techniques for Small Antennas," Peter J. Khan, et.al., University of Michigan, Quarterly Progress Report No. 1, U. S. Army Electronics Command, Contract No. DA 28-043 AMC-02246(E), October 1966, AD 807-047.

16. "Research on Antennas," Dr. H. H. Meinke, Institut fur Hochfrequenztechnik der Technischen Hochschule Munchen, Annual Summary Report, Air Force Avionics Laboratory, European Office of Aerospace Research, Contract AF 61(052)-506, October 1965, AD 476-739.

17. "Research on Compact and Efficient Antennas," J. F. Ramsey, et.al., Airborne Instruments Laboratory, Final Report, U. S. Army Electronics Command, Contract No. DA 28-043 AMC-00281(E), July 1965, AD 474-376.

18. "Study and Investigation of a UHF-VHF Antenna," J. A. M. Lyon, University of Michigan, Final Report, Air Force Avionics Laboratory, Wright-Patterson Air Force Base, Ohio, Contract AF 33(657)-10607, April 1965.

19. "Study and Investigation of a UHF-VHF Antenna," J. A. M. Lyon, et.al., University of Michigan, Quarterly Report No. 6, Air Force Avionics Laboratory, Wright-Patterson Air Force Base, Ohio, Contract AF 33(615)-3609, August 1967.

20. "Techniques for Integrating Solid-State Circuitry into Antennas," Ohio State University Research Foundation, Interim Technical Report, Air Force Avionics Laboratory, Wright-Patterson Air Force Base, Ohio, Contract AF 33(615)-3384, 1 June 1966, AD 488-097.

21. "Techniques for Integrating Solid-State Circuitry into Antennas," Ohio State University Research Foundation, Interim Technical Report, Air Force Avionics Laboratory, Wright-Patterson Air Force Base, Ohio, Contract AF 33(615)-3384, 3 March 1967, AD 808-530.

22. "Techniques for Integration of Active Elements into Antennas and Antenna Structure," J. F. Rippin, Jr., Ohio State University Research Foundation, Interim Engineering Report, Air Force Systems Command, Wright-Patterson Air Force Base, Ohio, Contract AF 33(657)-10386, 1 September 1965.

23. "Techniques for Integration of Active Elements into Antennas and Antenna Structure," J. F. Rippin, Jr., Final Engineering Report, Ohio State University Research Foundation, Air Force Systems Command, Contract AF 33(657)-10386, 20 December 1965, AD 476-943.

24. "Transistors Integrated with Electrically Small Radiators," Dr. Hans Meinke, Institute for High Frequency, Munich, Germany, Air Force Avionics Laboratory, Wright-Patterson Air Force Base, Ohio, October 1966.

DISTRIBUTION LIST FOR FINAL REPORT ON CONTRACT DAAB07-68-C-0189

No. of Copies	To
20	Defense Documentation Center, ATTN: DDC-IRS, Cameron Station (Bldg. 5), Alexandria, Virginia 22314
1	Technical Library, Dir. of Defense Research and Engineering, Room 3E-1039, The Pentagon, Washington, D. C. 20301
1	Naval Ships Systems Command, ATTN: Code 20526 (Technical Library), Main Navy Bldg., Room 1528, Washington, D. C. 20325
1	Director, U. S. Naval Research Laboratory, ATTN: Code 2027, Washington, D. C. 20390
1	Commanding Officer and Director, U. S. Navy Electronics Laboratory, ATTN: Library, San Diego, California 92152
1	AFSC STLO (RTSND), Naval Air Development Center, Johnsville, Warminster, Pa. 18974
1	Chief of Research and Development, Department of the Army, Washington, D. C. 20315
1	Commanding General, U. S. Army Materiel Command, ATTN: R&D Directorate, Washington, D. C. 20315
1	Redstone Scientific Information Center, ATTN: Chief, Documents Section, U. S. Army Missile Command, Redstone Arsenal, Alabama 35809
1	Commanding Officer, Aberdeen Proving Ground, ATTN: Technical Library, Bldg. 313, Aberdeen Proving Ground, Maryland 21005
1	Commanding Officer, U. S. Army Combat Developments Command, Communications Electronics Agency, Ft. Monmouth, N. J. 07703
1	Commander, U. S. Army Research Office (Durham), Box CM-Duke Station, Durham, North Carolina 27706
1	U. S. Army Security Agency, ATTN: OACofS, Dev, Arlington Hall Station, Arlington, Virginia 22212
1	Commanding General, U. S. Army Electronic Proving Ground, ATTN: Technical Information Center, Fort Huachuca, Arizona 85613

DISTRIBUTION LIST FOR FINAL REPORT ON CONTRACT DAAB07-68-C-0189
(Continued)

No. of Copies	To
1	Asst. Secretary of the Army (R&D), Department of the Army, ATTN: Deputy Asst. for Army (R&D), Washington, D. C. 20315
1	Commanding General, U. S. Army Electronics Command, ATTN: AMSEL-MR, 225 South 18th Street, Philadelphia, Pa. 19103
1	Headquarters, U. S. Army Combat Developments Command, ATTN: CDCLN-EL, Fort Belvoir, Virginia 22060
1	USAECOM Liaison Officer, MIT, Bldg. 26, Room 131, 77 Massachusetts Avenue, Cambridge, Mass. 02139
1	USAECOM Liaison Officer, U. S. Army Tank-Automotive Center, Warren, Michigan 48090
1	USAECOM Liaison Officer, Aeronautical Systems Division, ATTN: ASDL-9, Wright-Patterson Air Force Base, Ohio 45433
1	Commander, Rome Air Development Center, ATTN: EMCVI-2, Griffiss Air Force Base, New York 13440
1	Army Deputy Director, Electromagnetic Compatibility Analysis Center, ATTN: Col. Wilson, North Severn, Annapolis, Md. 21401
	Commanding General, U. S. Army Electronics Command, Fort Monmouth, New Jersey 07703
1	ATTN: AMSEL-PP
1	ATTN: AMSEL-IO-T
1	ATTN: AMSEL-RD-MAT
1	ATTN: AMSEL-RD-LNA
1	ATTN: AMSEL-XL-D
1	ATTN: AMSEL-NL-D
1	ATTN: AMSEL-WL-D

DISTRIBUTION LIST FOR FINAL REPORT ON CONTRACT DAAB07-68-C-0189
(Continued)

No. of Copies	To
	Commanding General, U. S. Army Electronics Command, Fort Monmouth, New Jersey 07703
1	ATTN: AMSEL-KL-D
1	ATTN: AMSEL-HL-CT-D
1	ATTN: AMSEL-BL-D
1	ATTN: AMSEL-VL-D
2	ATTN: AMSEL-RD-GF (Record Copies, Ida Wagner)
4	ATTN: AMSEL-RD-GF (Guy Johnson)

Security Classification

DOCUMENT CONTROL DATA - R&D

(Security classification of title, body of abstract and indexing annotation must be entered when the overall report is classified)

1. ORIGINATING ACTIVITY (Corporate author)	2a. REPORT SECURITY CLASSIFICATION
Georgia Institute of Technology, Atlanta, Georgia	Unclassified
	2b. GROUP

3. REPORT TITLE

ELECTROMAGNETIC INTERFERENCE MEASUREMENT METHODOLOGY, COMMUNICATION EQUIPMENT

4. DESCRIPTIVE NOTES (Type of report and inclusive dates)

Final Report, 1 February 1968 to 31 May 1969

5. AUTHOR(S) (Last name, first name, initial)

Free, William R. and Stuckey, Charles W.

6. REPORT DATE	7a. TOTAL NO. OF PAGES	7b. NO. OF REFS
October 1969	100	6

8a. CONTRACT OR GRANT NO.	9a. ORIGINATOR'S REPORT NUMBER(S)
DAAB07-68-C-0189	
b. PROJECT NO.	A-1075-F
1H6 20501 D449 0156	
c.	9b. OTHER REPORT NO(S) (Any other numbers that may be assigned this report)
d.	ECOM-0189-F

10. AVAILABILITY/LIMITATION NOTICES

This document has been approved for public release and sale; its distribution is unlimited.

11. SUPPLEMENTARY NOTES	12. SPONSORING MILITARY ACTIVITY
Radio Frequency Interference Communications	U. S. Army Electronics Command Fort Monmouth, New Jersey 07703 AMSEL-NL-C

13. ABSTRACT

This report summarizes the accomplishments on a program to develop improved test techniques and procedures for performing radiated measurements in shielded enclosures which can be correlated with measurements made in the open-field.

A set of three short hooded probe antennas to cover the 1 to 12 GHz frequency range were developed and evaluated. Results from this program indicate that reliable radiated measurements, which can be correlated with open-field measurements, can be made in shielded enclosures with short hooded probe antennas over the 200 MHz to 12 GHz frequency range.

Coupling nulls were observed in shielded enclosures in the frequency range from 10 to 100 MHz. The presence of these nulls could not be explained on the basis of cavity resonances or multi-path reflections from the enclosure walls since the dimensions on the enclosures were quite small in terms of wavelengths. It was concluded that a different coupling mechanism must be responsible for the existance of these coupling nulls. A theory was developed to explain the nulls in terms of near-field coupling between the radiating source and the enclosure walls and between the enclosure walls and the probe antenna. The results from extensive experimental measurements supported the validity of this theory. The coupling nulls were essentially eliminated by isolating the probe antenna from the enclosure walls.

DD FORM 1 JAN 64 1473

Security Classification

55/1200

14. KEY WORDS	LINK A		LINK B		LINK C	
	ROLE	WT	ROLE	WT	ROLE	WT
Electromagnetic Interference Measurement Methods Cavity-Backed Spiral Antennas Antennas Shielded Enclosures Near-Field Antenna Theory						

INSTRUCTIONS

1. ORIGINATING ACTIVITY: Enter the name and address of the contractor, subcontractor, grantee, Department of Defense activity or other organization *(corporate author)* issuing the report.

2a. REPORT SECURITY CLASSIFICATION: Enter the overall security classification of the report. Indicate whether "Restricted Data" is included. Marking is to be in accordance with appropriate security regulations.

2b. GROUP: Automatic downgrading is specified in DoD Directive 5200.10 and Armed Forces Industrial Manual. Enter the group number. Also, when applicable, show that optional markings have been used for Group 3 and Group 4 as authorized.

3. REPORT TITLE: Enter the complete report title in all capital letters. Titles in all cases should be unclassified. If a meaningful title cannot be selected without classification, show title classification in all capitals in parenthesis immediately following the title.

4. DESCRIPTIVE NOTES: If appropriate, enter the type of report, e.g., interim, progress, summary, annual, or final. Give the inclusive dates when a specific reporting period is covered.

5. AUTHOR(S): Enter the name(s) of author(s) as shown on or in the report. Enter last name, first name, middle initial. If military, show rank and branch of service. The name of the principal author is an absolute minimum requirement.

6. REPORT DATE: Enter the date of the report as day, month, year; or month, year. If more than one date appears on the report, use date of publication.

7a. TOTAL NUMBER OF PAGES: The total page count should follow normal pagination procedures, i.e., enter the number of pages containing information.

7b. NUMBER OF REFERENCES: Enter the total number of references cited in the report.

8a. CONTRACT OR GRANT NUMBER: If appropriate, enter the applicable number of the contract or grant under which the report was written.

8b, 8c, & 8d. PROJECT NUMBER: Enter the appropriate military department identification, such as project number, subproject number, system numbers, task number, etc.

9a. ORIGINATOR'S REPORT NUMBER(S): Enter the official report number by which the document will be identified and controlled by the originating activity. This number must be unique to this report.

9b. OTHER REPORT NUMBER(S): If the report has been assigned any other report numbers *(either by the originator or by the sponsor)*, also enter this number(s).

10. AVAILABILITY/LIMITATION NOTICES: Enter any limitations on further dissemination of the report, other than those imposed by security classification, using standard statements such as:

(1) "Qualified requesters may obtain copies of this report from DDC."

(2) "Foreign announcement and dissemination of this report by DDC is not authorized."

(3) "U. S. Government agencies may obtain copies of this report directly from DDC. Other qualified DDC users shall request through _____."

(4) "U. S. military agencies may obtain copies of this report directly from DDC. Other qualified users shall request through _____."

(5) "All distribution of this report is controlled. Qualified DDC users shall request through _____."

If the report has been furnished to the Office of Technical Services, Department of Commerce, for sale to the public, indicate this fact and enter the price, if known.

11. SUPPLEMENTARY NOTES: Use for additional explanatory notes.

12. SPONSORING MILITARY ACTIVITY: Enter the name of the departmental project office or laboratory sponsoring *(paying for)* the research and development. Include address.

13. ABSTRACT: Enter an abstract giving a brief and factual summary of the document indicative of the report, even though it may also appear elsewhere in the body of the technical report. If additional space is required, a continuation sheet shall be attached.

It is highly desirable that the abstract of classified reports be unclassified. Each paragraph of the abstract shall end with an indication of the military security classification of the information in the paragraph, represented as *(TS), (S), (C), or (U)*.

There is no limitation on the length of the abstract. However, the suggested length is from 150 to 225 words.

14. KEY WORDS: Key words are technically meaningful terms or short phrases that characterize a report and may be used as index entries for cataloging the report. Key words must be selected so that no security classification is required. Identifiers, such as equipment model designation, trade name, military project code name, geographic location, may be used as key words but will be followed by an indication of technical context. The assignment of links, roles, and weights is optional.

DD FORM 1 JAN 64 1473 (BACK)